Università degli Studi di Catania
Scuola Superiore di Catania

International PhD

in

Nanoscience

XXV cycle

Memory, metals and neurotrophins

Alessio Travaglia

Coordinator of PhD

Prof. Grimaldi

Tutor

Prof. Rizzarelli

Catania, 2012

Abstract

In the last decades, one of the main interests of neuroscientists has been to unravel the molecular mechanisms of memory.

Neurotrophins are proteins involved in development and survival of neurons as well as they are active player in memory formation and synaptic plasticity. d-block biometals, especially copper and zinc, are emerging as crucial player in the physiology of the brain.

As matter of fact, there is a significant overlap between brain areas in which the highest concentration of metals have been measured and those where the neurotrophins exert their biological activity. Metal ions can directly modulate their activities, through conformational changes, and/or indirectly by activating their downstream signaling in a neurotrophin-independent mode. Despite the importance of these modulations, there is the lack of experimental data regarding the coordination features of metal ions complexes with neurotrophins.

The N-terminal domain of neurotrophins is critical for the binding selectivity and activation of their receptors. We synthesized the N-terminus peptide fragments encompassing the human neurotrophins, characterized their copper(II) and zinc(II) complexes by means of potentiometric, spectroscopic (UV/Vis, CD, NMR and EPR) techniques and DFT calculations, tested the metal-driven biological effect. The coordination features of acetylated as well as single point mutated peptides have been also studied to prove the involvement of each donor group. The functional interaction of biometals with neurotrophins and related peptides has been tested by biological assay on SHSY5Y neuroblastoma cell, providing evidence of the correlation between biological activity and coordination environment.

Our biochemical characterizations of the neurotrophins signaling, both *in vitro* and *in vivo*, have shed some light on the possible use of neurotrophins and neurotrophins-like peptides in neurological disorders. Indeed, the use of neurotrophins in the early stages of neurodegenerative diseases has recently gained attention. However, there are limits to such therapy, e.g. insufficient permeability of the blood-brain barrier and inappropriate

activation of receptors that trigger side effects. The use of peptidomimetic combined with systems that guarantee their delivery might allow to overcome these restrictions. In view of application as functional nanoplatforms for smart drug delivery, supported lipid bilayers formed by neurotrophin peptidomimetics/small unilamellar vescicles adsorption on silica (both planar model and nanoparticles) have been characterized.

In conclusion, the interaction of metals and neurotrophins might represent a crossroad for neuronal physiology. Better understanding of metal ion-driven neurotrophins signal transduction and intercellular signaling, as well as vice versa, the role of neurotrophins in the control of metal ions homeostasis, could disclose helpful information and it is therefore strongly raising as one of the most critical step in the study of neurodegenerative diseases as well in the physiological mechanisms of memory.

1. Introduction

1.1 Memory Consolidation

Memory is the active process by which incoming information are elaborated, encoded, stored, and subsequently recalled.[1-2]

The brain is the most astonishing, complex and less understood organ in the human body. It is made up of about 100 billion neurons (or nerve cells), each of which may be connected to up to 10,000 other neurons through special junctions called synapses.[3-5] Whenever something is learned, circuits of neurons in the brain are created, altered, strengthened or weakened. [6-8] Thus, in physiological terms, memory is a set of encoded neural connections built up in the brain as a consequence of stimuli.[2,4] The sensory system collects outputs, from the outside world, which are converted in chemical and physical signals (encoding phase). Then, the memory traces have to be stored in specific brain regions to be maintained over time (storage phase). Last, the acquired information has to be recalled if required. [9-10]

Memory is usually divided into short- and long-term. [1-2,5,11] Short-term memory (STM) is the ability to hold and to recall small quantities of information for a short period of time, usually considered in the order of seconds. STM is due to transient patterns of neuronal connection, involving the paretial and the frontal lobe, especially the dorsolateral prefrontal cortex.[5] Long-term memories (LTM), as the name suggest, allow storing unlimited quantities of information for long-lasting duration, sometimes a whole life span. However, the difference between STM and LTM is not only the duration of the memory traces, but also the different biochemical mechanisms of encoding/storage.[2] Only a long-term memory triggers changes in neural pathways, necessary to store the information, that can be recalled even years later. It is believed that LTM are maintained through stable and permanent changes in neural connections widely spread throughout the brain.[1,5] The hippocampus is a brain region considered essential to learn new information.[2,12] Indeed, although it does not seem to store information itself, new memories are unable to be stored into LTM without the hippocampus.[13-14] The hippocampus seems to act as temporary transit point for long-term memories and it is essential to the consolidation of information

from short-term to long-term memory. [2,11,15] Furthermore, it is involved in changing neural connections for a period of three months or more after the initial learning.[2,11,15]

Memory consolidation is defined as the process that stabilizes a memory trace after its acquisition. Indeed, intriguingly, after the initial acquisition phase, the new learned information is in a labile form, sensitive to disruption. [2,16-17] Memory consolidation is distinguished into two specific processes, synaptic consolidation, which occurs within the first few hours after learning, and system consolidation, which lasts over a period of weeks to years. [2]

1.1.1 Synaptic Consolidation and Long-Term Potentiation

Synaptic consolidation has been observed across all species and occurs within the first few hours after learning. Long term potentiation (LTP) is one of the best understood forms of synaptic plasticity and synaptic consolidation.[12,18-19]

The most widely studied type of LTP is the N-methyl-D-aspartate receptor (NMDAR)-dependent LTP at the synapses between Schaffer collaterals and commissural neurons in area CA1 of the adult hippocampus [12,18] Much is known, at molecular level, about this process. Glutamate molecules, released into the synaptic cleft, bind NMDA receptor. Only in the presence of a coincident event of depolarization, Mg(II) ion is expelled from the NMDAR channel. When the channel is no more blocked by Mg(II) ion, the binding of glutamate molecules can open the NMDAR channel, allowing an influx of calcium(II) ions into the cell.[18,20] The calcium influx trigger the activation of protein kinases, such as Ca^{2+}/calmodulin-dependent protein kinase II (CaMKII) and protein kinase C (PKC).[21-22] In turn, these proteins, as well the extracellular signal-regulated kinase (ERK), activate transcription factors that trigger the synthesis of new proteins that maintain the LTP. [23-25]

1.1.2 System Consolidation

System Consolidation is a slow and dynamic process in which memory traces are "moved" from the regions in which are first encoded to the cortex, in a permanent form of storage.[2-3]

It is believed that memory is retained in the hippocampus for up to one week after initial learning. Then, the memory traces are slowly transferred to the neo-cortex, where it is permanently stored.

In this view, the neurogenesis in the adult hippocampus may facilitate to delete the old memories, creating new "space" for the incoming new memories.[26-27]

1.1.3 Memory Consolidation: Molecular Perspective

Neuroscientists have been prompted to go in deep on the details of long term memory formation since the discovery that, at the beginning of the consolidation process, memory formation can be prevented/disrupted by interferences.[3,17,28-29] These include seizure, trauma, neuronal inactivation and brain lesions, but also by new additional learning, inhibition of transcription or specific transcription factors, inhibition of protein synthesis or selective blockade of specific molecular pathways.[29-30] From the first discovery, a plenty of papers have shed light on the molecular mechanisms of memory consolidation, providing evidence on the role of specific biochemical events involved in long-term memory formation.[7,10,31-33]

What are the transcription factors involved in memory formation? What are they target genes and how they allow complex cognitive responses? Or, in other words, what are the proteins required for memory formation? In which brain regions are they necessary? What is the time course of transcription and protein synthesis requirements? Much has been done, but many points have not been completely unraveled.

Least but not last, an increasing number of evidences suggest a potential role of transition metal ions in neuromodulation/neurotransmission. The brain is an organ with extraordinary complexity and unique chemical composition and its inorganic chemistry is inherently rich and remains an open frontier to study. What metal ions are present in the brain? How are they distributed? Do they have a function role in memory formation?

Finally, besides mere knowledge of what transcription factors and proteins are involved in memory formation, it would be interesting to evaluate their interactions/regulations. In this context, metal ions might directly modulate the activities of biological macromolecules, likely through conformational changes, and/or indirectly by activating their downstream signaling.

1.2 Neurotrophins

Neurotrophins (NTs) are secreted proteins discovered because of their essential role in development, differentiation, and maintenance of specific populations of neurons.[34-36] Then, in the last decade, it has been reported that neurotrophins and their receptor match all the characteristics that a protein must have to play a consistent role in memory consolidation and synaptic plasticity:

1) Their expression, regulation and secretion are activity dependent.

2) They are expressed in the right place/time where memory consolidation takes place, and their receptors are localized in the same area.

3) As a consequence of its activity, they modulate the neuronal function, such as membrane excitability, neuronal morphology and connectivity.

Thus, besides their well-established actions in survival and development, today is known that they are involved in the wiring regulation of the central and peripheral nervous system during development, [37-38] can modulate synaptic plasticity[39-42] and cognitive functions, [39-41,43-44] as well they seems involved in the etiology/exacerbation of neurological disease, such as Alzheimer's Disease.

The neurotrophins family comprises nerve growth factor (NGF), brain-derived neurotrophic factor (BDNF), neurotrophin-3 (NT-3) and neurotrophin-4 (NT-4). The NTs are structurally and functionally related proteins, which exert their biological action as non-covalent dimmers.[45] They share a sequence homology close to 50% and a structural homology of about 60%. A single monomer of each NT has a core consisting of two pairs of antiparallel β-strands with well conserved sequences among the neurotrophins family members, and responsible for the dimer assembly. Whereas, the N- and C-termini, as well as loops 2 and 3, determine sequence diversity [46-48]

Discovered by Rita Levi-Montalcini and Stanley Cohen almost half century ago, NGF is the founding and best-characterized member of the neurotrophins family.[35] All the

neurotrophins are synthesized as precursor (pro-NTs) and cleaved by some proteases (plasmin, furin, MMP7 and MMP3)[49-50] to produce the C-terminal mature and active forms, which exert their biological action as non-covalent homodimer. Neurotrophins driven cell signaling operate through the interaction with two distinct classes of receptors: p75 and Trks (tropomyosin receptor kinase) receptors, thereby activating signal transduction cascades that trigger distinct biological responses.[47,51-53] In a simplified view, p75 transmits apoptotic signals, whereas Trks receptors trigger pro-survival outcome (Fig. 1).

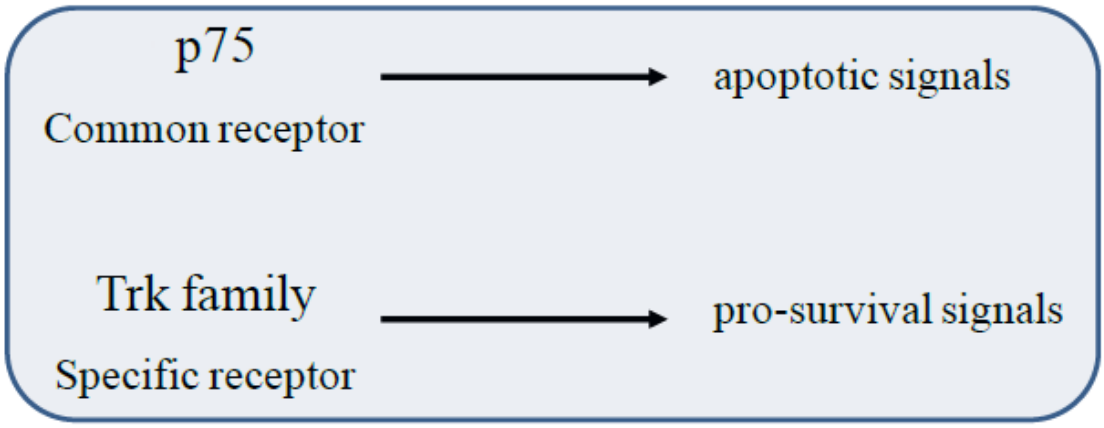

Figure 1. *Schematic representation of neurotrophins receptors and their response upon activation*

1.2.1 Neurotrophins Signaling

Low-affinity neurotrophins receptor, p75, is known as the common neurotrophins receptor, because of its ability to recognize all the NTs, even though with different kinetic constants. The receptor p75 plays a variety of roles in neurotrophins signaling, including the enhancement of Trk activity as well as Trk-independent signaling. Pathways that are independent from Trk activation may, under appropriate conditions, lead to an apoptotic cell death.[51-53]

p75 receptor, indeed, belongs to the "death domain" family of receptor proteins, which

includes Fas receptor, tumor necrosis factor receptor, and other receptors.

The intracellular domain of p75NTR lacks any intrinsic catalytic, thus the p75 signaling is believed to be the consequence of association/dissociation of various intracellular adaptor binding proteins.[51-53]

The Trk receptor belongs to a family of three different members: TrkA, TrkB and TrkC. The Trk receptor family shows a high degree of specificity (Fig 2) i.e. NGF binds TrkA; TrkB is the receptor for BDNF and NT-4, whereas NT-3 binds to TrkC. The latter one seems to be promiscuous, since it can also activate TrkA and TrkB.[51-53]

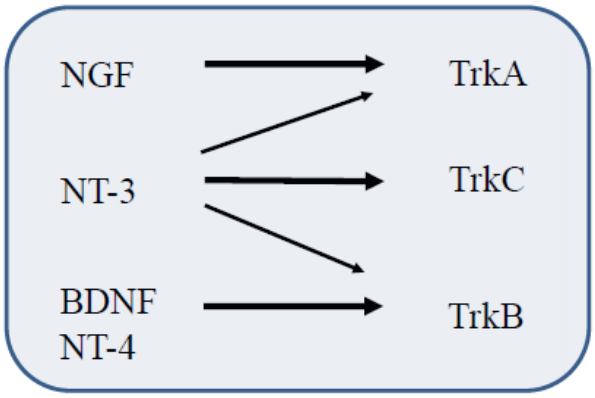

Figure 2. *Schematic representation of interaction between neurotrophins and their cognate Trk receptor*

The binding of NGF to TrkA induces receptor dimerization and the consequent trans-autophosphorylation of tyrosine residue in the intracellular domain of the TrkA. This event represents the beginning of a downstream signal, which involves several kinase cascades (Fig 3). The main signal transduction pathways due to TrkA activation include:

a) The classic MAPK cascade, involving activation of the G- protein Ras, and the kinases Raf and MEK, abbreviated as the reaction series Ras/Raf/MEK/MAPK. The major role of the Ras-MAPK pathway is the neurite outgrowth.

b) the phosphatidylinositol-3-kinase (PI3 kinase)/Akt pathway. The PI3K-Akt pathway is a key regulator of the anti-apoptotic/pro-survival response in neurons

c) the phospholipase C gamma (PLCγ) pathway. PLC activation leads to PI3 hydrolysis, with formation of IP3 (inositol trisphosphate) and DAG (diacylglycerol). Consequentially, IP3 induces the release of Ca^{2+} by stores, resulting in the activation of various Ca^{2+} regulated enzymes. This pathway may play a role in Ca^{2+}-mediated cellular degeneration in aging and disease by affecting oxidative stress systems.[51,54]

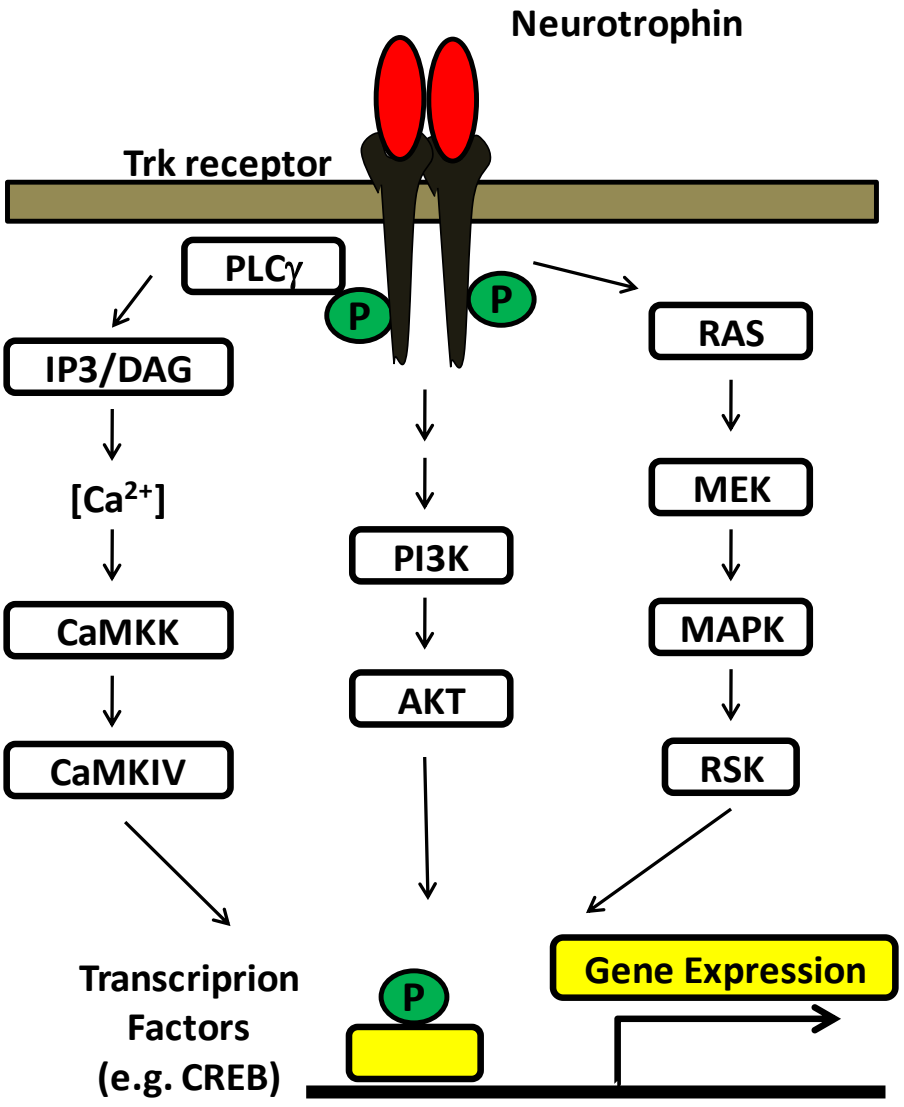

Figure 3. *Major Trk receptor signaling.*

The overall picture of neurotrophins-mediated signaling cascade is tangled by the activity of pro-forms, Indeed, pro-Neurotrophins have been initially considered the precursor of the mature (and active form) of the neurotrophins, thus molecules without any biological activity

Now it is recognized that pro-neurotrophins mediate cellular apoptosis [55] and inhibit neurite growth in many cell lines and primary neurons [56] through p75 receptor, even in the presence of TrkA, with the involvement of sortilin receptor, a member of Vsp10p-domain receptor. [57]

In summary, a strict, not fully understood, regulation of p75 and TrkA (and sortilin) pathways by NGF (and its precursor) is emerging as responsible for modulation of many different aspects of neuronal life, like neurite outgrowth and differentiation, pro-survival signals or pro-apoptotic outcome, and molecular mechanisms involved in physiological as well pathological conditions.[51,58-59]

1.2.2 Neurotrophins and Transcription Factors

Neurotrophins, through their downstream signaling that raise intracellular cAMP and Ca(II) ions concentration, ultimately trigger the activation of transcription factors.

Eric Kandel, Nobel Prize in 2000, has described the process of memory storage as a "dialogue between genes and synapses".[4] The genetic information carried by all organisms is expressed in any biological function via a series of processes that begins with DNA transcription, a process through which the information encoded in the DNA is copied into a molecule of RNA (which is then translated to a specific protein).

Beside to be the first regulatory step in gene expression, transcription is a molecular requisite for long-term synaptic plasticity and long-term memory formation.[9,24,60] Indeed, memory consolidation can be altered/prevented by agents able to interfere with protein transcription.[23,25,61-63] Thus, researchers have been focused on the identification of families of transcription factors required to mediate memory formation and to elucidate how they exert this function.[24-25,64] These include cAMP response element binding protein (CREB), CCAAT enhancer binding protein (C/EBP), methyl-CpG-binding protein 2 (MeCP2) activating protein 1 (AP-1), early growth response factor (Egr), and Rel/nuclear factor κB (Rel/NFκB).[24-25,64]

Among them, the transcription factor cAMP response element-binding protein (CREB) is probably the most studied. CREB is a 43 kDa protein widely expressed in the brain, especially in the regions essential for encoding learning and memory, including the hippocampus and cortex.[65-66] Neurotrophins, as previously mentioned, through their downstream signaling that raise intracellular cAMP and Ca(II) ions concentration, [67-68] trigger the phosphorylation and activation of CREB at Ser-133. The phosphorylated form of CREB (pCREB) binds specific DNA sequences, thus enhancing the expression of genes that results in synapse-specific structural changes.[66,69-70] CREB signaling is reputed essential for neuronal changes that mediate many important functions in the nervous system, including neurogenesis and neuronal survival, development, and differentiation, synaptic plasticity, and the conversion from short- to long-term memory.[42] Also, CREB

signaling has been recently involved in several neurodegenerative disease, such as Alzheimer's Disease.[66,69-71]

A transcription factor recently connected with the neurotrophins signaling and cognitive function is the methyl-CpG-binding protein 2 (MeCP2). MeCP2 has been first discovered because of its ability to bind methylated DNA. It is expressed throughout the body and is particularly abundant in the brain, where it seems to be essential for the normal function of neurons. [72-75] It has gained popularity and the attention of scientific community because its mutation cause the autism spectrum disorder Rett Syndrome (RTT).[76-77] This disease is mainly found in girls with a prevalence of around 1 in every 10,000. Strikingly, there is not sign of disease at the born, but after 6-18 months, RTT patients lose purposeful use of their hands and instead develop stereotypic hand movements. The onset of mental deterioration is accompanied by loss of motor coordination and deceleration of head growth.[78-79] The exact function of this protein is not known. It seems to act as a transcriptional repressor, thus preventing gene expression when is not needed. However, MeCP2, in addition to its long-term gene-silencing role, recent works point out that MeCP2 can also activate the gene expression, though it is still debated.[75,78]

Among the target genes of MeCP2, that encoding for BDNF is the most extensively studied, since the pivotal role played by this neurotrophin in neuronal survival, dendritic arborization, circuit formation and function of connected neurons.[44] MeCP2has been reported to specifically bind BDNF promoter III and functions as a negative regulator of BDNF expression. In response to membrane depolarization and consequent calcium influx into the neurons, MeCP2 becomes phosphorylated and is release from the BDNF promoter, thereby permitting BDNF transcription. [78,80-85] Also, despite the evidence that MeCP2 plays an important role in neurons, recent works have raised questions about what is the primary cell types (e.g. neuron, astrocytes or microglia) which lead to the manifestation of RTT phenotypes, despite the low abundance of MeCP2 in non-neuron cell types.[80-81]

1.2.3 Neurotrophins and Alzheimer's Disease

Neurodegeneration is the progressive loss of structure and/or function of neurons, and increasing the likelihood of death. [86-87] The increase of elderly population due to life span prolongation has unfortunately led to a high variety of age-related neurologic diseases particularly related to accumulation of misfolded proteins. Alzheimer's disease (AD) is the most common form of dementia in the elderly, the fourth cause of death in the western world (after heart disease, cancer and stroke); AD affects 24 million of patients and it is expected to double by 2020.[88]

The pathologic hallmark of AD is the formation of intracellular neuronal tangles and the deposition of amyloid plaques in the neural parenchyma. [89-90] Amyloid β (Aβ), a small peptide featured by 39 to 43 amino acids, is the principal component of plaques that originate from the type-I membrane protein, Amyloid Precursor Protein (APP), after cleavage by β- and γ-secretases. [91-92] According the 'amyloid cascade hypothesis', the excessive production and accumulation of Aβ triggers the pathogenesis of AD. [89] Indeed, plaques and tangles are present mainly in brain regions involved in learning, memory, and emotional behavior such as the entorhinal cortex, hippocampus, basal forebrain and amygdale. However, the amyloid cascade hypothesis is not completely convincing and accepted and the exact nature of the toxic species is debated. [93] It seems to be related to soluble oligomers rather than to plaques, [90] whereas monomers have been found to be neuroprotective. [94-95]

A large number of efforts have been made to contrast the deranged effects of neurodegeneration and to identify therapeutic interventions to prevent the progression of age-related cognitive decline.[92-93,96-97] In this respect, NTs and their receptors have gained most attention as potential targets. The homeostasis of different neurotrophins is indeed altered in specific brain areas during the pathogenesis of AD [98-99] In the central nervous system, the highest levels of NGF are present in the hippocampus, the brain area involved in learning and memory, and in the areas containing basal forebrain cholinergic neurons (BFCNs) [100]; all these findings led to the formulation of the "NGF hypothesis of AD" (Fig. 4). [101-103]

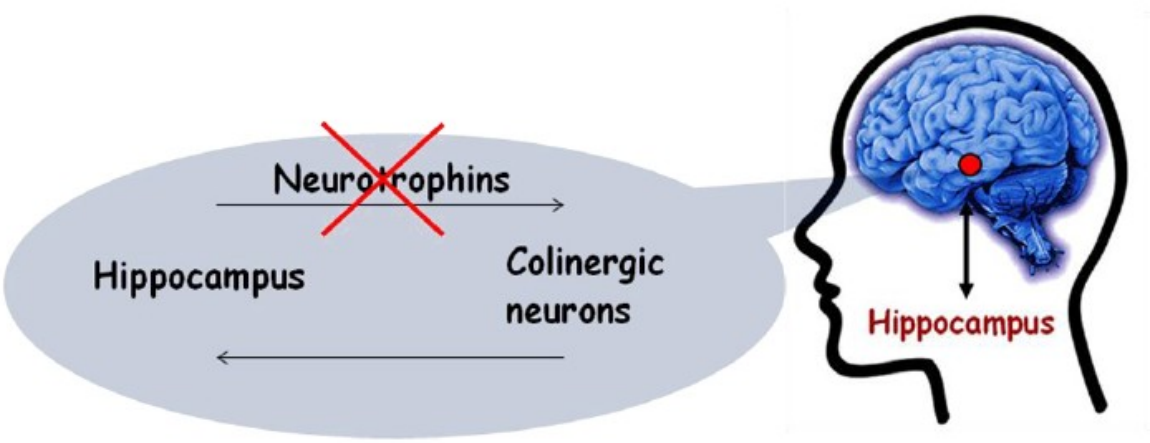

Figure 4. *The Neurotrophins hypothesis of Alzheimer's Disease suggests that an alteration in NFG/BDNF signaling is related with the etiology/exacerbation of neurodegenerative disease.*

It is worth noting that hippocampus is innervated by BFCNs. In turn, BFCNs are supplied with NGF by hippocampal neurons; namely NGF is taken up by the terminals of cholinergic neurons and retrogradely transported back to the cell bodies in the basal forebrain. It is accepted that NGF is essential to maintain the phenotype and the synaptic activity of BFCNs, as well as to prevent their age-related atrophy.[104] The degeneration and atrophy of BFCNs has been linked with memory impairment and cognitive dysfunction in AD. [105-106]

Impaired axonal transport has been suggested to decrease the level of NGF in BFCNs during the progression of AD, [107] although this model is not completely accepted. [108] Moreover, in support of the neurotrophins hypothesis of AD progression, a marked change in the expression levels of the neurotrophins receptors occurs during ageing, and TrkA expression has been reported to be downregulated in the AD parietal cortex and BFCNs. [109-114] At the same time, there is a progressive upregulation of p75 levels, [115] that indicates a disequilibrium in the TrkA/p75 ratio and consequently in the NGF-mediated signaling. This could play a relevant role in the etiology of AD [110-111,116]. Deficits in TrkA receptor phosphorylation signaling contribute to age-related default in long-term potentiation (LTP)

[117-119], one of the major cellular mechanisms involved in learning and memory (see paragraph 1.1.1). This can be likely the molecular mechanism for memory impairment in AD.

Contrasting NGF levels have been reported in AD. [111,120-123] Nonetheless, pro-NGF levels double in frontal and occipital cortex and in hippocampus of AD patients, [124] suggesting that defective cleavage of pro-NGF to mature NGF may occur in this disease. [49,125] Pro-NGF is, indeed, the predominant form of NGF in the brain of AD patients and increases with the progression of disease. [124,126] Intracerebral administration of pro-NGF has been found to causes AD-like learning impairments in mice, supporting the above mentioned relationship. [127] Intriguingly, intrahippocampal injection of Aβ oligomers elicits the upregulation of pro-NGF in rat. [128] The unbalance of NGF processing can therefore be suggested as the onset condition of AD neurodegeneration, but direct, still unexplored, effects of pro-NGF cannot be excluded.

More recently, BDNF is also emerging as a crucial player in the CNS. Its role is highlighted by the fact that hippocampus is the brain area with the highest BDNF expression. The BDNF mRNA expression is 50-fold higher than that of NGF. [129] With few exceptions, [130] the scientific community agrees that the reduced brain level of BDNF and its mRNA could contribute to the progressive atrophy and death of specific neuronal populations in the AD-affected brain. [99,122-123,131] Analogously to NGF, BDNF exists in the brain also as pro-BDNF but, differently from pro-NGF, pro-BDNF level decreases in AD brain. The reduced level of BDNF can, therefore, be correlated with the significant downregulation of the precursor. [132-133] A reduction of both pro-BDNF and mature BDNF levels has been linked with loss of cognitive functions. [134] The study of correlations of NGF processing with AD, or other age-related neurodegenerative diseases could open new perspectives for the particularly demanding challenge of definite therapeutic interventions.

Finally, an intriguing cross-talk between the "amyloid hypotheses" and the "NGF hypotheses" of AD is recently emerging. It has been found that an interruption of NGF signaling can activate the amyloidogenic pathway, inducing cell death through a not fully understood mechanism. [135] The block of NGF signaling has been shown to up-regulate APP, β- and γ-secretases, with deposition increase of amyloid plaques. [136] Similarly,

transgenic mice expressing recombinant antibodies able to neutralize up to 50% of endogenous NGF have been reported to develop AD-like features. [137] In addition, these AD-like features have been shown to be due to an imbalance of the TrkA/p75 ratio and signaling. [116] Indeed, the APP processing is differentially regulated by TrkA and p75 receptors, which reduce and activate the cleavage of APP, respectively.[138]

Further interest in the role of these receptors in the etiology of AD can be attributed to the finding that Aβ can activate TrkA [139] as well as p75 [140] receptors and a downstream cascade which leads to neuronal death. Aβ(1-42) doubles the level of p75 in SH-SY5Y human neuroblastoma cells and in the hippocampus of AD-transgenic mice[141], also inducing significant cell death in hippocampal neurons, whereas the same effect has not been observed in p75-deficient neurons. [142] A dose-dependent effect of Aβ has also been observed: i) high concentrations of Aβ determine apoptosis (10-100 μM) [143] or prevent NGF-induced activation of NF-kappaB (800nM) [144] ii) low concentrations of Aβ (25 nM), in contrast, have been reported to be pro-survival, inducing cellular effects similar to those triggered by NGF. [143] In addition, low levels of Aβ upregulate the BDNF mRNA at short times (3-5 h) but dramatically reduce it at longer times (24 or 48 h). One could speculate that aggregation of Aβ occurs [145] and cytotoxic activity of soluble oligomers of Aβ(1-42) will take place. [115]

1.2.4 Neurotrophins-based therapy and smart drug delivery

The results presented in the previous paragraph suggest the possibility to develop a neurotrophins-based therapy for neurological disease. However, there are some hurdles in the use of neurotrophins as drugs, due to their poor pharmacological properties, such as the low blood–brain barrier permeability and a wide range of adverse side effects, due to the activation of p75 receptor.[120,146-147]

Considerable efforts have been made to obtain agents that can mimic or antagonize the NGF activities, with the aim:

i) to cross the Blood-Brain Barrier and achieve adequate concentrations in the target regions of the brain

ii) to elicit certain but not necessarily all the signaling cascades triggered by NGF

Intracerebral injections of NGF, implantation of viral vectors and genetically modified cells/devices able to release NGF are invasive methodologies to be applicable. [148-151] On the other hand, intranasal delivery and topical application of NGF on the ocular surface are non-invasive approaches that need further investigations. [120] Micro- and nano-particles made of different polymeric materials, able to storage and release NGF, have been developed. [152-156] The encapsulation of NGF into liposomes has been reported to prevent enzymatic degradation, whereas the functionalization of the liposome is a good strategy to promote its permeability across the blood-brain barrier. [157]

Innovative strategies for immobilization and release of biomolecules are highly challenging. One intriguing approach has been recently proposed for ligand cell targeting. It is based on the multifunctional character of a nanoplatform, so-called ‘protocell’, consisting of hybrid materials, made of silica nanoparticles wrapped by fluid-phase lipid bilayers. [158-159] Indeed, lipid bilayers are able to mimic cellular membranes, due to their electric charge, thickness, and permeability. Moreover, they offer the advantage to anchor ligand molecules in a not rigid manner, representing a breakthrough of traditional rigid gel-phase liposome vesicle.[160] The non-covalent bond between ligand and drug carrier is a

fundamental pre-requisite to decrease the overall concentration of ligands – thus avoiding adverse biochemical signaling to the cell - but, at the same time, to allow a local enhancement of ligand in proximity of specific cells receptors. [158-159] Also, it has to be mentioned that the overall ligand concentration is only one of the crucial parameters for an efficient drug activity. A suitable ligand-receptors interaction on the target cell is critically driven by local concentration gradients as well as conformational states.

Some of the methodologies described can potentially guide the neurotrophins across the Blood-Brain Barrier. However, encapsulated or not, neurotrophins elicits both TrkA and p75 receptors, the latter responsible of side effects. To overcome this second issue, considerable efforts have turned to design small molecules able to interact selectively with the TrkA receptor mimicking or antagonizing the NGF activities. [146-147] To this aim, important clues derive from the comparison of the crystal structures of neurotrophins [45,161-169]

The Neurotrophins-Trkr interface consists of two patches: the first involves the β-sheet of the core of the homodimeric active form; the second appear to be formed by discontinuous stretches of amino acid residues distributed throughout the primary sequence of the molecule. [45] Comparing the structure of the neurotrophins with their cognate Trks receptor, it has been observed that the former domain constitute a conserved binding motif for all neurotrophins family member.[45,162-163] Strikingly, the latter contain residues not conserved among the neurotrophins family, suggesting that these patch can guide the specificity for a peculiar Trk receptor.

Among the non conserved residues, many biochemical studies have been focused on the N-terminus tail, unraveling its importance.

It has been reported that a truncated form of NGF, which lacks the first 9 residues of NGF, displayed more than 300-fold lower affinity for TrkA than the whole NGF, and 50-fold lower capacity in eliciting TrkA phosphorylation, without affecting folding, stability or conformation of the molecule.[170-171] Among the residues of the N-terminal domain, the His-4 has been reported to be critical. Diethyl pyrocarbonate modification of His-4 and His-8 in a NGF double mutant abolished neuritogenesis, binding to both receptors, and

phosphorylation of TrkA in PC12 cells. NGF(H4D) mutant showed a 1000-fold lower binding affinity for TrkA (compared with wild type NGF), at least 10-fold less efficacy in the TrkA autophosphorylation, and 30-fold less capacity in PC12 cell differentiation.[172-173]

These studies have been confirmed by computational calculations, which identified the residues lying at the ligand-receptor interface. These include His4, Glu11, Trp 21, Arg 59, and Arg103 of NGF, and Glu 295, Phe 303, Arg347, Asn 349, and Gln 350. [174-175] In particular, the His 4 and Glu 11 residues provide highly persistent H-bond interactions with the receptor, as well as Ile 6 and Phe 7 residues stabilize the binding of the N-term of NGF to TrkA through hydrophobic interactions. [174-175]

1.3 Metals and Memory

As previously mentioned, the brain is an organ with astonishing complexity and unique chemical composition. The role of s-block metals (Na^+, K^+, Ca^{2+}) in the brain has been studied in deep. Less is known about the role of transition metal ions. Actually, although they are often called "trace metals", their concentration (above all copper and zinc) is 10000-fold higher than common neurotransmitters and neuropeptides. The abundance in the synaptic cleft provide a clue of their functional role in the brain and, perhaps, in memory consolidation (Fig. 5).

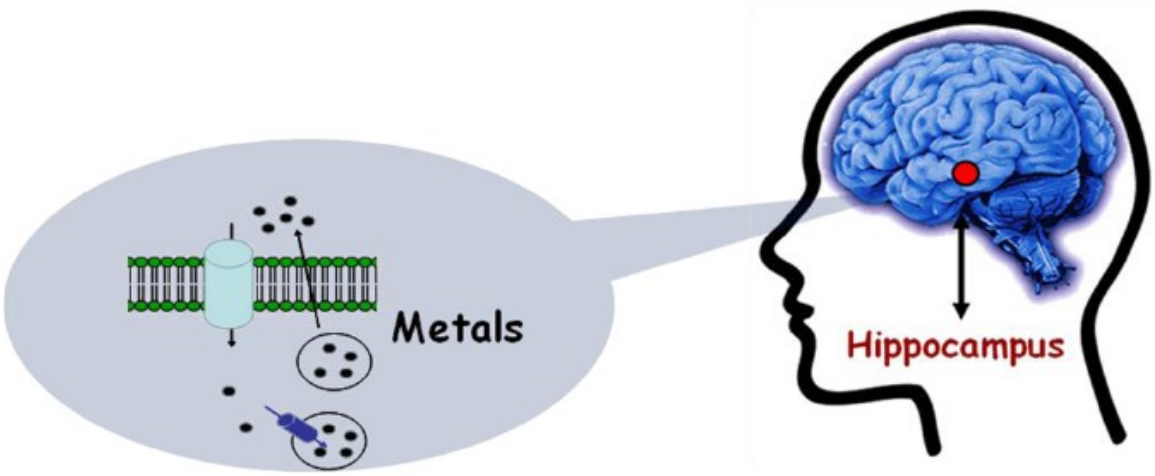

Figure 5. *Metals in the brain. Emerging evidences suggest that transition metal ions are released in the synaptic cleft and might take part in neuromodulation/neurotransmission.*

1.3.1 Metals and Metallostasis

Transition metal ions are essential catalytic and/or structural elements of many enzymes, transcription factors and/or other regulator agents, as well as emerging modulators if neuronal functions.[176] However, neurons (as well as all the other cells) need to maintain metal ions within a narrow range of concentrations that determine health. [177] In respect to

the optimum of concentration, lower and higher values are often detrimental to cells life. Thus, a highly orchestrated and regulated mechanism is required to guarantee metallostasis (metal ions homeostasis). [178]

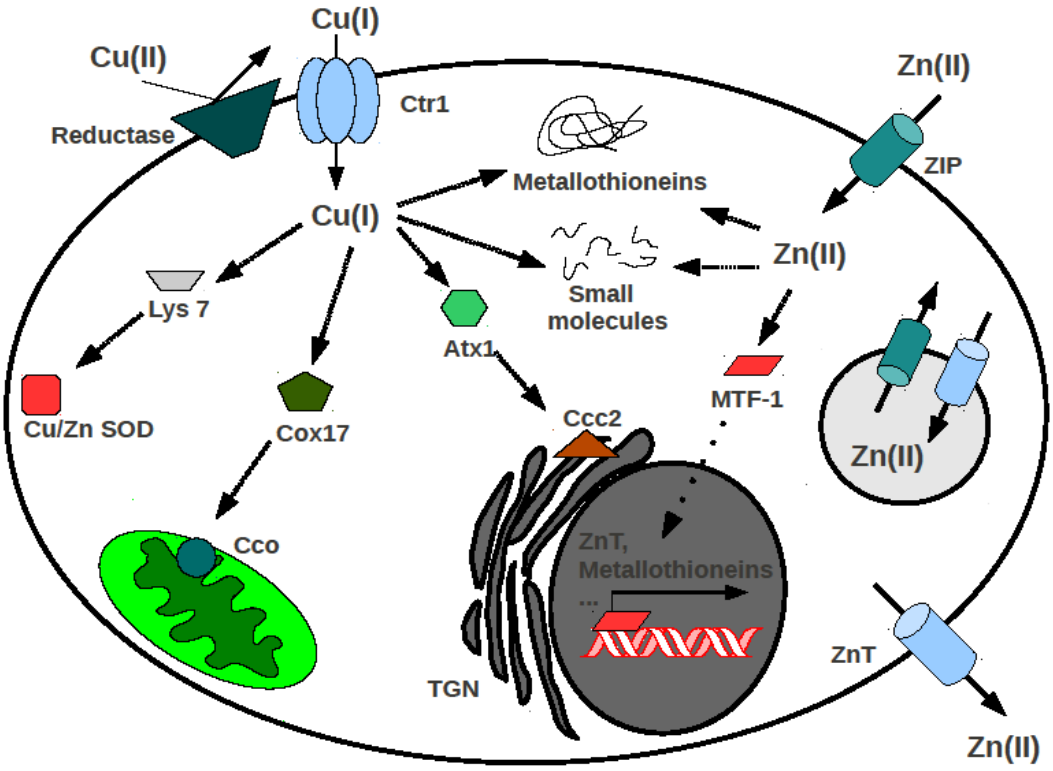

Figure 6. *Schematic model of copper and zinc homeostasis. Extracellular Cu^{2+} is reduced by plasma membrane reductases, then Cu^{+} enters the cell via Ctr1 (copper transporter-1). Cu^{+} can be funneled to its ultimate intracellular destinations through specific protein-based pathways. Lys7 is the copper metallochaperone for Cu/Zn superoxide dismutase (Cu/Zn SOD), Cox17 loads Cu^{+} into the cytochrome c oxidase (Cco), Atx1 shuttles Cu^{+} to the Ccc2 P-type ATPase transporter localized on post-Golgi network (TGN). ZIP proteins (zrt/irt-like proteins) are influx transporters that mediate Zn^{2+} uptake from the extracellular environment, or intracellular vesicles, into the cytoplasm. Otherwise, ZnT carriers (zinc transporter protein) are efflux transporter able to reduce the cytoplasmatic Zn by promoting zinc movement directly out the cell or into intracellular compartment. Metal transcription factor-1 (MTF-1) binds Zn^{2+} and translocates to the nucleus to upregulate metallostasis-involved proteins. Besides to be shuttled to various proteins and subcellular organelles, zinc as well as copper ions are buffered by metallothioneins and small molecules (e.g glutathione, ascorbic acid).[from [179]]*

Through a complex network of molecular interactions, metallostasis acts to balance the intracellular metal uptake, trafficking, storage, speciation and signaling (Fig.6). These intricate biochemical pathways allow the storage and delivery of metals to their proteic partner. Also, the strict balance of metallostasis is controlled by metals themselves, through transcription factors and post-transcriptional regulatory mechanisms.

A picture of zinc(II) and copper(II) ion cellular homeostasis is summarized in the following.

The ZnT (Zinc Transporter) [180-181] and the ZIP (Zinc regulated metal transporter, Iron-regulated metal transporter-like protein) families,[182] including 10 and 15 members, respectively, consist of multipass transmembrane proteins involved in zinc(II) ion homeostasis. [183] Zip proteins are influx transporters that mediate Zn^{2+} uptake from the extracellular environment, or intracellular vesicles, into the cytoplasm. ZnT carriers are efflux transporters that reduce the cytoplasmatic Zn^{2+} by promoting metal ion movement directly out the cell or into intracellular compartment.

It is worth to note that both ZnTs and Zips exhibit unique tissue- and subcellular- specific expression. For instance, ZnT1 is a cellular zinc exporter and is predominantly expressed on the plasma membrane of cells and seems to play a key role in early embryonic development and a protective role in the nervous system. [184]

ZnT3 transporter is particularly abundant in regions that have high levels of labile, chelatable Zn^{2+} and it has been suggested that it accumulates zinc in synaptic vesicles and it has a neuromodulatory role in synaptic transmission. It has been linked to degenerative neurological diseases such as Alzheimer's.[185-186]

Once inside the cell, besides to be shuttled to various subcellular organelles, zinc ions are bound by metallothioneins (MTs), a class of cystein-rich cytosolic protein with high affinity for metals. Although a single essential function of MT has not been demonstrated , MTs have been proposed as playing an important role in controlling whole body zinc metabolism.[187]

The expression of several genes, involved in zinc metabolism, is regulated by zinc itself. Indeed, zinc can be bound by specific transcription factor, such us the metal response element-binding transcription factor-1 (MTF-1). MTF-1, after the binding with zinc, translocates to the nucleus to bind the DNA in the metal response element (MRE), activating the expression of genes as ZnT-1, Metallothioneins and gamma glutamylcysteine synthetase (an enzyme that is essential for glutathione synthesis).[188-190]

The uptake of copper(II) ion has been well studied in yeast and, more recently, in human.[191] Cu^{+} is transported across the plasma membrane by the high-affinity transporter Ctr1 (Copper transporter 1), after to be reduced by plasma membrane reductases, then Cu^{+} is buffered by metallothioneins or, through a variety of protein-based pathways, delivered by specific copper chaperone proteins to the mitochondria (for insertion into cytochrome c oxidase), to cytosolic enzymes (e.g Cu/Zn superoxide dismutase) and to post Golgi compartments (Fig. 6). [192-193]

1.3.2 Zinc and Memory

Zinc is the second most abundant transition metal in the body. The brain is the organ with the highest zinc concentration, but it is not homogeneously distributed and it is mostly present in the hippocampus, amygdala and neocortex.[194]

Over 90% of the Zn^{2+} found in the brain and the body have been classified as static, playing structural roles in transcription factors and enzyme, whereas histochemically reactive zinc, revealed by Timm's sulfide-silver staining method, represent the other 10% of zinc(II) ions. The latter predominantly exists in presynaptic vesicles and increasing evidences have suggested it plays a role in neuromodulation and synaptic plasticity.[195-197]

In the extracellular space, the basal Zn^{2+} concentrations have been estimated to be very low (10^{-8} M) [198] though Zn^{2+} concentration has been reported to increase in both extracellular and intracellular compartments by excitation of zincergic neurons. [199] Studies with live hippocampal slices have supported the idea that Zn^{2+} is co-released with glutamate from

zincergic presynaptic mossy fiber boutons,[200-202] Strikingly, it has been measured concentration values that are up to 10000-fold higher than common organic neurotransmitters. [194-195,203] For instance, Zn^{2+} concentrations can reach up to 300 μM in the mossy fiber boutons of hippocampal neurons that extend from the dentate gyrus to neurons in the CA3 fields.[185,195-196] Similar input-output systems in the cortex, amygdala, and olfactory bulb also require such "zinc containing neurons". [194-195] From a cognitive perspective, the abundance of vesicular zinc in synapses of the cortex, hippocampus, and amygdala suggests a possible role in learning and memory.

However, despite indications of synaptic Zn^{2+} release by many laboratories, the precise roles for these mobile zinc stores remain controversial. [204]

Many studies have been focused on the effect of zinc on Long-Term Potentiation [205-206] as well on the interactions between Zn^{2+} and NMDA receptors (NMDAR), shedding light on the potential role(s) for synaptic Zn^{2+}. Zinc is a known antagonist of NMDARs, thus it has been proposed that Zn^{2+} can modulate the activity of this receptor, shaping the NMDAR response at these synapses. NMDARs, in turn, can reduce the neurotoxicity of excess Zn^{2+} stores by blocking their entry into postsynaptic dendrites. [207]

Among multiple pathways, AMPA and NMDA receptors, as well voltage-dependent calcium channels (VDCC) seems the channels involved in zinc-mediated synaptic activities.[208-211] Indeed, it is worth to note that Zn^{2+} released into the synaptic cleft has the unique ability to potentially enter the postsynaptic neuron, a phenomenon not observed with other neurotransmitters or neuromodulators. However, it is unknown whether the moderate increase in Zn^{2+} in the cytosolic compartment affects memory processing in the hippocampus.[212] Also, no organelle-based storage pool for labile intracellular Zn^{2+} has been identified, though metallothioneins have been proposed to buffer the zinc content. [213]

Although it is likely that many zinc-binding proteins and transporters act in concert to modulate transient changes in cytosolic zinc ion concentration, zinc uptake into synaptic vesicles requires the zinc transporter protein ZnT-3.

Supporting the role of Zn^{2+} signal in learning and memory, it has been reported that ZnT-3 KO mice exhibit age-dependent deficits in learning and memory. Intriguingly, these deficits have been linked with reduced activation of the Erk1/2 MAPK in hippocampal mossy fiber terminals, as well as of the BDNF pathway.[214-216]

1.3.3 Copper and Memory

Copper is the third-most abundant transition metal in the brain, after zinc and iron. The copper concentration in the human brain has been estimated to be on the order of 0,1 mM. However, copper is distributed unevenly within brain tissue.[217-219] Experiments in rats showed that copper is particularly abundant in the medial geniculate nucleus (the center processing visual information), superior colliculus (a component of the midbrain associated with motor functions) and periaqueductal grey (the neural region responsible for physiological responses to stress and panic). [220-222] Copper concentration is also high in the lateral amygdala (groups of nuclei involved in memory and emotional reactions) and in the dorsomedial aspect of the diencephalon (the part of the forebrain containing thalamus, hypothalamus and the posterior portion of the pituitary gland). Strikingly, copper distribution within the brain varies between species. For example, human hippocampus has the highest copper concentration compared to other regions, providing clue of a higher metabolic demands or a specific – still unraveled- role of this metal in this brain region. What is more, copper levels change during brain development, increasing with age. [223-224] Rat neonatal brain has low copper levels, which rapidly increase during the first two weeks after birth, especially between the postnatal day 7 and 14, when the striatum, thalamus, and superior colliculus show marked and preferential accumulation of copper. Increase in copper concentration have been also observed in patients with neurological symptoms related to dementia; in Alzheimer's-like dementia copper has been reported to be 2-fold higher than in age matched controls[225-226]

The next important frontier of copper neurobiology is to provide mechanistic understanding of copper metabolism in the central nervous system and its regulation in different cell types as well as the entire brain.

It is been proposed a direct link between copper homeostasis and neuronal activation in central nervous system. Indeed, postsynaptic NMDA neuritis have been recently reported to release copper(II) ions upon NMDA activation. [227] It has been observed a mechanism that correlates Ca^{2+} entry (through NMDA receptor) and ATPase 7A translocation toward the synaptic cleft. Thus, after NMDA receptor activation, copper (II) ions are releases in the synaptic cleft, where copper(II) can act as a switch, blocking NMDA receptor and exerting a protective action against NMDA-mediated excitotoxicity and abnormal influx of calcium.[228] In this context, lack of secretable copper in Menke's disease might results in a decreased ability of the neuron to modulate NMDA receptor activation, suggesting a role for Menkes ATPase in memory and learning.[227-228]

It has also been reported that copper ions are able to activate the phosphoinositide 3-kinase (PI3K)/Akt signaling cascade, a biochemical pathway known to be antiapoptotic and cytoprotective, deeply involved in the regulation of gene expression and, intriguingly, overlapping with neurotrophins signaling. [51,229-232] Exposure to copper(II) salts elicits an activation of Akt in various cell types. [229-232] Akt has a key role in cell signaling, integrating incoming messages about cell growth, differentiation, apoptosis and metabolism. The PI3K/Akt cascade, in addition to its role in regulating apoptosis and proliferation, is a major mediator in insulin signaling. This pathway act through the involvement of Glycogen synthase kinase-3 (GSK-3), an *in vivo* substrates of Akt phosphorylated upon exposure of cells to metals, as well as the FoxO-family transcription factors. [233]

Intriguingly, a similar effect on the activation of Akt has been observed in several cell types exposed to Zn^{2+}, but this metal elicits the same effect due to copper with approximately 10-fold higher dose, perhaps due to a different strength of the complex formed.

Many researchers are investigating the use of ionophores/metal complexes able to modulate this pathway, as well regulate the metal ion homeostasis. [234] For instance, it has been proposed that the mechanism of action of clioquinol-copper complexes is through the activation of the PI3K/Akt pathway and subsequent phosphorylation of JNK and ERK1/2.[230,235]

1.3.4 Alteration of Metallostasis and Neurodegeneration

Homeostasis of metals needs to be controlled spatiotemporally for proper brain functions, and their dyshomeostasis is associated with neurological diseases. [199]

As, previously mentioned (see paragraph 1.3.1), modulators of metallostasis are metal chaperones, metal transporters, metalloproteins, small molecules and metal transcription factors. [194,236] All together, they can partially correct metal ion dys-homeostasis (e.g., sequestering the metal ion in cytoplasmic vesicles or increasing its efflux/influx) that contributes to a broad range of human diseases, mostly linked to ageing. [237] Normal ageing and, particularly neurodegenerative diseases, have been reported to be also characterized by metal homeostatic machinery alteration, although it is not well understood why this occurs. [238] This represents one of the major challenges in understanding the molecular basis of neurodegeneration.

Indeed, the AD metal hypothesis that involves transition metal ions as prominent factors has been proposed in the development and exacerbation of Neurodegeneration. [239] This hypothesis emerged from the observation that metal ions are particularly abundant in AD plaques. [240] The binding of zinc(II) and copper(II) to Aβ can induce changes in the secondary structure, [241] which in turn can favor the aggregation of amyloidogenic peptide in vitro,[242] with pathological consequences such as oxidative stress in AD brains. [243] Otherwise, metal chelators have been found to be able to dissolve Aβ aggregates in AD post-mortem brains. [244] An early diagnosis of AD can be particularly helpful for more efficacious therapeutic approaches. Squitti et al have reported that the serum copper(II) level, not bound to ceruloplasmin, is higher in AD patients, an observation that could be indicative about the pathophysiology of the AD brain condition, [245-246] leading to the hypothesis that an association between copper metabolism deregulation and unfavorable evolution of Alzheimer's disease occurs. [247] This approach could not be reliable because the alteration of metallostasis is reflected in the intricate network of metal transporters and chaperones, [178] which have been found to be deregulated in AD.

However, there are few evidences of the molecular mechanisms involved in metallostasis and there is the lack of knowledge of the chemical species involved in metal

dys/homeostasis, e.g. if the deregulated species in pathologic condition are metal-transporters, -chaperones, or -transcription factors.

Of note, several zinc(II) ion transporters have been linked with protein aggregation, amyloid plaque formation, and the early progression of Alzheimer disease. [248-249] Both ZnTs and ZIPs exhibit unique tissue-specific expression. ZnT3, the main zinc transporter in the brain, [250] accumulates zinc in synaptic vesicles, and it has been suggested to play a neuromodulatory role in synaptic transmission as well as in neurodegenerative diseases such as AD. [185-186] This is indeed strongly supported by the evidence that double transgenic hAPP(+)/ZnT3-null mice display reduced levels of synaptic zinc(II) ion, and, in turn, a reduced plaque formation.[251] At the same time, the role of Cu^{+} chaperone ATPase7b has been correlated with the AD pathology. In fact, a genetic experiment has been carried out to investigate how this metal ion might modulate Aβ-dependent pathologies in vivo; the transgenic (Tg) CRND8 line of TgAPP mice in conjunction with a mutant allele of the CuATPase7b copper transporter showed a Cu^{+} accumulation, exhibiting a reduced number of amyloid plaques and diminished plasma Aβ levels. [252]

1.4 Metals and Neurotrophins

The above findings are drawing a new perspective in which metallostasis seems to play fundamental roles in neuromodulation/neurotrasmission. This is particularly relevant for glutamatergic synapses in the hippocampus, the brain area involved in learning and memory and the place of early occurrence of Aβ amyloid plaques, as well brain areas in which the highest concentration of Zn^{2+} and Cu^{2+} have been measured and where and neurotrophins exert their activity (Fig.7).

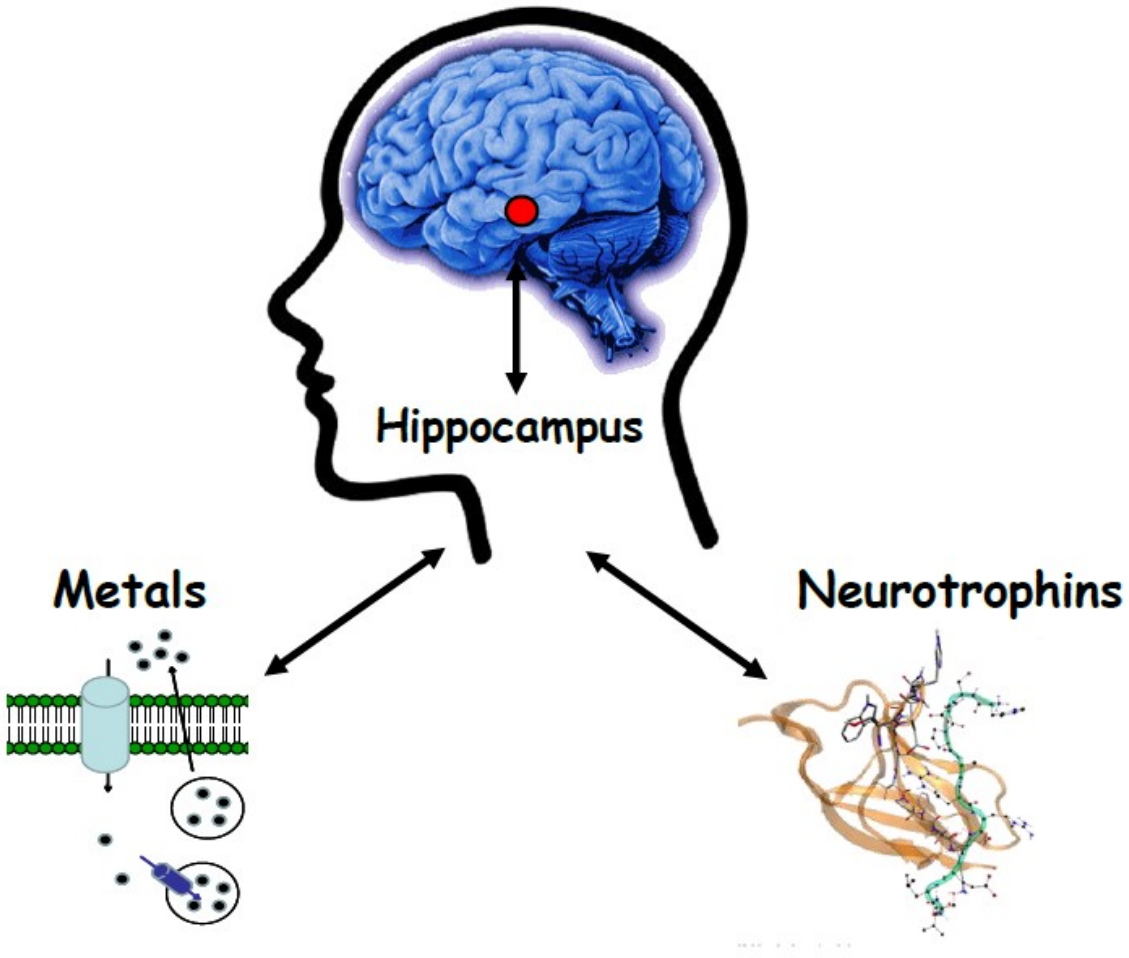

Figure 7. *Metal ions can modulate the activities of the neurotrophins, likely through conformational changes, and/or indirectly by activating their downstream signaling in a neurotrophin-independent mode.*

Four neutrophic factors, BDNF, CNTF (Ciliary neurotrophic factor), PEDF (Pigment epithelium-derived factor), GDNF (Glial cell-derived neurotrophic factor), have been reported to increase the intracellular Zn^{2+} level in RPE (retinal pigment epithelium) cells, modulating the expression of zinc(II) transporters which increase metal ion uptake. [253] The expression of the influx transporter ZIP2 is regulated by all four neurotrophic factors, whereas other zinc(II) transporters are regulated in a selective mode. In particular, CNTF and PEDF decrease the expression of ZIP4 and ZIP14, CNTF and GDNF decrease ZnT6, whereas PEDF and GDNF promote the expression of ZnT2, and only PEDF stimulates the expression of ZnT. [253] Although these data are referred to the regulation of zinc(II) transporters in retinal cells, one could reasonably speculate that similar mechanisms control the metal homeostasis in other cells.

On the other hand, it has been reported that metal ions affect neurotrophin activities. High concentrations of Zn^{2+} and Cu^{2+} have been reported to inhibit the effects of NGF as well as BDNF, NT-3 and NT-4/5 in vitro. Namely, these metal ions have been shown: i) to block the NGF-mediated neurite outgrowth in chick dorsal root ganglia (DRG); ii) to decrease the cell viability: [254] and iii) to counteract the NGF-mediated protection from oxidative stress in pheochromocytoma (PC12) cells. [255] These effects have been attributed to metal-induced conformational changes, which can alter the NGF binding to TrkA receptor, and, as a consequence, the activation of its downstream pathways. [256] Otherwise, recent contributions have singled out the presence of Zn^{2+} as a key factor for the protective activity of NGF, [257] showing that zinc(II) ion loading on native NGF increases its ability to trigger TF1 cell proliferation and mediates PC12 cell survival. Zinc(II) and copper(II) ions have also been found to antagonize p75-driven apoptosis in chick neural retina. [258] Previous studies demonstrated that NGF-mediated apoptosis, due to the p75 receptor pathway, occurs in the normal development of chick neural retina [58,259] In these cells, p75 is the only receptor available to interact with NGF, as TrkA has not been detected with chemical cross-linking and immunoprecipitation. [258] Interestingly, 100 μM of zinc(II) or copper(II) ions, but not other cations, block the NGF binding to p75, attenuating its pro-apoptotic signaling cascade in chick embryonic cell cultures. Therefore, metal ions have been proposed to cause an apoptotic outcome, avoiding the activation of the TrkA mediated signal and, at the same time, they show an anti apoptotic effect, interrupting p75

cascades. [254-256,258,260]

Until recently, Trk receptors have been reported to activate only by the binding of a specific neurotrophin, whereas zinc(II) ion transactivates TrkB. [261] This is characterized by a ligand-independent and indirect activation of a receptor. In response to neural activity, endogenous zinc stored in secretory vesicles has been shown to be released at the mossy fiber CA3 pyramidal synapses, which are the most Zn^{2+} enriched in the brain. Herein, zinc(II) ions are able to transactivate TrkB in vivo, with a mechanism distinct from BDNF-induced activation. This activation process has also been observed in BDNF null mutant (−/−) neurons, namely those that do not express BDNF. [261] Zinc(II) ions act as trans-synaptic messengers. They enter postsynaptic neurons through voltage-gated calcium channel (VGCCs) and N-Methyl- D-Aspartate receptor (NMDA) receptors. Once inside postsynaptic terminals, Zn^{2+} activates Src family kinase (SFK), then TrkB receptor is activated through Src kinase-mediated phosphorylation at specific tyrosine residues. The activation of TrkB in a neurotrophin-independent manner seems to play a role in long-term potentiation (LTP). Indeed, exogenous zinc(II) ion has been found to potentiate the efficacy of the hippocampal mossy fiber -CA3 pyramid synapse, whereas the LTP is impaired chelating zinc by mean of EDTA. [262] Moreover, the treatment with BDNF in the presence of Zn^{2+} (10-300 μM) has been reported to slightly inhibit TrkB phosphorylation. [263] This has been correlated to Zn^{2+} induction of metalloproteinases (MMPs) activity and pro-BDNF processing. Similar results have been reported on the Cu^{2+} ability to activate TrkB in a metalloproteinase-assisted manner. [264] Thus, $Zn^{2+}$and Cu^{2+} are able to decrease the intracellular level of pro-BDNF and to increase the level of pro- and mature BDNF in the cell culture medium.

Levels of BDNF and NGF have been shown to decrease in zinc(II) deficient mice, [265] hence zinc(II) dietary supplementation seems to replenish the NGF [266] as well as the BDNF level. [267] Moreover, chronic treatments with zinc(II) ion induced the upregulation of BDNF mRNA in the cortex and hippocampus, [268] strongly suggesting a more direct role of this metal ion in the neurotrophins expression.

The neuronal survival and differentiation during NGF signal transduction has been recently correlated with copper(II) ion, in particular it has been reported that NGF is able to

increase the cellular level of this metal ion that is required for optimum neurite outgrowth of PC12, [269] highlighting the role of this biometal in signal transduction.

1.4.1 Binding details of copper(II) and zinc(II) ions with neurotrophins

The above findings suggest that zinc(II) and copper(II) ions may be required in different but not yet fully understood aspects of neurotrophins activities that mediate neuronal differentiation and protection. This stresses the need for major insight into the molecular details of the interaction of Cu^{2+} and Zn^{2+} with neurotrophins, shedding light on the intricate mechanisms involving biometals.

Pattison and Dunn have provided the first proof of the direct interaction between metal ions and NGF, [270] showing that zinc(II) ion is specifically bound to native 7S NGF (e.g., an oligomeric protein composed of 5 non-covalently linked subunits: 2α, 1β, 2γ). The active NGF has also been found to bind zinc(II) ions in the native protein, with an uncommon Zn^{2+} to NGF molar ratio of 1:14.6 (determined by means of flameless atomic absorption spectroscopy measurements). This presence of Zn^{2+} in the native molecule contributes to significant conformational changes and increased biological activity of the protein.[257] It is interesting to underline the high occurrence of histidine residues in TrkA (14 His) and in NGF (4His), facing the extracellular space (Fig. 8 and Fig 9). Of great interest is the close proximity of negatively charged residues, such as Asp and Glu, to the His residues (Fig 9). These are structural requisites for the binding of metal ions, as zinc(II) and copper(II) ions.

The crystal structure of NGF reveals potential metal ion binding sites, with the involvement of His84 and Asp105. [161] According to Holland et al. a knot motif confers structural stability and maintains the position of these two residues, preserving the metal ion binding site.[161,260]

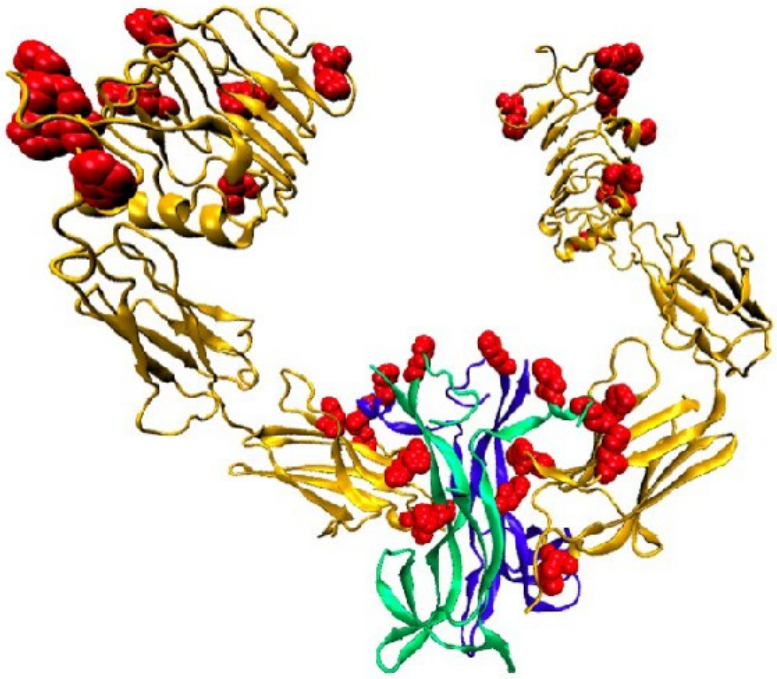

Figure 8. *Representation of the extracellular domain of the NGF/TrkA dimer. NGF chains are shown in green and blue, D1-D5 TrkA sub-units are shown in yellow. His residues are shown in red according to the vdw radii. [From [179]]*

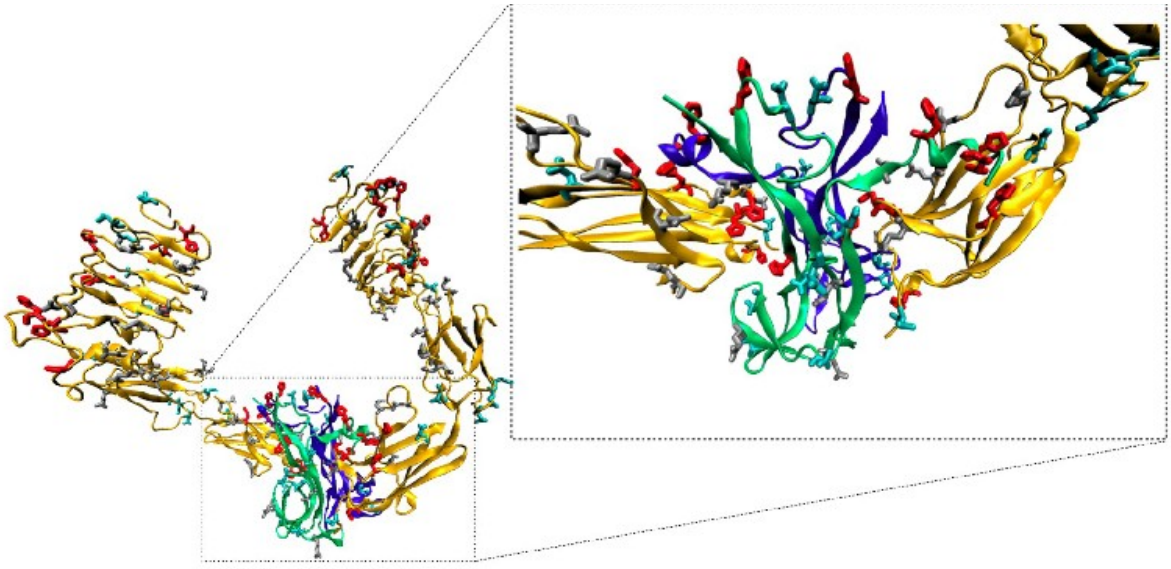

Figure 9. *Representation of the extracellular domain of the NGF/TrkA dimer. The negative charged residues, Asp and Glu, are shown in cyan and gray respectively. Both of them are close to His residues, shown in red. [From [179]]*

To the best of our knowledge, the coordination features of metal-ion complexes with NGF have been determined only by theoretical methods. [255-256,271] The computational results suggested a model in which Zn^{2+} alters the conformation of NGF by forming a pentacoordinate complex. This metal ion has been found to bind to the imidazole nitrogen atoms of His4 and His8 of one monomer and to the imidazole nitrogen atom of His84 and both oxygen atoms of Asp105 of the other unit of the NGF dimer; [255-256] the same coordination environment has been proposed for Cu^{2+}. [271] As a consequence of the conformational change resulting from metal chelation, no cross-link between primary amino groups of Ser1 of a NGF unit and Lys115 of another unit takes place, unlike for the active dimeric form of NGF in the absence of metal ions. Thus, it has been suggested that the binding of metals is responsible for the alteration of NGF conformation and, in turn, for the inhibition of its biological activities. [256] Also, computational approaches have been carried out to investigate the interaction of NGF with other transition metal ions. [260,271] It is interesting to note that copper(II) ion has been reported to be the only metal ion able to bind the imidazole nitrogen stronger than a proton at pH values higher than 6-6,5. At lower pH values, the imidazole is unable to coordinate Cu^{2+}. [271] Moreover, it has been proposed that NGF might interact with its receptors as a complex with zinc(II) ion.

2. Aims of the work

On the basis of the literature data above reported, we have investigated the issue of the interactions of the metal ions with the neurotrophins.

To the best of our knowledge, the coordination features of metal ions complexes with neurotrophins have been determined only by theoretical methods and only for NGF. No experimental data inherent the coordination features been reported, neither one of the hypotheses according to which Zn^{2+} and Cu^{2+} could have different binding environments, or Ser1 α-amino group could be involved in coordination have been supported.

Crystallographic, biochemical and computational studies converge to suggest that the N-terminal residues are crucial for specific activities of the neurotrophins. However, nobody has tested if just this small sequence is able to mimic the whole protein or at least some of its biochemical signaling. Among them, the activation of transcription factors is particularly attractive, because they are involved in gene expression but also in memory consolidation.

The use of neurotrophins in the early stages of neurodegenerative diseases has gained attention. However, there are limits to such therapy, e.g. insufficient permeability of the blood-brain barrier and activation of receptors that trigger adverse side effects. The use of peptidomimetic combined with appropriate systems that guarantee their delivery might allow to overcome these restrictions.

Briefly, the work has been summarized in sub-aims:

1) Synthesis of the peptide fragment encompassing the sequence 1-14 of the human NGF amino-terminal domain (NGF(1-14)) , blocked at the C-terminus, and characterization of its Cu^{2+} and Zn^{2+} complexes by means of potentiometric and spectroscopic (UV-vis, CD, NMR and EPR) techniques. N-terminus acetylated form of NGF(1-14) has also investigated to evaluate the involvement of Ser1 α-amino group in the metal ions coordination. The functional interaction of Cu^{2+} and Zn^{2+} ions with NGF peptides and with

the whole NGF protein has been tested measuring the effects on the proliferation rate of SHSY5Y neuroblastoma cell line culture.

2) Synthesis of the peptide fragment encompassing the sequence 1-12 of the human BDNF protein, blocked at the C-terminus, and characterization of its metal complexes by means of potentiometric and computational simulation. The coordination features of the acetylated form, Ac-BDNF(1-12), have also been characterized to put into light the involvement of the terminal amino group. Whereas, an analogous peptide, BDNF(1-12)D3N, in which the aspartate residue has been substituted by an asparagine, has been synthesized in order to provide evidence on the possible role of carboxylate group in metal coordination. The functional interaction of metal ions with BDNF, peptides or whole protein, has been tested of SHSY5Y neuroblastoma cell line culture.

3) *In vitro* and *in vivo* biochemical characterization of the neurotrophins signaling. After the chemical characterization, the synthesized peptide NGF(1-14) has been tested in PC12 cell line to ascertain its ability to act as agonist of NGF , to activate the TrkA pathway and to induce the phosphorylation of the transcription factor CREB. The collaboration with the EBRI (European Brain Research Institute) ensured the necessary expertise.

4) *In vivo* studies on the molecular mechanisms of BDNF in memory formation have been performed at New York University in collaboration with Prof. Alberini. We have tested the hypothesis that the transcription factor MeCP2 is a target of BDNF and it is regulated in different brain region after training of Inhibitory Avoidance Task.

5) Supported lipid bilayers, formed by the NGF(1-14)-SUV adsorption on silica (both planar model and nanoparticles), have been characterized in view of application as functional nanoplatforms for smart drug delivery. Preliminary measurements of cells interaction with the differently charged lipid membrane nanoplatforms have been performed in order to check the biocompatibility of the prepared materials.

3. Materials and Methods

Materials. All N-fluorenylmethoxycarbonyl (Fmoc)-protected amino-acids, and 2-(1-H-benzotriazole-1-yl) -1,1,3,3-tetramethyluronium tetrafluoroborate (TBTU), were obtained from Novabiochem (Switzerland); Fmoc- PAL-PEG resin, N,N-Diisopropyl-ethylamine (DIEA), N,N-dimethylformamide (DMF, peptide synthesis grade) and 20% piperidine-DMF solution were provided by Applied Biosystems; N-hydroxybenzotriazole (HOBT), triisopropylsilane (TIS) and trifluoroacetic acid (TFA), were purchased from Sigma/Aldrich.

NGF (kindly provided by Prof. Calissano) was purified from male mouse submaxillary glands.

POPC (1-palmitoyl-2-oleoyl-sn-glycero-3-phosphocholine) and POPS (1-palmitoyl-2-oleoyl-*sn*-glycero-3-phospho-L-serine (sodium salt) were purchased from Avanti Polar Lipids (Alabaster, AL), whereas the fluorescent labeled lipid probe, rhodamine-DHPE (1,2-dihexadecanoyl-sn-glycero-3-phosphoethanolamine) by Invitrogen, Carlsbad,CA.

All the other chemicals were of the highest available grade and were used without further purification.

Peptide synthesis and purification. All the peptides were synthesized on a Pioneer^{TM} Peptide Synthesiser using the solid phase peptide synthesis strategy. All amino acid residues were added according to the TBTU/HOBT/DIEA activation method for Fmoc chemistry on Fmoc-PAL-PEG resin (substitution 0.22 mmol/g, 0.33 mmol scale synthesis, 1.5 g of resin). N-terminal acetylation for AcNGF1-14 was performed by treating the fully assembled and protected peptide resins (after removal of the N-terminal Fmoc group) with a solution containing acetic anhydride (6% v/v) and DIEA (5% v/v) in DMF.

The peptides were purified by means of a preparative reversed-phase high-performance liquid chromatography (rp-HPLC). Purification was performed on a Varian PrepStar 200 model SD-1 chromatography system equipped with a Prostar photodiode array detector with detection at 222 nm. The peptides were eluted with solvent A (0.1% TFA in water)

and B (0.1% TFA in acetonitrile) on a Vydac C_{18} 250x22 mm (300 Å pore size, 10-15 μm particle size) column, at flow rate of 10 mL/min. Analytical rp-HPLC analyses were performed using a Waters 1525 instrument, equipped with a Waters 2996 photodiode array detector with detection at 222 nm.

The peptide samples were analysed using gradient elution with solvent A and B on a Vydac C_{18} 250x4.6 mm (300 Å pore size, 5 μm particle size) column, run at a flow rate of 1 mL/min.

The peptides were eluted according to the following protocol: from 0 to 5 minutes isocratic gradient in 5 % B, a linear gradient from 5 to 25% B for 25 min, and, finally, an isocratic gradient in 25%B from 30 to 40 minutes. All the peptides were characterized by ESI-MS.

- SSSHPIFHRGEFSV-NH_2 (NGF1-14): [R_t= 26.10 min]. Calculated for $C_{71}H_{103}N_{22}O_{20}$ Mass= 1584.73, ESI-MS [Obsd *m/z*: $(M+H)^+$ 1586.7; $(M+2H)^{2+}$ 793.7].

- Ac-SSSHPIFHRGEFSV-NH_2 (Ac-NGF1-14): [R_t= 27.00 min]. Calculated for $C_{73}H_{106}N_{22}O_{21}$ Mass = 1627.78, ESI-MS [Obsd *m/z*: $(M+H)^+$ 1628.5; $(M+2H)^{2+}$ 816.0].

- HSDPARRGELSV-NH_2 (BDNF(1−12)): [Rt= 25.2 min]. Calculated mass for C54H91N21O18 M= 1322.4, ESI-MS [Obsd m/z: $(M+H)^+$ 1323.2; $(M+2H)^{2+}$ 662.1].

- Ac-HSDPARRGELSV-NH_2 (Ac-BDNF(1−12)): [Rt= 28.0 min]. Calculated mass for C56H93N21O19 M= 1364.5, ESI-MS [Obsd m/z: $(M+H)^+$ 1365.4; $(M+2H)^{2+}$ 683.2].

- HSNPARRGELSV-NH_2 (BDNF(1−12)D3N): [Rt= 34.2 min]. Calculated mass for C54H92N22O17 M= 1321.5, ESI-MS [Obsd m/z: $(M+H)^+$ 1322.4; $(M+2H)^{2+}$ 661.7].

Preparation of small unilamellar vesicles (SUV) dispersions Small unilamellar vesicles were prepared from chloroform solutions of POPC (1-palmitoyl-2-oleoyl-sn-glycero-3-phosphocholine) and POPS (1-palmitoyl-2-oleoyl-*sn*-glycero-3-phospho-L-serine (sodium salt). A fluorescent labeled lipidprobe, rhodamine-DHPE (1,2-dihexadecanoyl-sn-glycero-3-phosphoethanolamine) was added (1 wt%) to 5 mg/mL solutions of 100 % POPC or 3:1

POPC:POPS in a round glass flask, then the chloroform was removed under Ar blowing and after under vacuum resulting in a thin lipid film on the glass flask. The lipid film was hydrated with PBS buffer (0.010 M PBS buffer with 0.140 M NaCl 0.0027 M KCl, Aldrich, pH 7.4) or 600 μM NGF(1-14) in PBS to a concentration of 5 mg/mL. The lipid mixture was extruded using a mini extruder (Avanti Mini-Extruder, Avanti polar lipids, Alabaster, AL) utilizing polycarbonatemembranes having pore sizes of 100 and 30 nm, 11 times for each membrane.

Prior to the FRAP and QCM-D investigations, the vesicles were diluted using PBS buffer to a final concentration of 0.1 mg/mL. Lipid adsorption experiments from the lipid micellar dispersion (100 μg/mL in PBS) were performed on glass (for LSM) or silicon dioxide (for QCM-D) substrates.

Potentiometric titrations. Potentiometric titrations were performed with a computer-controlled Metrohm digital pH meter (Model 654) and Hamilton digital dispenser (Model 665). The titration cell (2.5 ml) was thermostated at 298.0 ± 0.2 K and all solutions were kept under an atmosphere of argon, which was bubbled through the solutions. The combined microelectrode was calibrated on the pH = $^{-}\log[H^{+}]$ scale by titrating HNO_3 with CO_2 free KOH. Base solutions were added through a Hamilton burette equipped with 1 cm^3 syringes. The ionic strength of all solutions was adjusted to 0.1 mol dm^{-3} (KNO_3). All solutions were prepared with doubly distilled water. The analytical concentrations of peptides were 2.0×10^{-3} mol dm^{-3}. Metal to ligand ratios between 2:1 and 1:1, were employed. Stability constants for proton complexes were calculated from three peptide titrations carried out over the pH range 2.3–9.0. Triplicate titrations were performed to determine the copper(II) complex stability constants in the pH range 2.5-8.0 and the zinc (II) complexes in the pH range 2.5–7.0.

All the equilibrium constants are expressed as overall association constants (β) and refer to the general equilibrium given in equation 1

$$pM + qL + rH \leftrightarrows [M_pL_qH_r] \qquad (1)$$

where L is the fully deprotonated form of each peptide (charges are omitted for simplicity).

The overall association constant β, referring to the equilibrium given in equation 1, is defined by equation 2

$$\beta_{pqr} = [M_pL_qH_r]/[M]^p \cdot [L]^q \cdot [H]^r \qquad (2)$$

All potentiometric data were handled using the HYPERQUAD suite [272] that minimizes the error-square sum of the differences between measured and calculated electrode potentials and also allows for the simultaneous refinement of data from different titrations. Distribution diagrams were calculated by the HYSS program. Errors in stability constant values are reported as three times standard deviations.

Spectroscoscopic studies

UV-vis spectra were recorded at 25°C, by using a Cary 500 spectrophotometer equipped with 1 cm path length quartz cuvette. The concentrations of the peptides and copper(II) used to record absorption spectra were the same as those used for the potentiometric titrations. Measurements were performed in a 3 ml quartz cuvette with a 1 cm path length. Spectroscopic data were processed by using the HYPERQUAD program. [272]

Mother solutions in water of silica nanoparticles dye-doped with coumarin (NP) were diluted in 10 mM PBS (pH=7.4 at 25 °C) at the final concentration of 2.7×10^{-6} M. Spectra were acquired upon progressive additions of SUV (or SUV-NGF) in a molar ratio ranging from 10:1 to 1:10 (NP to lipid dispersions). UV-vis spectra were recorded in the wavelength range of 200-700 nm. Fluorescence spectra were carried out using λ_{exc}380 nm (for coumarin) and λ_{exc}540 nm (for rhodamine).

CD spectra were obtained at 25° C under a constant flow of nitrogen on a Jasco model 810 spectropolarimeter, which was calibrated with an aqueous solution of (1R)-(-)-10-camphorsulfonic acid. Measurements were carried out in water at different pH values using 1 cm path length cuvettes. The CD spectra of the copper(II) complexes as a function of the pH were obtained both in the 200-400 and 300-800 nm wavelength regions. All the solutions were freshly prepared using doubly distilled water. The copper(II) ion and

peptides concentrations used for the acquisition of the CD spectra in the visible region were identical to those used in the potentiometric titrations. Far UV CD spectra were acquired by using copper(II) ion and peptides concentrations ranging from 5.0×10^{-6} to 1.0×10^{-5} mol dm^{-3}.

EPR measurements were carried out on a Bruker Elexsys E500 CW-EPR spectrometer driven by a PC running XEpr program under Linux and equipped with both a Super-X microwave bridge, operating at 9.3-9.5 GHz, and a SHQE cavity. All EPR spectra of frozen solutions of copper(II) complexes were recorded at 150 K by means of a ER4131VT variable temperature apparatus. EPR magnetic parameters were obtained directly from the experimental EPR spectra, calculating them from the 2nd and the 3rd line to eliminate second order effects. Instrumental settings of frozen solution EPR spectra recording were as follow: number of scans 1-5; microwave frequency 9.344-9.376 GHz; modulation frequency 100 kHz; modulation amplitude 0.2-0.6 mT; time constant 164-327 ms; sweep time 2.8 min; microwave power 20-40 mW; receiver gain 1×10^4-2×10^5. Copper complexes were prepared by adding the appropriate amount of isotopically pure copper ion ($^{63}Cu(NO_3)_2$ 0.05 M solution), to the pertinent peptide solution. The metal-to-ligand ratios were 1:1 for all the copper-L systems. To obtain a good quality glass upon freezing, copper complexes solutions were prepared in 10% methanol–water mixture.

NMR sample solutions (2 mM) were prepared by dissolving the crude peptides in H_2O/D_2O 90/10 (v/v). Deuterated D_2O (99.9% relative isotopic abundance) was purchased from Cambridge Isotope Laboratories. All the NMR spectra were recorded at 298 K using a VARIAN UNITY 500 spectrometer, operating at 500 MHz. The proton chemical shifts were referenced to external TMS. Two-dimensional phase sensitive TOCSY, NOESY, ROESY and DQFCOSY spectra were collected using the States and Haberkorn method; water suppression was achieved by DPFGSE sequence. A spectral width of 6000 Hz was used in both dimensions; typically, 4096 was the number of complex points collected in the ω_2 dimension and 512 in the ω_1 dimension; the data were zero-filled to 2K in ω_1. Squared shifted sine-bell functions were applied in both dimensions *prior* to Fourier transformation and baseline correction. TOCSY, NOESY and ROESY experiments were

recorded with mixing times of 70 ms, 300 ms and 180 ms, respectively. Water suppression was achieved utilising the DPFGSE sequence .The data were processed and analysed using the VNMRJ and XEASY software. The Zn^{2+} metal ion coordination was studied at 1/0.95 peptide/Zn^{2+} molar ratio; the samples were prepared adding Zn(II) as $ZnCl_2$ water solution (0.1 M) to the above mentioned peptide solutions. To analyze the copper coordination features of both peptides, freshly prepared samples were titrated with different aliquots of a stock solution of $CuSO_4$ (10 mM in H_2O/D_2O 90/10 vv) to give molar ratios of the paramagnetic metal relative to peptide of 0.05, 0.1, 0.2, 0.3 and 0.4. The pH value of all the peptide solutions was adjusted with HCl and NaOH. For each samples ^{1}H-NMR experiments were acquired at 298 K; during Cu(II) titration the amide and side-chains protons affected in the monodimensional (TOCSY) ^{1}H NMR spectra were identified by comparing their intensities (I) with those of the same peak (I_0) in the data set of samples without metal. In order to obtain intensity profiles the I/I_0 ratios of not-overlapping peaks were plotted as a function of the peptide sequences. Pulse Field Gradient (PFG) diffusion measurements with the PG-SLED (pulse gradient-stimulated echo longitudinal encode-decode) sequence permitted to obtain D_{trans} which is proportional to the decay rate of the NMR signal attenuation as a function of gradient strength. Each diffusion data set contained a series of 13 monodimensional ^{1}H spectra with gradient strength from 0.5 to 30 G/cm. For the obtainment of the translational diffusion coefficient D_{trans} the DOSY package of the VNMRJ software was used.

Fourier Transform infrared (FT-IR) spectra were recorded on a Bruker Tensor 27 spectrophotometer, equipped with a room temperature DTGS detector, mid-IR source (4000 to 400 cm-1), and a KBr beamsplitter. Each spectrum was acquired at 4 cm-1 resolution (16 scans).

Laser scanning confocal microscopy (LSM) and Fluorescence recovery After Photobleaching (FRAP). Prior to the FRAP investigation, a glass bottom 96-well plate (uncoated, γ-irradiated, MatTek Corporation, Ashland, MA) was unpacked and immediately 200 μL of lipid dispersion were dispensed in each well. After 15 minutes, the lipid dispersion was removed and each well was washed several times with PBS. A final volume of 200 μL of PBS was left in each well to keep the adlayer hydrated for the whole

FRAP experiment. LSM observations were carried out by using an Olympus FV1000confocal laser scanning microscope equipped with a HeNe laser, oil immersion objective (60xO3 PLAPO) and spectral filtering system. Excitation wavelength was set at 543 nm, and emitted light was detected at 591 nm. The detector gain was fixed at a constant value, and images were taken for all of the samples, at random locations throughout the area of the well. For the FRAP investigations, time-solved snapshots were acquired as follows: three images before bleach, then bleaching by using high intensity (95% power) on the laser, and other micrographs every 5 seconds up to 2 minutes. By translating the sample stage, an average of 10 spots per substrate was photobleached in a given experiment. Fluorescence recovery curves were analyzed by ImageJ software (FRAP Profiler macro). The data were normalized to the initial (pre-photobleach) value, which enables the percentage of photobleaching and the percentage fluorescence recovery within the laser region to be determined. For each sample, the emission recorded from the bleached spots was compared with that coming from contiguous non-bleached areas.

Quartz crystal microbalance with dissipation monitoring (QCM-D) measurements were carried out in flow mode (50µl/min) on a Q-sense E1 unit (Biolin Scientific, Finland). Prior to each measurement series, the SiO_2-coated sensor crystals (AT-cut quartz crystals with a fundamental resonance frequency of 5 MHz) were cleaned by immersion in 10 mM sodium dodeceyl sulfate (SDS, > 1 h), followed by rinsing with Millipore water (MQ), Ar blow dried nitrogen and treated by UV-Ozone (30 min). Further cleaning was performed in situ in the measurement cell, by two subsequent steps of rinsing with MQ and SDS.

In vitro experiments

Cellular experiments Human neuroblastoma SH-SY5Y cells were grown in DMEM (Dulbecco's modified eagle's medium) purchased from Lonza, supplemented with 10% fetal bovine serum (FBS; Lonza), 1% penicillin/streptomycin, 2 mM L-glutamine and maintained in a in a humidified atmosphere of 95% air 5% CO_2 at 37°C in an incubator (Hera Cell 150)

SHSY5Y cells were treated with the peptides investigated (in the range from 10 to 100 μM), NGF and BDNF (from 10 to 100 nM) also in presence of $CuSO_4$ and $ZnSO_4$ solutions (10 uM).

Treatments of SHSY5Y cells were performed in the same culture medium. Proliferation and differentiation was qualitatively estimated after 72h through microscopy observation (LEICA DMI 4000 B) and quantified through cell counting, after 72h. This was achieved by Hoechst staining of nuclei and analyses of the captured images using the tool provided by Image-J, image analyses software (NIH).

Biocompatibily assay were performed according the following protocol. Cells were plated at a density of $1x10^5$ on the glass bottom 96-well plate in which small unilamellar vesicles (SUV) dispersions had been pre-adsorbed in DMEM-F12 medium with 5% fetal bovine serum. After 24hr cells were rinsed with PBS and treated for 15 min at 37°C in 5% CO_2 with the lysosomal markerLysoTracker Green DND-26 (Molecular Probes, 500 nM in PBS). After that, cells were rinsed with fresh PBS and observed at the confocal microscope.

In vivo experiments

Long Evans adult male rat (Harlan, Indianapolis, IN) weighing between 200-250 grams at the beginning of the experiments were used. Rats were housed individually on a 12 hour light-dark cycle with *ad libitum* access to food and water. All experiments were done during the light cycle between 9 AM and 6 PM. All rats were handled for 2-3 minutes per day for 5 days before any behavioral procedure. All protocols complied with the National Institute of Health Guide for the Care and Use of Laboratory Animals.

Cannulae implants and hippocampal injections Rats were anesthetized with ketamine (65 mg/kg, i.p.) and xylazine (7.5mg/kg, i.p.), and stainless-steel guide cannulae (22-gauge) were stereotactically implanted to bilaterally target the dorsal hippocampus (4.0 mm posterior to the bregma; 2.6 mm lateral from midline; and 2.0 mm ventral). The rats

were returned to their home cages and allowed to recover from surgery for 7 days. At the indicated time points before or after training, rats received bilateral injections of compounds as specified. All hippocampal injections were carried out in 1μl per side. Hippocampal injections used a 28-gauge needle that extended 1.5 mm beyond the tip of the guide cannula and connected via polyethylene tubing to a Hamilton syringe. The infusions were delivered at a rate of 0.33 μl/minute, using an infusion pump. The injection needle was left in place for 2 minutes after the injection to allow complete diffusion of the solution. The anti-BDNF antibody was purchased from Millipore (Billerica, MA) dissolved in 1xPBS. Anti-BDNF antibody was injected out at 1μg/injection/side. Control sheep IgG was purchased from Sigma Aldrich and dissolved in 1xPBS and injected at 0.5 μg/injection/side.

Western blot analysis. Several brain regions were punched from frozen slices. Protein extracts from rat were obtained by polytron homogenization in cold lysis buffer with protease and phosphatase inhibitors (0.2 M NaCl, 0.1 M HEPES, 10% glycerol, 2 mM NaF, 2 mM Na4P2O7, aprotonin 4U/ml, DTT 2mM, EGTA 1mM, microcystin, 1μM, benzamidine, 1mM). Protein concentrations were determined using the BioRad protein assay (BioRad Laboratories, Hercules, CA). Equal amounts of total protein (10-20 μg/lane) were resolved on denaturing SDS-PAGE gels and transferred to Hybond-P membranes (Millipore) by electroblotting. Membranes were dried and then reactivated in methanol for 5 minutes and then washed with 3 changes of water. The membrane was then blocked in 5% milk/TBS or according to manufacturers' instruction for 1 hour at room temperature, and then incubated with primary antibody overnight at 4°C in solution per manufacturers' suggestion. The membranes were washed, treated with secondary anti-rabbit or anti-mouse antibody for 1h at room temperature, and then washed again. Membranes were collected using a LICOR Odyssey scanner and quantitative densitometric analysis carried out using the Odissey Software, using actin as loading control for all markers.

Immunohistochemistry and immunofluorescence

Animals were anaesthetized and transcardially perfused with ice cold 4% paraformaldehyde in 0.1 M phosphate buffer, pH 7.4. After perfusion, the brains were

dissected and kept in the same fixatives overnight at 4°C, then cryoprotected by immersion in 10%, 20%, and 30% sucrose solutions and subsequently cut using a cryostat. 30-µm sections were collected in phosphate buffered saline (PBS, 0.01 M, pH 7.4) and processed for free-floating immunohistochemistry. After a blocking step in a PBS solution containing 0.05% Triton X-100 and 10% normal goat serum (NGS), sections were then incubated overnight at room temperature with primary antibodies. Antibodies were diluted in PBS with 3% NGS and 0.05 Triton X-100. Sections were then washed in PBS (3 x 10 min), incubated for 1 hour with labeled secondary antibodies diluted in 3% NGS and 0.05% Triton X-100 in PBS. Sections were mounted on gelatine-coated glass slides and observed with light and confocal microscopes.

4. Results and discussion

4.1 Characterization of NGF(1-14) and its complexes

An NGF N-terminus peptide fragment encompassing the residues 1–14 blocked at the C terminus, namely, SSSHPIFHRGEFSV-NH2 (NGF (1-14), L) has been synthesized to ascertain the coordination features of Cu^{2+} and Zn^{2+} complexes with the NGF N-terminal domain. The coordination features of the acetylated form Ac-SSSHPIFHRGEFSV-NH2 (AcNGF(1-14), L') have been characterized to prove (or disprove) the involvement of the terminal amino group in metal binding. The Cu^{2+} and Zn^{2+} complexes with NGF peptides have been studied by means of potentiometric and spectroscopic (UV/Vis, CD, NMR and EPR) techniques. The functional interaction of Cu^{2+} and Zn^{2+} ions with NGF peptides or with the whole protein has been tested by measuring the effects on the proliferation rate of SHSY5Y neuroblastoma cell line culture, suggesting important correlation between biological activity and coordination environment.

4.1.1 Metal-hosting capability of NGF N-terminus peptide fragments and effect of Cu^{2+} and Zn^{2+} on peptide conformation

Far-UV CD spectra reveal that both peptides adopt predominantly a random-coil conformation over the investigated pH range of 4–11 (Fig. 10).

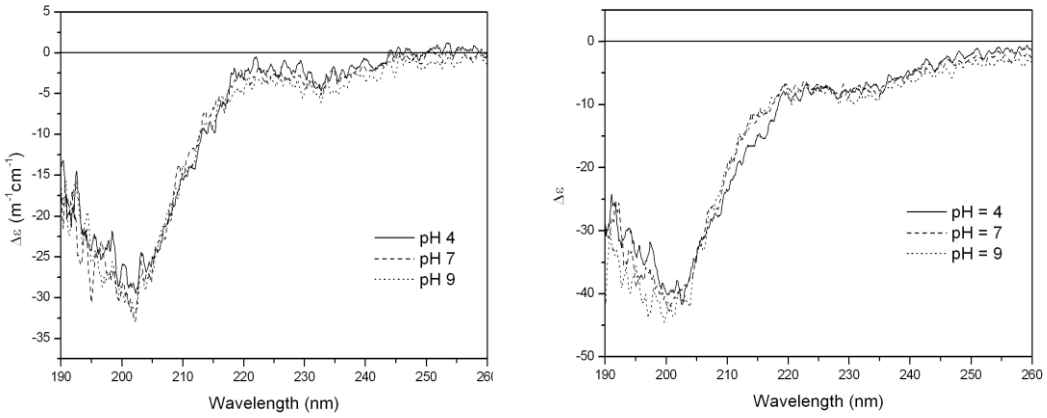

Figure 10. *Far-UV CD spectra of NGF(1-14) (left) and AcNGF(1-14) (right).*

NMR spectroscopic measurements have been carried out in a limited pH range due to the low solubility of the two peptides above pH 7. The narrow range of HN resonance dispersion, the absence of NOE effects diagnostic of secondary structure and the chemical shift index diagrams [273-275] clearly confirm that both peptides do not assume a definite conformation, in agreement with the far-UV CD results (Fig. 10). Figure 11a shows far-UV CD spectra for the titration of NGF(1-14) with Cu^{2+} at pH 7.4.

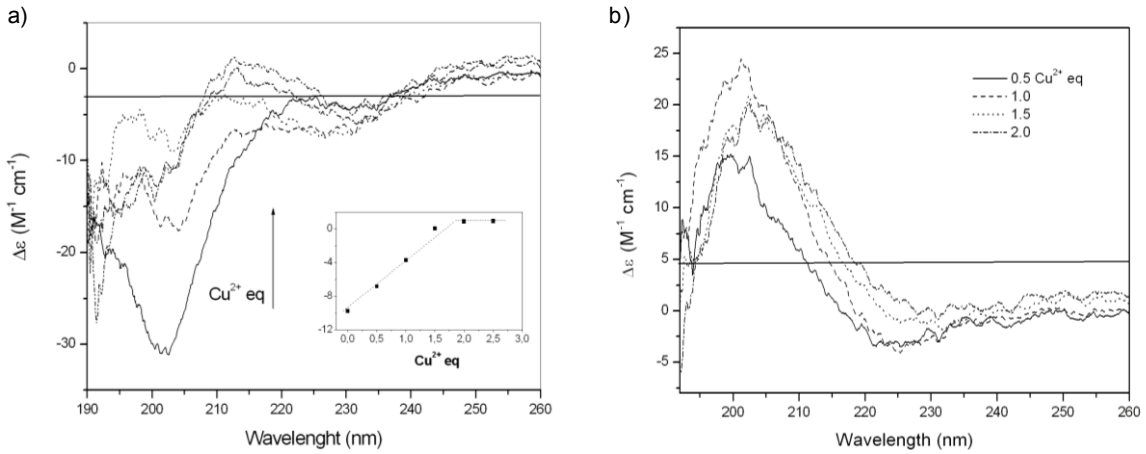

Figure 11. *a) Far-UV CD spectra at pH 7.4 of a) Cu^{2+} titration of NGF(1-14) <up to two molar equivalents of copper ions. Inset: Cu^{2+} binding curves monitored at 213 nm. b) The apo-subtracted difference spectra of the Cu^{2+} titration*

The secondary-structure region indisputably changes upon Cu^{2+} addition. Gradual loss of intensity of the negative signal at λ=202 nm and appearance of a positive band at λ=213 nm are observed with increasing Cu^{2+} concentration. The disappearance of the signal at λ=202 nm suggests reduced random-coil character of NGF(1-14) caused by interaction with the metal ion, even though a possible contribution due to the presence of induced charge-transfer bands cannot be excluded. The binding curve for titration of NGF(1-14) with Cu^{2+} is shown in the inset of Figure 11a.

The CD band at 213 nm increases in intensity with Cu^{2+} addition up to two molar equivalents; beyond this point no further changes are recorded up to three molar equivalents, where precipitation takes place. These data imply a 2:1 metal-to ligand

stoichiometry. The apo-subtracted difference spectra for the titration of Cu^{2+} with NGF(1-14) (Fig. 11b) give a better perception of the changes induced by interaction with metal ions. The CD spectral differences indicate an increase in the turn conformation of the peptide, resulting from the involvement of backbone amide nitrogen atoms in Cu^{2+} coordination (see below). The shift of the maximum and a slight decrease in the intensity are observed in the difference spectra beyond one equivalent of Cu^{2+}, which suggests that NGF(1-14) binds two copper ions but the metal ions experience different coordination environments. Far-UV CD spectra for the titration of NGF(1-14) with Zn^{2+} show a decrease in the minimum of the band centered at λ=202 nm. The band shape does not change as significantly as for Cu^{2+} (Fig. 12a), and this is due to the smaller amount of zinc peptide complexes formed. The changes in band intensity of the secondary-structure region reach a plateau at one molar equivalent of Zn^{2+} (Fig.12a). The difference spectra show only a slight increase in turn structures, suggesting that the Zn^{2+} coordination environment does not involve backbone nitrogen atoms but only the side chain groups.

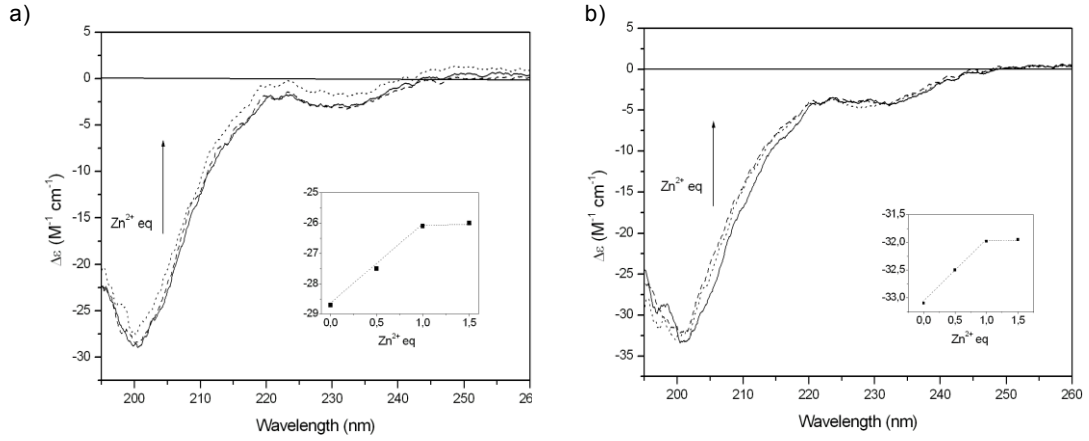

Figure 12. *Far-UV CD spectra for Zn^{2+} titration at pH 7.4 of a) NGF1-14 up to 1 mole equivalent of zinc ions; Zn^{2+} binding curve monitored at 201 nm (inset); b) AcNGF1-14, up to 1 mole equivalent of zinc ions; Zn^{2+} binding curve monitored at 201 nm (inset).*

Figure 13a shows the far-UV CD spectra for the titration of the acetylated peptide AcNGF(1-14) with Cu^{2+} at pH 7.4. A decrease in the intensity of the minimum at λ= 201 nm is also observed for this system, which is indicative of the loss of the random-coil

conformation resulting from metal binding. However, neither a positive band at λ=213 nm nor the other significant changes observed in the NGF(1-14) titration are detected in the CD spectra of the acetylated analogue. For this reason, the binding curve for the titration of Cu^{2+} with AcNGF(1-14) could be determined only at λ=201 nm. The intensity of this band decreases up to the addition of one equivalent of metal ions (inset to Fig. 13a) and a precipitate forms when two molar equivalents are added. Ac-NGF(1-14) is able to bind Cu^{2+} with a 1:1 metal-to-ligand stoichiometry. The difference spectra obtained for the Cu^{2+} titrations indicate an increase in turn structures of AcNGF(1-14) (Fig. 13b), even though this effect is less evident than that observed for NGF(1-14).

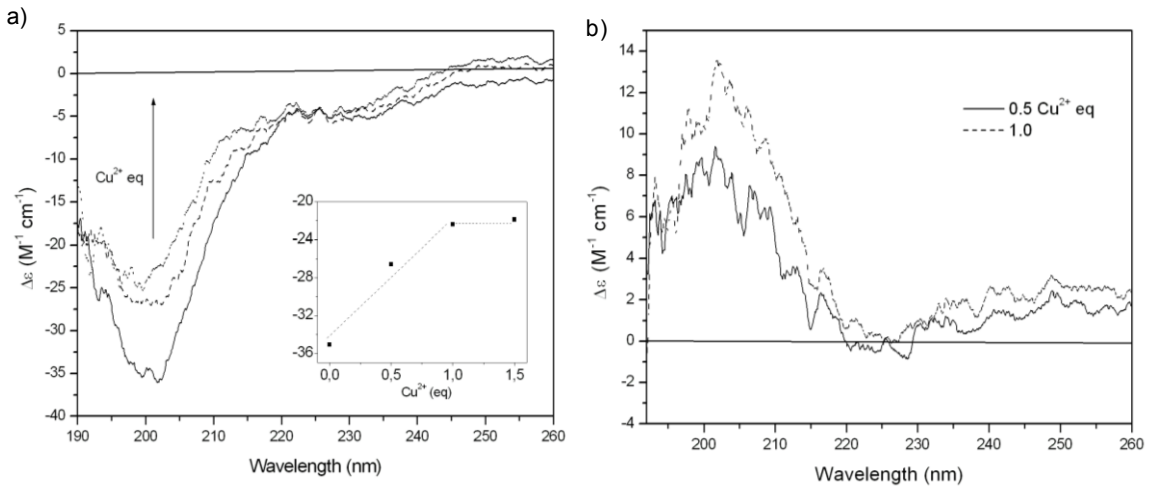

Figure 13. *Far-UV CD spectra at pH 7.4 of a) Cu^{2+} titration of AcNGF(1-14) up to 1 mole equivalent of copper ions. Inset: Cu^{2+} binding curve monitored at 201 nm. b) The apo subtracted difference spectra of the Cu^{2+} titration*.

The far-UV CD spectra for the titration of AcNGF(1-14) with Zn^{2+} (Fig. 12b) resemble those observed for NGF(1-14), that is, no major changes and a slight decrease in the minimum at λ=201 nm (addition of 1 equiv). The amount of Zn^{2+} complexes formed is less than that formed by Cu^{2+}, whereas the difference spectra suggest a slight increase of the turn structure.

4.1.2 Speciation, stability constants and coordination modes of the zinc(II) complexes with AcNGF1-14 and NGF1-14

Protonation constants of the peptides AcNGF(1-14) and NGF(1-14) have been determined by potentiometric titrations (Table 1); as expected**,** AcNGF(1-14) and NGF(1-14) have three and four proton-accepting centers, respectively. The Ser-1 amino group is the most basic center, while the two histidyl residues take up the two protons in two overlapping steps; however, the average value for the protonation of the imidazole residues closely recalls that obtained for similar His-containing peptides [276]. Also the acidity of the glutamyl γ-carboxylic function nicely agrees with that found for other peptides containing glutamic acid[276-277]

***Table** 1. Protonation constants (log β_{pqr}) and pK values for NGF(1-14) and AcNGF(1-14) (T= 298 K, I=0.10 mol dm^{-3} KNO_3).*

Species	AcNGF(1-14)	NGF(1-14)
LH	6.67 (2)	7.56 (6)[a]
LH_2	12.67 (2)	14.13 (7)
LH_3	16.86 (4)	20.14 (9)
LH_4	-	24.44 (9)
pK(Ser1-NH_2)	-	7.56
pK(Imidazole of His4 and His8)	6.67	6.57
pK(Imidazole of His4 and His8)	6.00	6.01
pK(-COOH of Glu11)	4.19	4.13

[a] Standard deviations (3σ values) are given in parentheses; L is referred either to NGF(1-14) or AcNGF(1-14)

The stability constant values of the complexes of Zn^{2+} with AcNGF(1-14) and NGF(1-14) are listed in Table 2.

Table 2. *Stability constants (log β_{pqr}) for the Zn^{2+} and Cu^{2+} complexes with NGF(1-14) and AcNGF(1-14) (T= 298 K, I=0.10 mol dm^{-3} KNO_3).*

Species	*AcNGF(1-14)*	*NGF(1-14)*
[ZnLH]	-	11.41 (2) [a]
[ZnL]	3.90 (2)	5.05 (1)
[CuLH]	-	14.09 (2)
[CuL]	6.37 (3)	8.72 (2)
[$CuLH_{-1}$]	0.60 (6)	3.27 (2)
[$CuLH_{-2}$]	-6.59 (9)	-4.02 (2)
[$CuLH_{-3}$]	-13.97 (9)	-

[a] Standard deviations (3σ values) are given in parentheses; L is referred either to NGF(1-14) or AcNGF(1-14). Charges are omitted for clarity.

As expected, the acetylation of the terminal amino group simplifies the species distribution. In fact Zn^{2+} does not form any complex with AcNGF(1-14) up to pH 5 (see Fig. 14a); above this pH only the $[ZnL']^{2+}$ species forms.

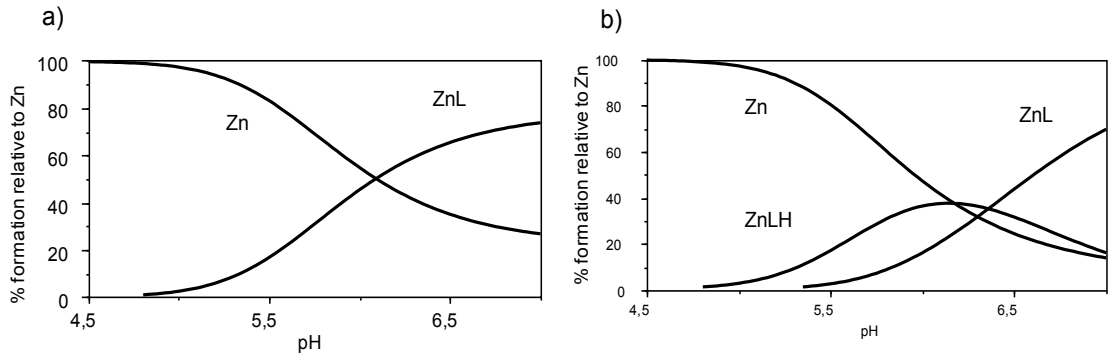

Figure 14. *Species distribution diagram for the Zn(II) complexes in aqueous solution a) AcNGF1-14 and b) NGF1-14. $[Zn^{2+}] = 2\times10^{-3}$ M. Ligand to metal molar ratio is 1:1. Charges are omitted for clarity.*

The stability constant value calculated for this complex species (log K=3.90) is indicative of the presence of two imidazole nitrogen atoms and a carboxylate group in the coordination sphere of Zn^{2+} (see Fig. 15). Such an arrangement is supported by the similarity between Zn-AcNGF(1-14) binding constant value and that obtained for an analogous Zn^{2+} complexes of a N-terminus Aβ peptide fragment (log $K_{Aβ\ fragment}$ = 3.63); in latter peptide the metal ion has been shown to be bound to two imidazole nitrogen atoms and to the carboxylate group of a Glu residue, leading to a macrochelate with a 2N1O ($2N_{Im}$,COO^-) binding mode. [278] A large molar fraction (see Fig. 14a) of uncomplexed metal ion is present over the entire pH range explored (3-6.5); this is responsible for the formation of a precipitate (likely zinc(II)-hydroxide or mixed hydroxo complexes) that is detected as neutrality is reached.

The protonated species formed by NGF1-14 with zinc(II), $[ZnLH]^{3+}$, displays a stability constant value ($logK_{(111)} = log\beta_{(111)} - logK_{p(011)}$= 3.85) similar to that of the species formed by the acetylated peptide. This indicates that the zinc(II) experiences the same coordination environment ($2N_{Im}$,COO^-) involving the side chains of His4, His8 and Glu11. The $[ZnL]^{2+}$ is the prevailing complex species in the pH range 6.5-7 (Fig. 14b).

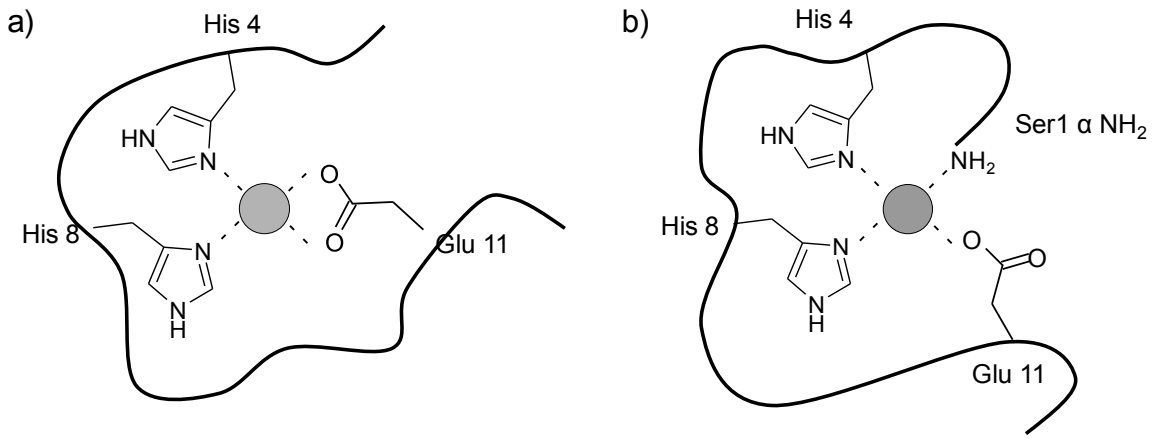

Figure 15. *A schematic representation of the Zn^{2+} coordination environment in the[ZnL] complex species of a) AcNGF(1-14) and b) NGF(1-14).*

Its stability constant value (log $\beta_{(110)}$ = 5.05) clearly indicates the formation of a more stable complex species with respect to the protonated one, with the involvement of a further donor atom, which substitutes a water molecule in the zinc(II) coordination sphere. This leads to conclude that the Ser1 free amino group is the "additional" group available for the coordination of zinc(II); thus, zinc(II) that turns out to be bound to N_{NH2}, $2N_{Im}$, and COO^-. A further evidence of this coordination mode results by the absence of analogous complex species in the acetylated peptide, in which the amino group is blocked. Further increase of pH value induces the formation of a precipitate due to the hydrolytic species formation.

NMR measurements have been carried out at two different pH values (5.5 and 6.9) and at peptide/Zn^{2+} 1/0.95 molar ratio, to further support the set of donor atoms indicated by the stability constant values. The translational diffusion coefficient, D_{trans}, (2.2 x 10^{-10} m^2s^{-1}) remains unchanged upon Zn^{2+} addition, ruling out metal ion mediated peptide-peptide aggregation phenomena within the concentration range investigated with the NMR experiments. Several amino acid residue resonances turned out to be perturbed, shifted and/or broadened, upon Zn^{2+} addition at pH 5.5, indicating both the involvement of these aminoacids in the metal coordination and/or their proximity to the metal binding site. The graphs reporting the perturbation of backbone chemical shift [279] for Zn-NGF(1-14) and Zn-AcNGF(1-14) present remarkable similarities at this pH value (Fig. 16), indicating that zinc(II) binding involves the same donor atoms in both peptides.

The resonances assigned to the histidine imidazole rings shift upfield and broaden upon addition of zinc(II), with the His4 and His8 Hε experimenting the larger shifts (Fig. 16), indicating that the two Nδ imidazoles are the metal anchoring sites[280-282] The βCH_2 and γCH_2 signals of the Glu11 residue show small but significant chemical shift changes (0.01-0.05 ppm) indicating that this residue is involved in the metal coordination. In addition, the methylene resonances of Gly10, that degenerate in the free form of the peptides, split into two well-resolved signals in the presence of the metal ion, as a result of a different magnetic environment experimented by the two nuclei.

These data further corroborate the involvement of the side-chain carboxylate group of the Glu11 residue in addition to the two histidines, in keeping with the potentiometric data. The C-terminal amino acid residue resonances assigned to Ser13 and Val14 are affected by the presence of the metal ion neither for NGF1-14 nor for AcNGF1-14 (Fig. 16)**.** The resonances of the three serine residues present in the N-terminus of AcNGF1-14 have been sequentially assigned and turn out be identical both in presence and absence of zinc(II); the same applies to the Ser2 and Ser3 in the N-terminus of NGF1-14, while the resonance of Ser1 in the absence and presence of metal ion could not be assigned. This is in agreement with the indication that at acidic pH the predominant Zn(II) complex species formed by the two peptides has the same coordination environment.

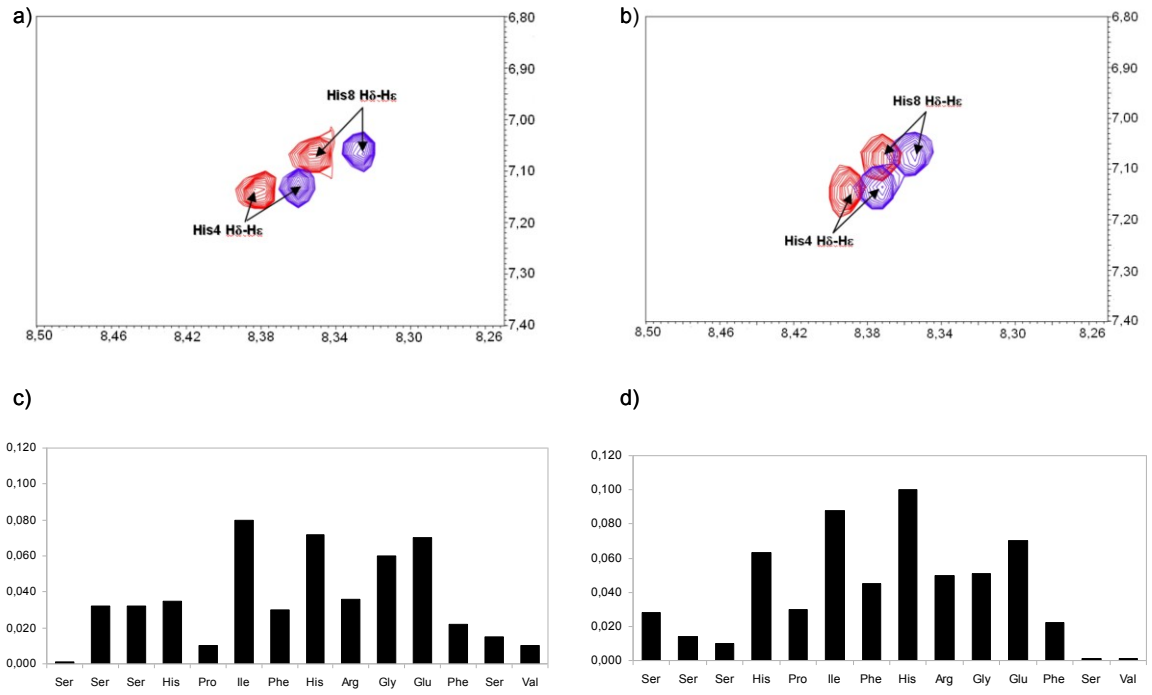

Figure 16. *Histidines imidazole regions of the TOCSY spectra of NGF (panel a) and AcNGF (panel b) before (red) and after (blue) the Zn^{2+} addition. Panels c and d report the chemical shift changes (ppm) of NGF(1-14) and AcNGF(1-14), respectively, resulting from the Zn^{2+} addition*.

At pH 6.9, most of the NH protons are too broad to be detected; nevertheless, on the basis of the remaining signals, the trend observed at pH 5.5 for some amino acid residues of both peptides may be confirmed. As observed in the acidic region, the histidines side chains experience a downfield shift consistent with a Nδ binding to metal ion with except the His8 of AcNGF1-14; at pH 6.9 the imidazole protons are equally shifted by the metal binding suggesting a Nε Zn^{2+} coordination mode.[282] The absence of the NH signal of N-terminal residues in the Zn-NGF1-14 system at this pH, does not permit to conclude that the Ser1 amino group is directly involved, but the trend observed for the Glu11 indicate that the carboxylic group is somehow involved in the metal coordination. Based on both the thermodynamic and NMR data, we can conclude that in the main zinc(II) complex species with NGF1-14, the amino group, two imidazole nitrogen atoms and one carboxylate group (N_{NH2}, $2N_{Im}$, COO^-) are involved in the coordination at physiological pH (Fig. 15).

4.1.3 Speciation, stability constants and coordination environments of the copper(II) complexes with AcNGF1-14 and NGF1-14

The stability constants of the Cu^{2+} complexes are also listed in Table 2, while the metal ion speciation at 1:1 metal ion-to-ligand ratio for both peptides is shown in Figure 17.

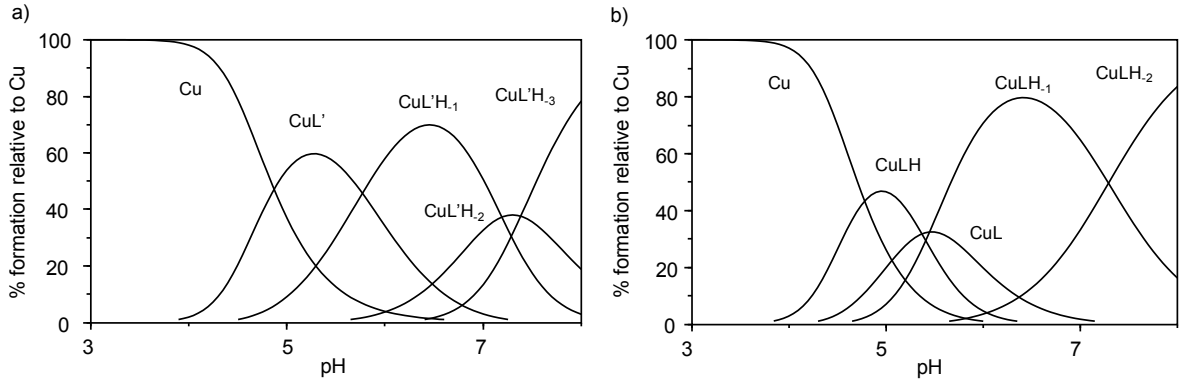

Figure 17. *Species distribution diagram for the Cu^{2+} complexes in aqueous solution with a) AcNGF(1-14) and b) NGF(1-14). [Cu^{2+}] = 2x 10^{-3} M. Ligand to metal molar ratio is 1:1. Charges are omitted for clarity.*

AcNGF(1-14) does not complex Cu^{2+} up to pH 4; at this pH value $[CuL']^{+}$ starts forming and reaches its maximum percentage at pH 5 (Fig 17a). The stability constant value (log K = 6,37) is two logarithmic units larger than that of similar copper(II) complexes of peptide fragments in which the metal forms a macrochelate with a N_{im} and COO^{-} binding mode [283] while it is similar to that reported for Aβ peptide fragments where the metal ion has been shown to form a macrochelate with a $2N_{im}$, COO^{-} coordination environment (log K = 6.18).[284] This suggests that two histidine imidazole nitrogen atoms and the glutamate carboxylate group are involved in Cu^{2+} binding to AcNGF1-14. The spectroscopic parameters are reported in Table 3. The CD spectra in the visible region show an extremely low intensity, supporting that the metal ion coordinates through side chains donor atoms that are distant from chiral centers of peptide backbone. The UV-vis parameters (λ_{max} = 710 nm ε= 55 $M^{-1}cm^{-1}$) and the EPR parameters ($g_{\|}$ = 2.312 and $A_{\|}$ = 158x10^{-4} cm^{-1}) are consistent with a 2N1O coordination mode and suggest a slight distortion of the equatorial plane. The NMR results are in line with these binding features.

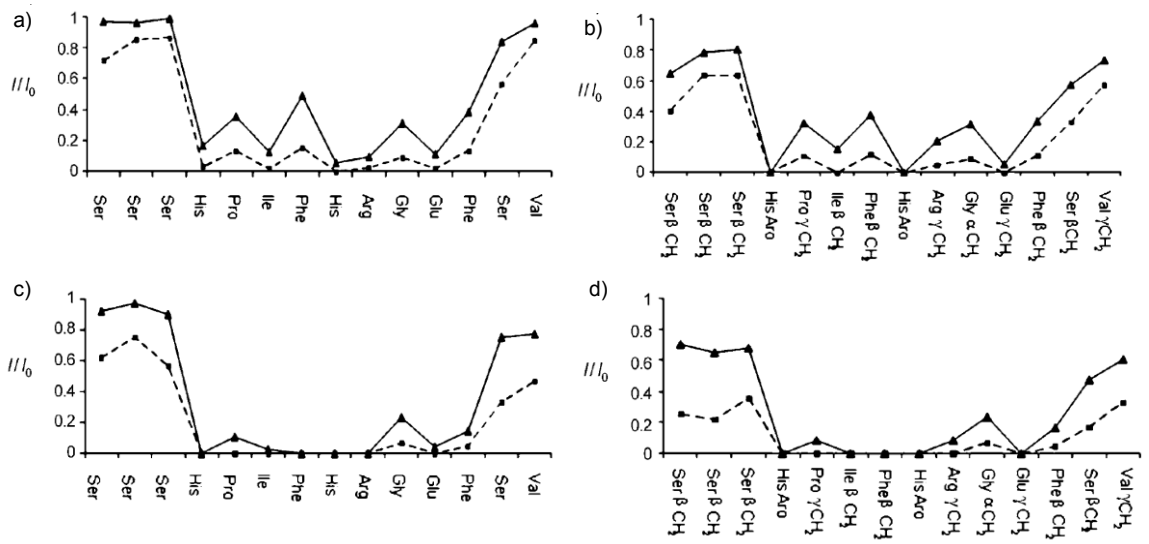

Figure 18. *I/I_0 profiles of the ^1H signals of Cu(II)-AcNGF1-14 system at pH 4.8 a) backbone, b) side chain atoms, and pH 5.9 c) backbone, d) side chain atoms, in the presence of 0.05 (▲) and 0.1 (■) of Cu^{2+}.*

pH values of 4.8 and 5.9 for the NMR copper titrations have been chosen to maximally represent in solution the CuAcNGF and $CuAcNGFH_{-1}$ species. Diffusion NMR experiments, recorded at the different pH values in presence of different aliquots of the metal ion, indicate that no peptide/peptide aggregation occurs. In all measurements, the paramagnetic Cu^{2+} strongly affects the width of the signals. The more affected residues have been identified by comparing their intensities (I) with those of the same peak (I_0) observed in the absence of the Cu^{2+} ion: the I/I_0 ratios of protons that do not overlap are reported in Figure 18 as a function of the peptide sequence. In agreement with the distribution diagram, at pH 4.8 and in the presence of a peptide excess, Ac-NGF1-14 forms only one complex, $[CuL']^{2+}$; this complex species is populated only for about 20%, whilst 80% of the ligand is still free (Fig.17). Figure 18a clearly evidence that the two terminal regions (residues 1-3 and 12-14) are not in close proximity or directly coordinated to the metal ion. On the other hand, Hε1 and Hδ2 resonances of the two histidine residues and the γ protons of the Glu11 side chain, as well as the Hα protons, are extensively broadened at a peptide/Cu(II) molar ratio of 1/0.05, confirming the suggested 2N1O coordination mode ($2N_{Im}$, COO^-).

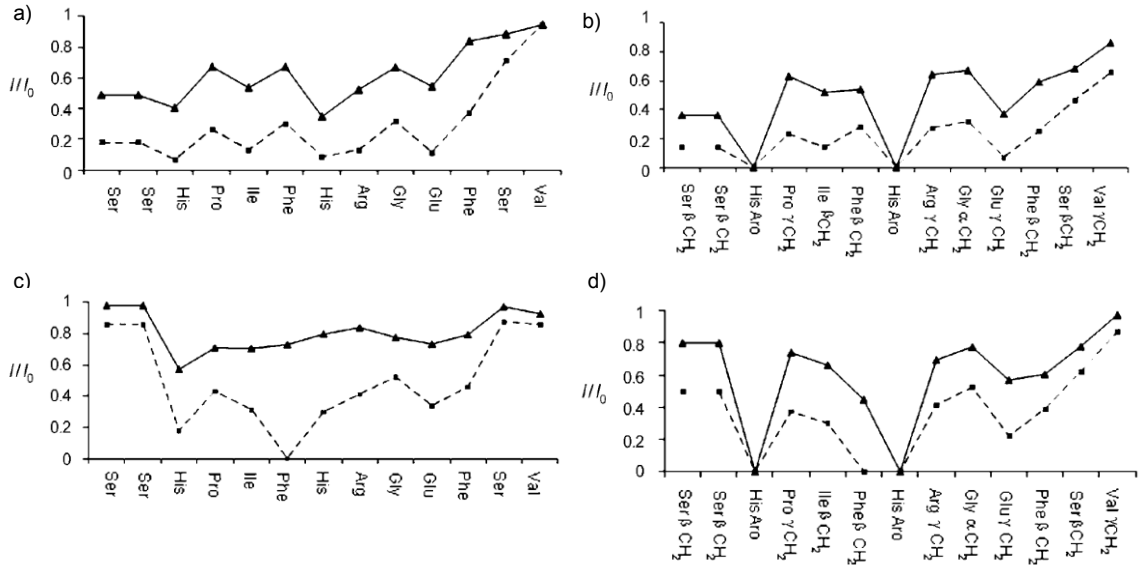

Figure 19*: I/I₀ profiles of the ¹H signals of Cu²⁺-NGF(1-14) system at pH 4.8 a) backbone, b) side chain atoms, and pH 5.4 c) backbone, d) side chain atoms, in the presence of 0.05 (▲) and 0.1 (■) of Cu²⁺.*

Table 3. *Spectroscopic parameters for the Cu^{2+} complexes with AcNGF(1-14) and NGF(1-14). $[Cu^{2+}]$= [Ligand] = 1×10^{-3} mol dm^{-3}*

	pH	Species	UV-vis $\lambda_{max}(\varepsilon)$ [nm($M^{-1}cm^{-1}$)]	CD λ_{max} ($\Delta\varepsilon$) [nm($M^{-1}cm^{-1}$)]	EPR $g_{\|\|}/A_{\|\|}$ ($10^{-4}cm^{-1}$)	
AcNGF(1-14)	5	CuL'	710 (54)	-	2.312 (2)	158 (4)
	6	$CuL'H_{-1}$	598 (69)	693 (-0.13);. 325 (+0.36); 295 (-0.2);.290 (0.90)	2.270 (4)	184 (4)
	7	$CuL'H_{-2}$	580 (100)	580 (-0.22);. 323 (+0.68); 297 (-0.1); 257 (3.4)	2.212 (3)	190 (4)
	8	$CuL'H_{-3}$	550 (80)	558 (-0.25). 321 (+0.43); 297 (-0.1); 261 (3.2)	2.195 (4)	198 (4)
NGF(1-14)	5	CuLH	674 (71)	644 (-0.22); .322 (+0.21); 279 (-0.17); 253(+0.50)	-	-
	6-7	$CuLH_{-1}$	610 (104)	632 (-0.58); 340 (+0.52) sh; 328 (+0.95); 284(-1.40); 255(+0.50)	2.226 (2)	162 (3)
	8	$CuLH_{-2}$	560(134)	557 (-0.13); 340 (+ 0.40) sh.; 325 (+0.6); 285 (-1.80); 255 (+0.50)	2.205 (2)	190 (2)

Errors in $\lambda = \pm 2$ nm and $\varepsilon = 5\%$. Charges are omitted for clarity.

$[CuL'H_{-1}]^+$ has the stepwise constant $\log K_{11-1} = 5.77$ ($\log K_{11-1} = \log\beta_{(110)} - \log\beta_{(11-1)}$). This value clearly refers to the deprotonation of one amide nitrogen of the peptide backbone. The CD band at 340 and the shoulder around 310 nm result from the binding of both imidazole and amide nitrogen atoms to copper(II), respectively, again supporting the potentiometric results. In addition, the involvement of the imidazole side chain in the metal ion coordination, is further corroborated by the presence of the diagnostic π_2 N_{Im} -Cu(II) c.t band at 260 nm. The λ_{max} measured for this complex species is significantly blue-shifted in comparison with that observed for the $[CuL']^{2+}$ species. This is due to the formation of a strong equatorial field in which the nitrogen amide atom is involved in the formation of two chelate rings. The EPR parameters assigned to $[CuL'H_{-1}]^+$, corroborate both the

thermodynamic data and the UV-Vis results, indicating the formation of a smaller macrochelate ring, entailing the in-plane coordination of three nitrogen donor atoms ($2N_{Im}$, 1N) (see scheme 3). The NMR experiments, carried out at pH 5.9, show a trend similar to that observed at lower pH. The N-terminal 1-3 and C-terminal 12-14 residues are not significantly affected by copper(II) addition, while the signals the His and Glu residues signals broaden. An important difference is represented by the Phe 7 and Ile6 signals which show a pronounced intensity reduction even at low Cu^{2+} concentrations (Fig. 18c,d) suggesting that the amide deprotonation occurs in the proximity of the His 8 residue. The intensity decrease of glutamic residue signal is to be ascribed to the contemporary presence of the $[CuL']^{2+}$ species at this pH.

$[CuL'H_{-2}]$ is a minor species, and the stepwise constant ($\log K_{11-2} = 7.19$) is consistent with the deprotonation of an additional amide group. The EPR parameters of $[CuLH_{-2}]$ could not be obtained owing to the contemporary presence of different complex species whilst the spectroscopic parameters ($\lambda_{max} = 580$ and $\varepsilon = 100$) could be determined by UV-vis titrations carried out at room temperature. These parameters are similar to those obtained for $[CuL'H_{-1}]^{+}$ and are indicative of a 3N coordination mode; however, in this species an imidazole nitrogen atom has been substituted by an amide nitrogen ($1N_{Im}$, $2N^{-}$).

$[CuL'H_{-3}]^{-1}$ is the predominant complex species at pH 8. The blue-shift of the absorption maximum band, the increase in the CD spectra of $N^{-} \rightarrow Cu(II)$ charge transfer band at 310 nm and the EPR parameters (see Table 3) clearly indicate the deprotonation of a third amide nitrogen atom leading to a copper(II) 4N (N_{Im}, $3N^{-}$) coordination mode. Since the deprotonation of the first amide group takes place in the proximity of His8, the deprotonation steps for the species $[CuL'H_{-2}]$ and $[CuL'H_{-3}]^{-1}$ should involve Phe7 and Ile6. This implies that the imidazole side chain of His4 is not involved in the copper(II) coordination at all; this is in line with the EPR parameters that indicate a planar arrangement around the metal ion.

The distribution diagram (Fig. 17b) shows that copper(II) forms complexes with NGF1-14 above pH 4. At this pH a protonated species forms, $[CuLH]^{3+}$, the stepwise stability constant ($K_{(111)} = \beta_{(111)} - K_{(011)} = 6.53$) of which is similar to that of the analogous complex

species $[CuL]^{2+}$ formed by AcNGF1-14. This indicates that at low pH value both peptides have the same coordination mode ($2N_{Im}$, COO^-) which is also corroborated by the NMR measurements. Similarly to the Cu-Ac-NGF1-14 system, the aromatic proton signals of the two histidine and glutamate residues are markedly affected by Cu^{2+} addition (Fig. 19). The C-terminal domain is not affected, while the N-terminal region shows a different trend. The broadening of Ser2-Ser3 resonances, more pronounced that in AcNGF1-14 system, indicates that the amine group of Ser1 is somehow involved in the metal coordination. However, the UV-vis parameters obtained at room temperature for the analogous complex species of the two peptides are different. This may be due to the presence of different coordination isomers involving both $2N_{Im}$, COO^- and N_{NH2}, N_{Im} (histidine 4 or 8), COO^-. Unfortunately, we have been not able to obtain the EPR parameters of the predominant species at acidic pH.

$[CuL]^{2+}$ is only a minor species and its spectral parameters could not be determined. However, this species displays a larger stability constant value ($\log \beta_{(110)}$= 8.72) compared to that of the analogous Cu-AcNGF1-14 system. This indicates the presence of the amino group and two imidazole nitrogen atoms. The NMR results at pH 5.4 reported in figure 19 indicate some interesting differences with those obtained for AcNGF1-14 peptide. Glu11 signals vanish with a slower rate if compared to AcNGF while serine resonances experience a more pronounced broadening that in AcNGF. These data indirectly suggest the involvement of the free amino group in the metal coordination.

As pH increases, $[CuLH_{-1}]^{-1}$ becomes the predominant species. The stepwise constant value $\log K_{(11-1)}$, ($\log K_{(11-1)} = \log\beta_{(110)} - \log\beta_{(11-1)}$= 5.45) indicates the deprotonation of an amide nitrogen atom. Such value is quite similar to that obtained for the deprotonation of the first backbone nitrogen atom of the acetylated peptide. NMR measurements at pH higher than 5.5 are scarcely informative due to an excessive broadening of the signals.

$[CuLH_{-1}]^{+}$ CD spectra show dichroic signals that are diagnostic of the coordination environment. The bands at 285, 320, the shoulder at 340 nm and the strong positive dichroic signal centered at 260 nm result from the amino group-Cu^{2+} charge transfer (c.t.), the amide$\rightarrow Cu^{2+}$ c.t., the π_1 $N_{Im}\rightarrow Cu^{2+}$ c.t., and the π_2 $N_{Im}\rightarrow Cu^{2+}$ c.t , respectively (see table 3). The EPR parameters ($g_{\|}$ = 2.226 and $A_{\|}$ = 162 10^{-4} cm^{-1}) are very similar to those

reported for both the copper(II) complexes of Gly_5His peptides and some Aβ peptide fragments supporting the same (NH_2, N^-, N_{Im}) coordination mode.[278,284] These parameters are indicative of the presence of three nitrogen donor atoms in a highly distorted environment. This distortion from a square planar or pseudo-octahedral geometry is ascribable to the presence of an apical oxygen (e.g. a carboxylate) or an imidazole nitrogen atom.

It is worth to note that the absence of a complex species with parameters similar to those of AcNGF1-14 , strongly supports the formation of a five-membered chelate ring originating from the coordination of Ser1 NH_2 and Ser2 deprotonated amide nitrogen, the N_{Im} atom of a histidine residue, likely His4.

NMR measurements carried out on the Cu-NGF1-14 system at pH higher than 5.5 show a pronounced broadening of the signals. The NMR results obtained at pH 5.4 are reported in figure 19. At this pH values different complex species coexist (Fig 17b), and this prevents the assignment of the coordination environment. However, the NMR data indicate some interesting differences between the free and the acetylated peptide. In particular, the signals related to the N-terminal Ser residues are affected by Cu^{2+} addition, suggesting the involvement of the amino group.

At pH 8, $[CuLH_{-2}]$ is the predominant species. The UV-vis parameters (λ = 560 nm, ε = 130) and the increase of the amide band intensity indicate the involvement of four nitrogen atoms in this species, *i.e.* $1N_{NH2}$, $2N^-$ and $1N_{Im}$. The Hamiltonian parameters ($g_{\|}$ = 2.205 and $A_{\|}$ = 190 (10^{-4} cm^{-1}) corroborate the presence of a 4N chromophore with the donor atoms arranged in a planar coordination mode.

4.1.4 Proliferative effects of NGF and its N-terminus peptide fragments on SHSY5Y cells

The proliferative effect of NGF1-14, AcNGF1-14 and the whole protein NGF has been tested on neuronal cell line culture (neuroblastoma SHSY5Y), both in the presence and in the absence of metal ions. Dose response experiments showed a slight dose dependent increase (about +20% *vs* the control) of the number of cells following the addition of both NGF (10 to 100nM) and peptide fragments (10 to 100µM) (Fig. 20).

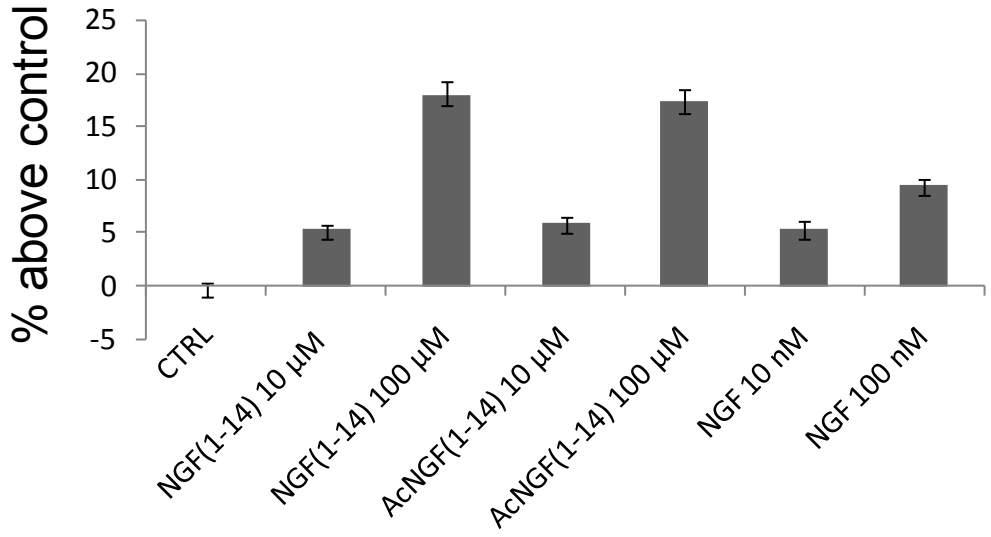

Figure 20. *Dose-dependent proliferative effect of NGF(1-14) (10 µM and 100 µM), AcNGF(1-14) (10 µM and 100 µM), and of the whole protein NGF (10 nM and 100 nM) on neuroblastoma SHSY5Y.*

These data indicate that both peptides can mimic the activity of the whole protein in these conditions, although the same proliferative effect is achieved when the concentration of NGF1-14 or AcNGF1-14 is 100-fold higher than NGF concentration. Of note, the proliferative effect induced by the acetylated AcNGF1-14 is the same as that of the amino free NGF1-14 (Fig. 20). This is in agreement with the crystal structure of the complex between NGF and its TrkA receptor binding site, which shows that Ser1 is not involved in the interaction.

The results of the co-treatments with both peptide fragments and metal ions (Cu^{2+} and Zn^{2+}) are reported in Figure 21.

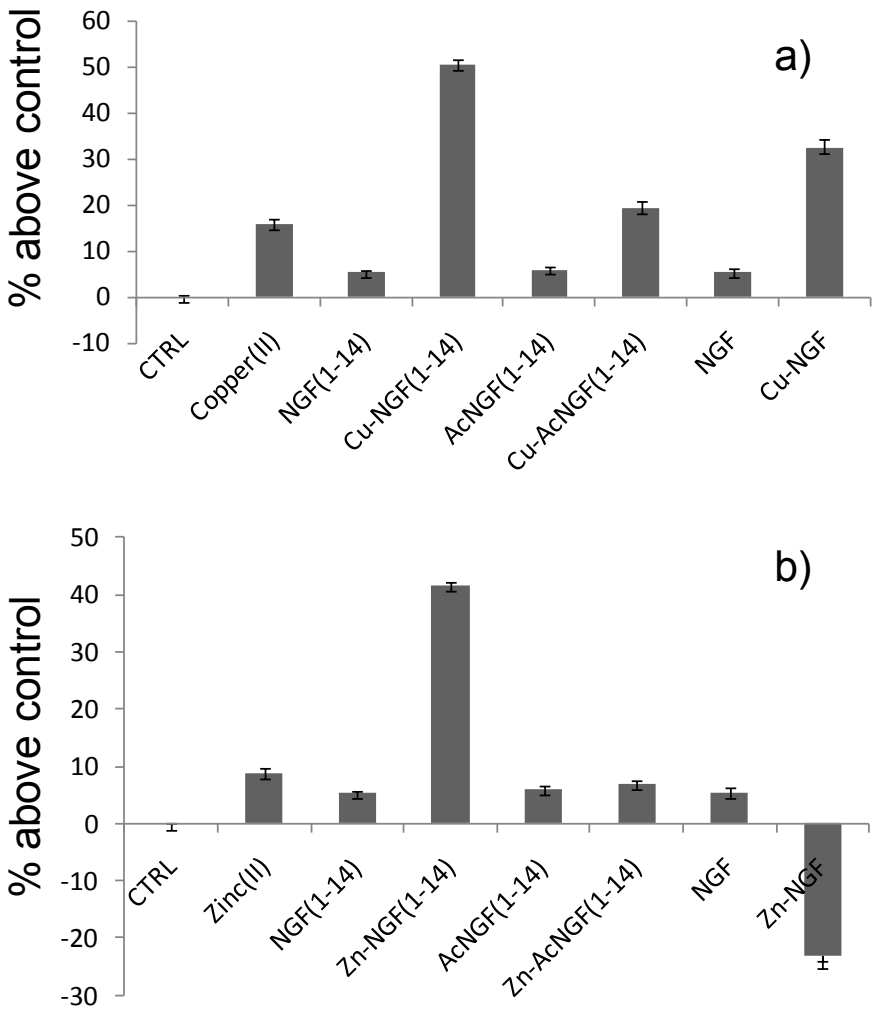

Figure 21: *Proliferative effect of NGF(1-14) (10 μM), AcNGF(1-14) (10 μM) and the whole protein NGF (10 nM) on neuroblastoma SHSY5Y, as evaluated without and with addition of 10 μM Cu^{2+} (a) or 10 μM Zn^{2+} (b). The data are normalized with respect to control samples set to zero*.

Copper(II) and zinc(II) increase the proliferative effect (+15% and +8%, respectively) over the control experiments; on the other hand, the proliferative activity of NGF1-14 significantly increased in the presence of Cu(II) (+50%) (Fig. 21a) or Zn(II) (+45%) (Fig 21b). These effects are synergic, since the cell number grows up by more than the sum of

the effects caused separately by the metals or the peptide. The same synergic effect is not detected in the presence of Cu-AcNGF1-14 and Zn-AcNGF1-14, highlighting the critical role played by the free amino group. The role of metal ions has been also studied on NGF by using the metal-protein molar ratio reported in a previous study. The SHSY5Y cell culture treated with 10 nM NGF and copper (10 μM), shows a synergic increase of the cell number (+32%). On the contrary, co-treatment with 10 μM Zn^{2+} and NGF 10 nM inhibits the cell growth by 25%.

Intriguingly, preliminary studies suggest that the co-treatment with NGF(1-14) and copper(II) induce the increase in the intracellular copper concentration (Fig. 22 and Fig 23). Such effect has not been observed neither after the treatment of copper(II) nor with NGF(1-14).

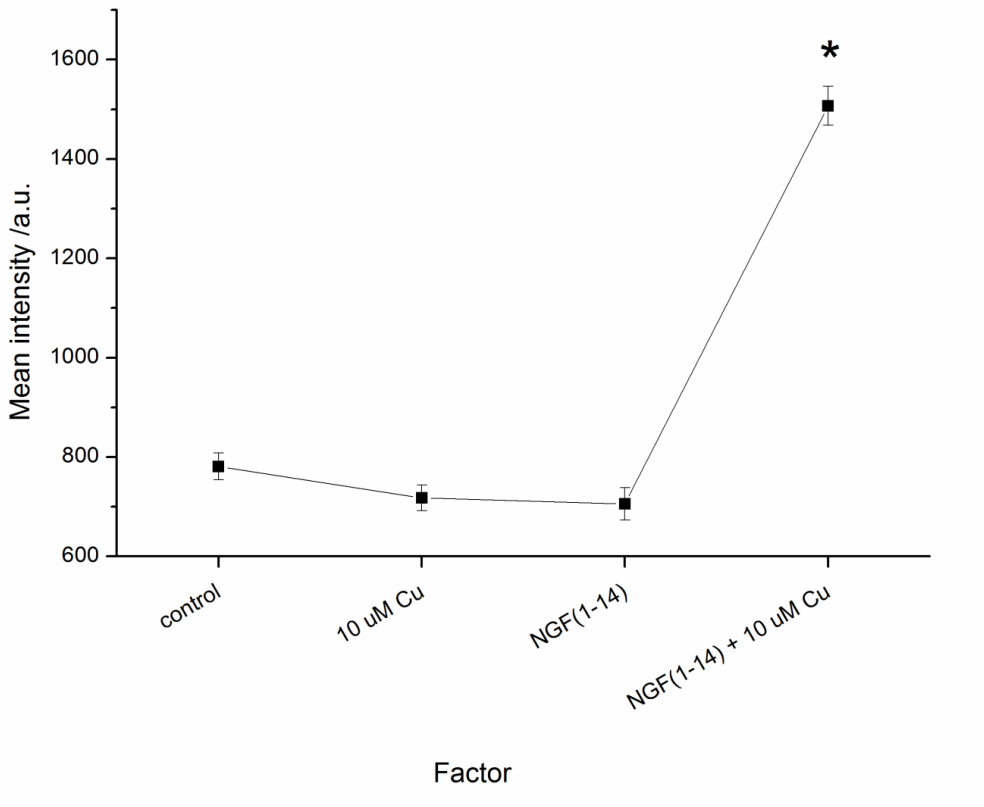

Figure 22. *Mean values of fluorescence intensities (λex=543, λem=550-620 nm) for neuroblastoma SH-SY5Y cells treated by 500 nM 1@NP copper(I)sensor. Mean values +/- S.E.M. (*= means difference is significant at the 0.01 level).*

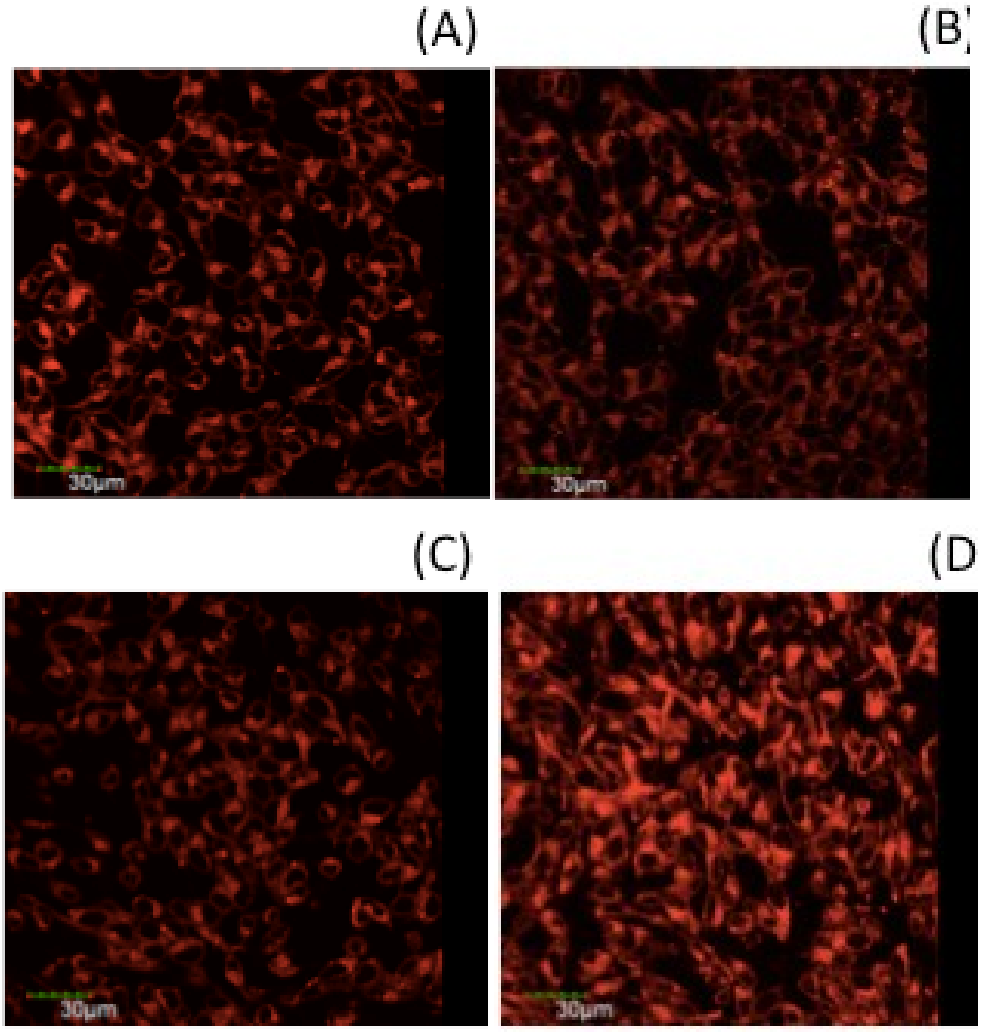

Figure 23. *Live-cell imaging results from LSM analysis of neuroblastoma SH-SY5Y cells treated with 500 nM 1@NP in PBS (10 mM, pH=7.4): control cells (A) and cells supplemented during 24 hrs in the culture medium with 10 μM $CuSO_4$ (B); NGF(1-14) (C); 10 μM $CuSO_4$ + NGF(1-14) (D).*

4.2 Characterization of BDNF(1-12) and its metal complexes

A BDNF N-terminus peptide fragment encompassing the residues 1–12 blocked at the C-terminus, namely, HSDPARRGELSV-NH_2 (BDNF(1-12), Fig. 24) has been synthesized to ascertain the coordination features of Cu^{2+} complexes with the BDNF N-terminal domain. The Cu^{2+} complexes with BDNF(1-12) have been studied by means of potentiometry, spectroscopic techniques (UV/Vis, CD, NMR and EPR), parallel tempering simulations and DFT-based geometry optimizations. The coordination features of the acetylated form Ac-HSDPARRGELSV-NH_2 (AcBDNF(1-12)) have been also characterized to prove (or disprove) the involvement of the terminal amino group (see Fig. 24). In addition, the role of the Asp residue has been assessed by the synthesis of a single mutated peptide HSNPARRGELSV-NH_2 (BDNF(1-12)D3N). Moreover, the functional interaction of Cu^{2+} with BDNF peptides or with the whole protein has been tested by measuring the effects on the proliferation rate of SHSY5Y neuroblastoma cell line culture.

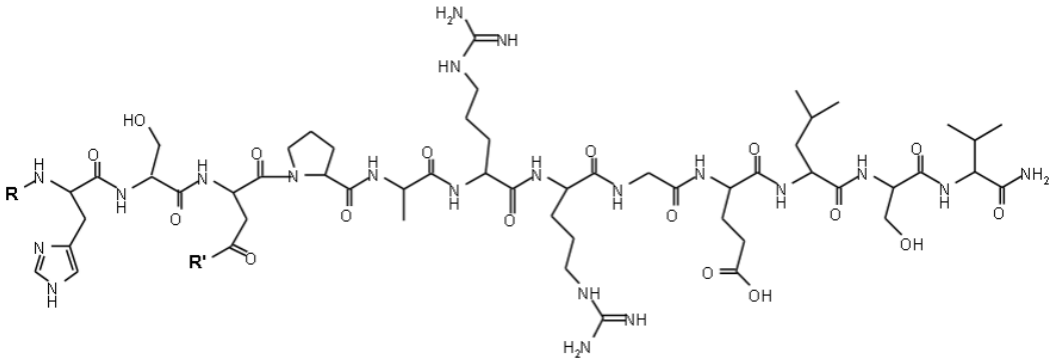

Figure 24. *Schematic view of primary sequences of peptides investigated BDF(1-12), Ac-BDNF(1-12) and BDNF(1-12)D3N*.

4.2.1 Protonation constants and conformational features of BDNF(1-12), BDNF(1-12)D3N and Ac-BDNF(1-12)

Protonation constants of the studied peptides have been determined by potentiometric titrations and are reported in Table 4.

Table 4. *Protonation constants (log β_{pqr}) and pK values for BDNF(1-12), BDNFD3N(1-12) and Ac-BDNF(1-12) (T = 298°K, I = 0.1 mol dm^{-3} KNO_3).*[a]

Species	*BDNF(1-12)*	*BDNF(1-12)D3N*	*Ac-BDNF(1-12)*
LH	7.44 (1)	7.50 (1)	6.44 (1)
LH_2	12.97 (1)	12.99 (2)	10.75 (1)
LH_3	17.19 (1)	17.02 (2)	14.07 (1)
LH_4	20.39 (1)	-	-
pK COO^-	3.20	-	3.32
pK COO^-	4.22	4.03	4.31
pK His	5.53	5.49	6.44
pK NH_2	7.44	7.50	-

[a] Standard deviations (3σ values) are given in parentheses. Charges are omitted for clarity.

The ligands show four (BDNF(1-12)) and three (Ac-BDNF(1-12), BDNF(1-12)D3N) proton-accepting centers, as expected. The amino group is the most basic center of BDNF(1-12) and BDNF(1-12)D3N. The two protonation equilibria of the aspartic and glutamic residues in BDNF(1-12) and Ac-BDNF(1-12) partly overlap; the comparison with the pK value of glutamate residue of BDNFD3N suggests that the lowest pK values of the wild type peptides belongs to the aspartic residue. This assessment is in agreement with the general finding indicating aspartic β-carboxylic group is more acidic than glutamic γ-carboxylic one and the pK value obtained agrees with that found for other peptides containing aspartic and glutamic residues.[278,284-286] Taking into account the low differences in the pK values of BDNF(1-12) and the mutated BDNF(1-12)D3N, an electrostatic interaction between the aspartic carboxyl group and the amino group of Histidine residue can be ruled out. The imidazole basicity of the histidine residue in BDNF(1-12) and BDNF(1-12)D3N is lower than that displayed by the heterocyclic residue in the acetylated

peptide Ac-BDNF(1-12). This difference in the pK values is originated by electrostatic interaction with the more basic amino group, an effect observed in other peptides encompassing the histidine in the first position of the sequence.[287]

Parallel tempering simulations confirm the potentiometric data: the conformations of BDNF(1-12), Ac-BDNF(1-12) and BDNF(1-12)D3N span extended and bent states which are shown in Figure 25. Those are featured by intra-chain hydrogen bonds. The N-terminal amine group is prone to form hydrogen bonds involving Nε nitrogen of His-1 in those peptides which are not N-terminally blocked, as BDNF(1-12) and BDNF(1-12)D3N (Fig. 25) justifying the different pK values of imidazole in comparison with the acetylated peptide. Moreover, the carboxyl groups of Asp-3 belonging to BDNF(1-12) and Ac-BDNF(1-12) form hydrogen bonds with Arg-6 or Arg-7 (Fig. 25b and 25c of Ac-BDNF(1-12)). The former weak interactions are lost in Ac-BDNF(1-12) concerning the amine group and in BDNF(1-12)D3N concerning Asp-3 residue (Fig. 25).

On the whole the investigated peptides do not display a definite secondary structure region and the far-UV CD spectra confirm that all three peptides adopt predominantly a random coil conformation over the pH range investigated (4-11).

The addition of Cu^{2+} does not induce significant changes on the secondary structure region of BDNF(1-12) and BDNF(1-12)D3N peptides differently to that observed for the acetylated fragment Ac-BDNF(1-12) (Fig. 26).

In the Cu-BDNF(1-12) system a maximum at 215 nm appears at increasing pH values and the apo-subtracted difference spectra show a slight increase of a turn structure determined by copper(II) amide nitrogen atoms binding (Fig. 26a and inset). This effect is less evident in the analogous system with the mutated peptide BDNF(1-12)D3N (Fig. 26b). The copper(II) addition to the Ac-BDNF(1-12) peptide induces a gradual loss of intensity of the negative signal at 199 nm and the appearance of a positive band at 210 nm (Fig. 26c). The CD spectra differences indicate a clear increase of the turn conformation of the peptide, resulting from the involvement of backbone amide nitrogen atoms in Cu^{2+} coordination.[288]

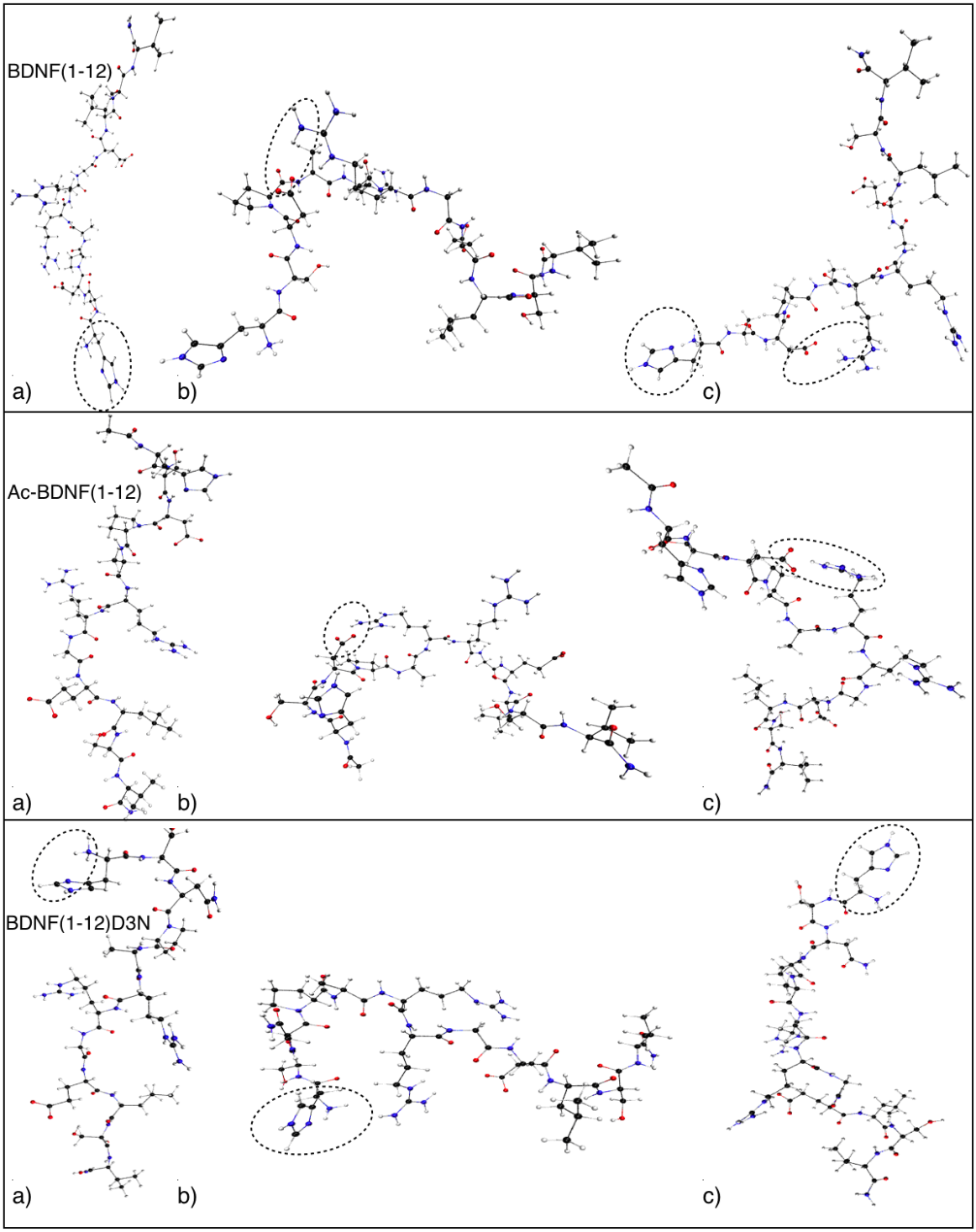

Figure 25. *The three main clusters of BDNF(1-12), Ac-BDNF(1-12) and BDNF(1-12)D3N. The hydrogen bonds involving the N-terminal amine and the Nε nitrogen of His-1 can occur only in BDNF(1-12) (a,c) and BDNF(1-12)D3N (a,c). The hydrogen bonds involving Asp-3 and Arg-6 or arg-7 can occur only in BDNF(1-12) (b,c) and Ac-BDNF(1-12) (b,c). Carbon atoms are shown in black, nitrogen in blue and oxygen in red spheres.*

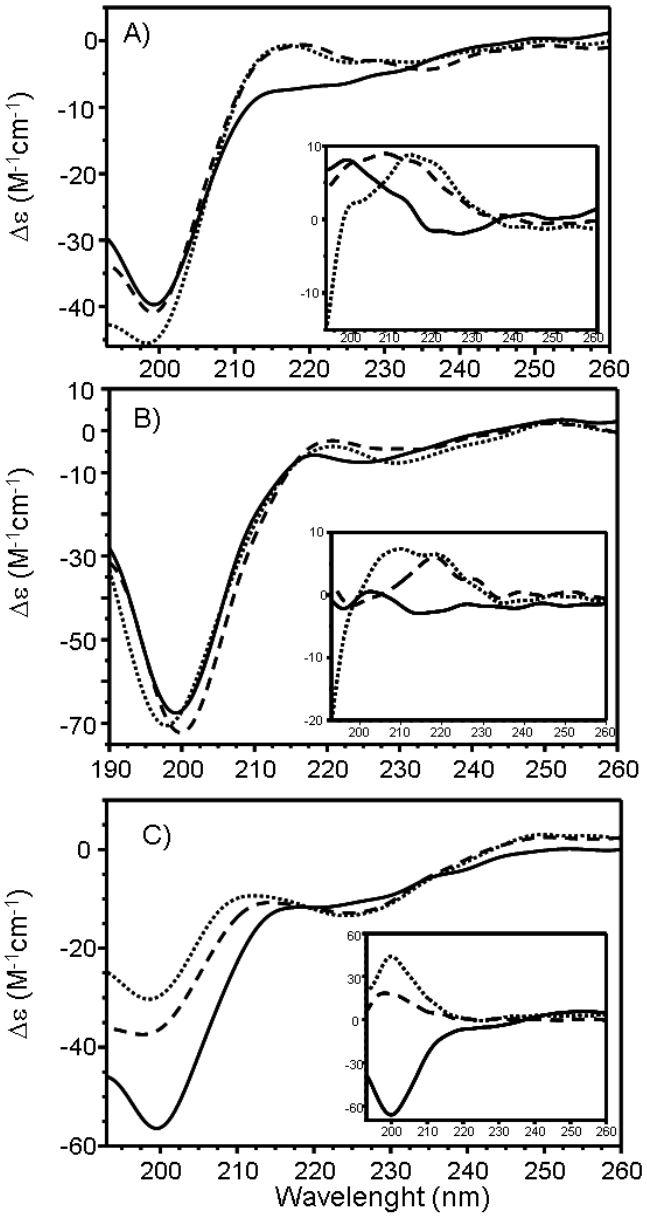

Figure 26. *Far-UV CD spectra at pH 5, 7.4 and 10 of copper(II) complexes with a) BDNF(1-12), b) BDNF(1-12)D3N and c) Ac-BDNF(1-12). Inset: The apo subtracted difference spectra.*

The comparison of CD data indicate that the involvement of the amino group in copper(II) binding in BDNF(1-12) and BDNF(1-12)D3N (see next section) induces less conformational change in the peptide backbone in comparison to the acetylated peptide fragment.

4.2.2 Speciation, stability constants and coordination modes of copper(II) complexes with BDNF(1-12), Ac-BDNF(1-12) and BDNF(1-12)D3N

The overall stability constant values of the metal complexes with the peptides are listed in Table 5, while the distribution diagrams are reported in Figure 27.

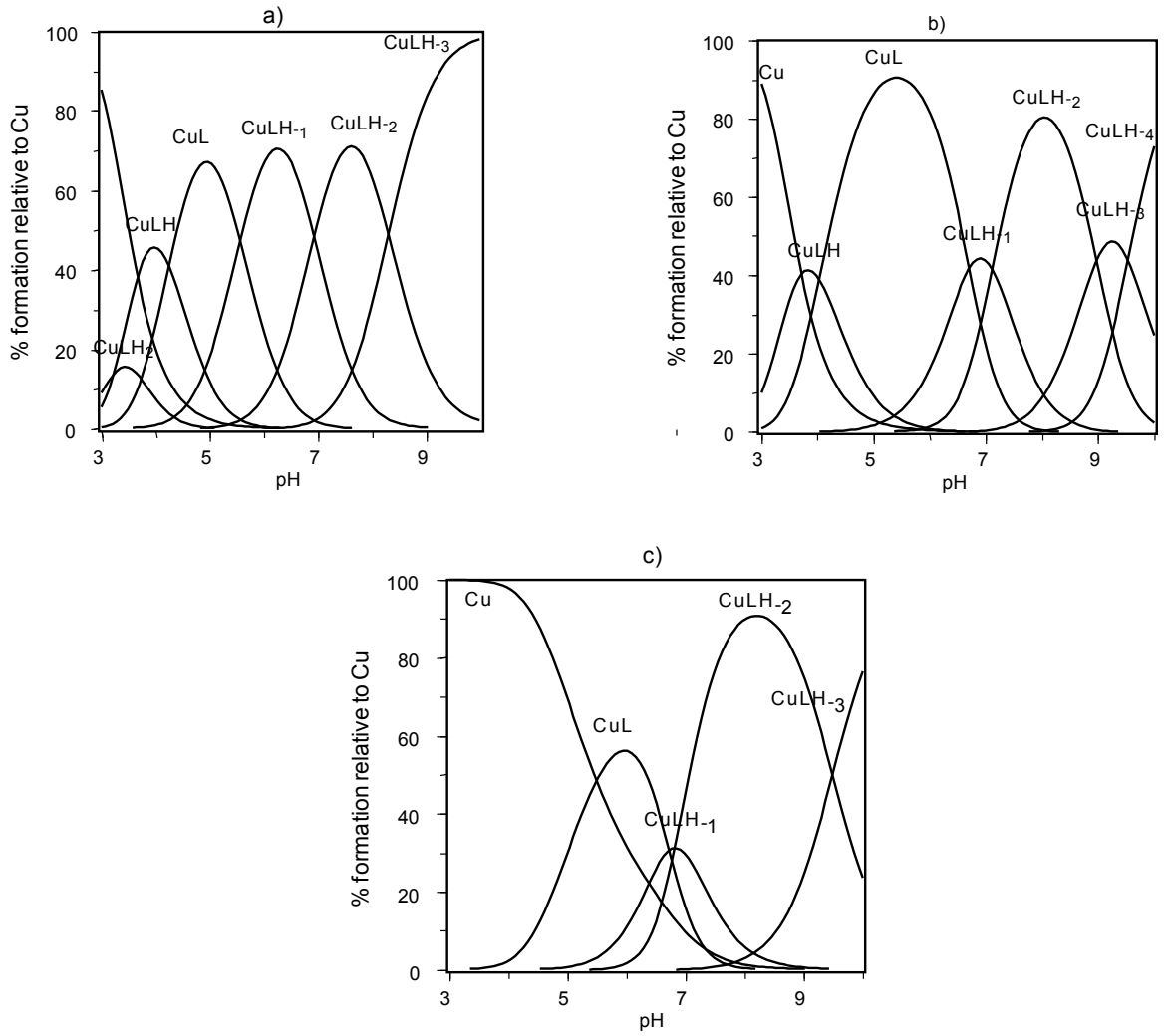

Figure 27. *Species distribution diagram for Cu(II) complexes with A) BDNF(1-12), B)BDNF(1-12)D3N and C) Ac-BDNF(1-12) Charges are omitted for clarity. [L]=1x10-3 mol dm-3, M/L molar ratio 1:1.*

Table 5. Stability constants (log β_{pqr}) and pK values of Cu (II) complexes with BDNF(1-12), BDNFD3N(1-12) and Ac-BDNF(1-12) (T= 298°K, I= 0.1 mol dm^{-3} KNO_3).[a]

Species	*BDNF(1-12)*	*BDNF(1-12) D3N*	*Ac-BDNF(1-12)*
	$log\beta_{pqr}$	$log\beta_{pqr}$	$log\beta_{pqr}$
$CuLH_2$	16.40 (5)	-	-
CuLH	13.18 (2)	12.86 (1)	-
CuL	8.93 (2)	8.83 (1)	4.03 (2)
$CuLH_{-1}$	3.37 (2)	2.12 (2)	-2.68 (3)
$CuLH_{-2}$	-3.56 (3)	-5.25 (1)	-9.51 (3)
$CuLH_{-3}$	-11.87 (3)	-13.97 (2)	-19.00 (3)
$CuLH_{-4}$	-	-23.50 (2)	-

[a] *Standard deviations (3σ values) are given in parentheses. Charges are omitted for clarity.*

The first species formed by BDNF(1-12) is $[CuLH_2]^{2+}$. The stepwise stability constant value calculated for this complex species ($logK = log\beta_{121} - log\beta_{021} = 3.43$) suggest the involvement of one nitrogen atom without the assistance of a carboxyl group.[276] Taking into account the strong acidic pH range of this species formation, it is possible that the glutammate carboxylate group is still protonated with one between amino and imidazole nitrogen atom deprotonated.[289] Due to its low percentage of formation it is not possible to determine its spectral parameters.

The stability constant value calculated for the next complex species $[CuLH]^+$ ($logK = log\beta_{111} - log\beta_{011} = 5.74$) indicates the coordination of two nitrogen atoms to the metal ion.[48] The logK value calculated for the analogous species formed with single mutated peptide BDNF(1-12)D3N is similar ($logK = log\beta_{111} - log\beta_{011} = 5.31$) and in agreement with the hypothesis of a histamine-like coordination of copper ion with the glutamate group still protonated. The slight higher value for BDNF(1-12) is due to a weak interaction of aspartic carboxylate group in copper(II) binding. However, the contemporary presence of other complex species does not permit the determination of spectroscopic parameters.

Increasing the pH, the deprotonation of the glutamate γ-carboxylate group occurs and this is not bound to the metal ion in the [CuL] ($logK = log\beta_{111} - log\beta_{101} = 4.25$; pK $COOH_{Glu}$ = 4.22). The stability constant value for the analogous species formed by BDNF(1-12)D3N is similar and also in this case the log K deprotonation step corresponds to pK value of

glutammic carboxylate group (Table 4). However, the UV-vis parameters (λmax= 648 ε= 55) indicate a stronger ligand field around copper(II) ion for Cu-BDNF(1-12) system, in comparison with the analogous species formed by BDNF(1-12)D3N, indicating the formation of a CuN_2O_2 chromophore with the metal ion bound to two nitrogen atoms and one carboxylate (N_{NH2}, N_{im}, COO^-_{Asp}, $2O_{water}$) (Fig. 28). The UV-vis parameters of $[CuL]^+$ formed by BDNF(1-12)D3N are similar to those reported for the analogous species formed by histamine and His-Gly in which the metal ion shows a N_{NH2}, N_{Im} coordination mode (Fig. 28).[286,289] Moreover, for this last species it has been possible to determine the EPR parameters at pH 5 ($g_{||}$ = 2.283 and $A_{||}$ = 179 $\times 10^{-4}cm^{-1}$) which confirm a histamine-like coordination.[290-291]

Noteworthy, in the case of Cu-BDNF(1-12) system, it has not been possible to determine EPR parameters for the poor resolution of the spectra up to pH 6.The cause of a similar logβ value for these two copper(II) complex species in which the metal ion display a different coordination environment lies in the loss of different intramolecular weak interactions between the two peptides as determined by parallel tempering simulations (see previous section). Therefore, the increase of stability constant determined by the coordination of carboxylate group to metal ion is counterbalanced by the break of electrostatic bonding between the Asp-4carboxylate and guanidine group of Arg-6 and/or Arg7.

The CD parameters, determined by combined pH-metric and spectroscopic titrations (see experimental section) for [CuL] species (Table 6) are similar to those reported for other copper(II) complexes, in which the metal ion is bound to donor atoms in a macrochelate ring, without the involvement of the peptide backbone.

The copper(II) complex with BDNF(1-12) shows a band at 270 nm due to the presence of the amino group in the metal ion coordination environment.[292] A further support to the amino group binding is provided by the absence of this band in the analogous [CuL] species formed by the acetylated peptide Ac-BDNF(1-12).

Table 6. *Spectroscopic parameters of copper(II) complexes with BDNF(1-12), BDNF(1-12)D3N, Ac-BDNF(1-12). [L] = 1x10^{-3} mol dm^{-3}.*

	Species	UV-vis $\lambda_{max}(\varepsilon)$ [nm($M^{-1}cm^{-1}$)]	CD λ_{max} ($\Delta\varepsilon$) [nm($M^{-1}cm^{-1}$)]	EPR $g_{\|\|}/A_{\|\|}$ ($10^{-4}cm^{-1}$)	
BDNF (1-12)	CuL	648 (44)	304 (-0.156); 686 (0.255)	-	-
	$CuLH_{-1}$	555 (102)	312 (0.256); 502 (0.158); 686 (0.181)	-	-
	$CuLH_{-2}$	540 (128)	312 (0.564); 502 (0.204)	2.200 (1)	204 (3)
	$CuLH_{-3}$	540 (130)	310 (0.568); 500 (0.208)	2.200 (1)	201 (3)
BDNF (1-12) D3N	CuL	670 (40)	334 (-0.113); 701 (0.129)	2.283 (1)	179 (3)
	$CuLH_{-1}$	-	300 (-0.495); 639 (0.172)	-	-
	$CuLH_{-2}$	550 (140)	313 (0.903); 490 (0.222); 585 (-0.225)	2.200 (1)	200 (3)
	$CuLH_{-3}$	525 (130)	310 (0.696); 491 (0.495); 565 (-0.452)	2.174 (1)	201 (3)
	$CuLH_{-4}$	525 (130)	308 (0.610); 490 (0.492); 565 (-0.614)	-	-
Ac-BDNF (1-12)	CuL	708 (51)	305 (0.319); 361 (-0.100)	2.323 (1)	160 (3)
	$CuLH_{-1}$	-	305 (-1.051); 357 (0.886); 511 (0.100); 581 (-0.104); 649 (0.319)	-	-
	$CuLH_{-2}$	620 (110)	305 (-1.402); 357 (1.211); 491 (0.104); 567 (-0.252); 653 (0.369)	2.235 (1)	167 (3)
	$CuLH_{-3}$	581 (114)	301 (-0.506); 352 (0.601); 521 (-0.626); 663 (0.357)	2.200 (1)	185 (3)

Errors in $\lambda = \pm 2$ nm and $\varepsilon = 5\%$. Charges are omitted for clarity.

The [CuL] is the first complex species formed by Ac-BDNF(1-12), with a (N_{im}, COO^-_{Asp}, $2O_{water}$) coordination mode. This copper complex species results to be the prevailing metal complexes up to pH 6.5. The stability constant value is 4.03, a value higher than that generally reported for the coordination of only one imidazole nitrogen, clearly indicating the metal binding of aspartate β-carboxyl group besides water oxygen atoms (Fig. 28).

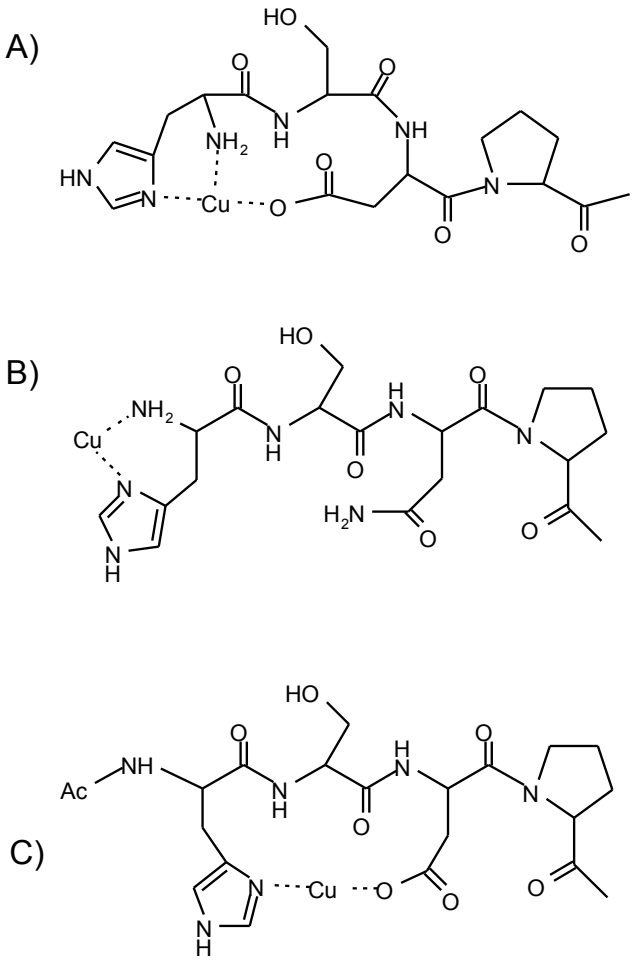

Figure 28. *Schemes of [CuL] complex species: A) L= BDNF(1-12); B) L= BDNF(1-12)D3N; C) L= Ac-BDNF(1-12). Metal ion coordination environment is completed by water molecules and/or carbonyl group (not shown).*

It is interesting to note that the logβ value determined is lower to that reported for analogous system in which copper ions display a similar coordination environment and a similar membered macrochelate ring, [287,290] but also in this case the logβ value is influenced by the break of the weak electrostatic interaction between the carboxylate and

the guanidine group present in the apo-ligand. The EPR parameters reported in Table 6 ($g_{||}$ = 2.323 and $A_{||}$ = 160 $\times 10^{-4}cm^{-1}$), confirm the involvement of both, the carboxylate group together with the imidazole nitrogen atom in metal binding. [287,290] The parallel hyperfine coupling constant value ($A_{||}$) is higher than those reported for other $CuNO_3$ chromophores, in which the metal is coordinated by an imidazole nitrogen and a carbonyl oxygen atom, being indicative of a stronger equatorial field due to the negative charge of the carboxylate oxygen.[293]

The involvement of the glutammic carboxylate group in the metal ion coordination can be ruled out for all studied peptides, taking into account the primary sequence (the aspartic is in third position whereas Glu is the ninth amino acid residue). However, in general the glutammic γ-carboxylic group has a lower influence in comparison with the shorter β-carboxilic side chain group of the aspartic residue.[285]

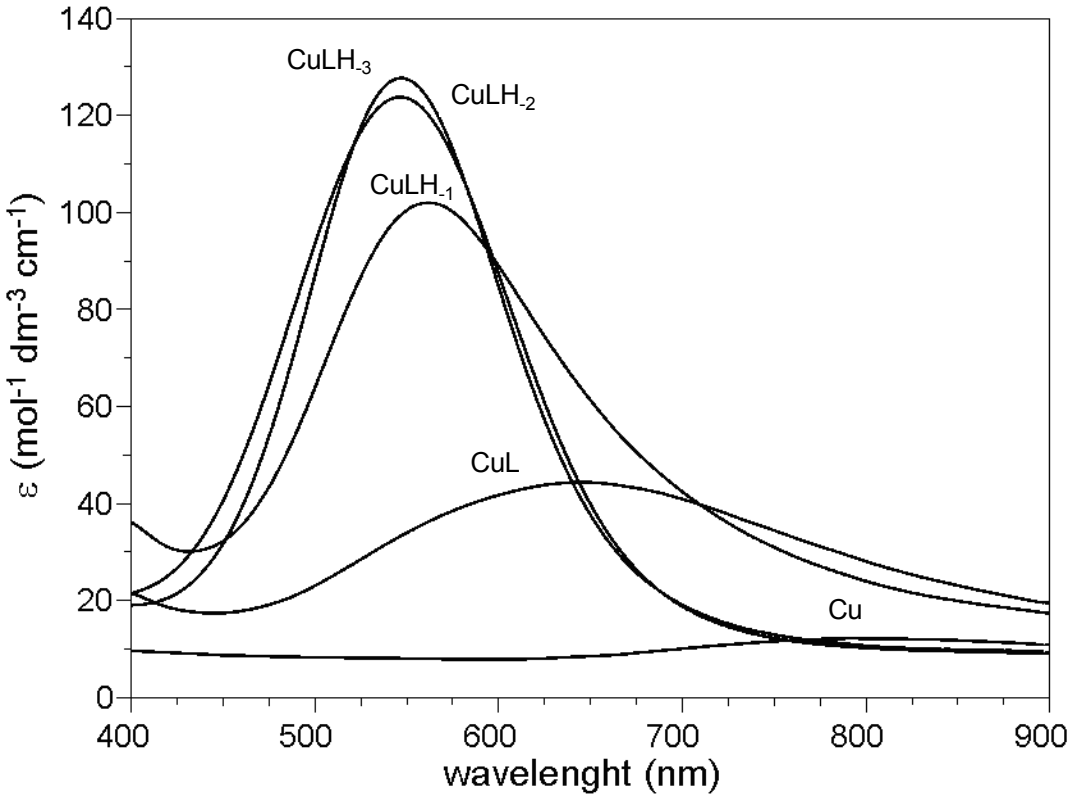

Figure 29. *UV-vis spectra of Cu-BDNF(1-12) system obtained by titration experiments and processed by means of HYPERQUAD program*.

The formation of [$CuLH_{-1}$] involves the deprotonation of an amide nitrogen atom. The pK value (Table 5) for Cu-BDNF(1-12) system indicates that this deprotonation is favoured by the coordination of the carboxylate group. The pK value of the analogous species formed with the mutated BDNF(1-12)D3N is one logarithmic unit higher (Table 5). The UV-vis parameters calculated by means of titration experiments (λ= 555 nm; ε = 102 mol^{-1} dm^{-3} cm^{-1}) show a strong blue-shift in comparison with the [CuL] species. The amino and imidazole nitrogens, one deprotonated amide nitrogen and the carboxylate group bind Cu^{2+}. This coordination mode results in a slightly distorted geometry: the three nitrogen donors cannot contemporary coordinate in the equatorial plane without give rise to a significant distortion of metal coordination geometry. The EPR parameters determined at pH 6.5 in which the $[CuLH_{-1}]^-$ is the predominant species, are indicative of a planar disposition of at least three nitrogen atoms. Indeed, the UV-vis spectra obtained for this species display a wide band caused by the presence of two isomers in which the metal has a different coordination environment (Fig. 29). An analogous system in which the copper(II) ion is bound to N_{NH2}, N_{Im}, N^-, COO^- shows λ_{max} around 600 nm. [285,290] The comparison with spectroscopic data UV-vis and CD assigned to [$CuLH_{-2}$] species indicate that one isomers may be [$CuLH_{-2}$(H)] with two deprotonated amide and the imidazole protonated. The deprotonation and coordination of the second amide nitrogen results in the formation of a very stable [$CuLH_{-2}$] species, with a [5,5,6] chelation rings, due to the presence in the third position of aspartic residue (Fig. 30).[278,285,290]

The EPR parameters are unchanged in the pH range 6.5-10 and strongly support the absence of ligand in axial position. The Uv-vis parameters (Table 6) are in agreement with the presence of N_{NH2}, 2N-, COO- donor atoms in the metal equatorial plane, and the CD spectrum shows an increase of the $N^- \rightarrow Cu^{2+}$ charge transfer band at 355 nm, while the band centered at 270 nm is unaffected.

To evaluate the metal coordination geometry in [$CuLH_{-1}$] and [$CuLH_{-2}$] DFT-based geometry optimizations have been carried out. The minimum energy structures of the former complexes predicted through DFT are reported in Figure 31.

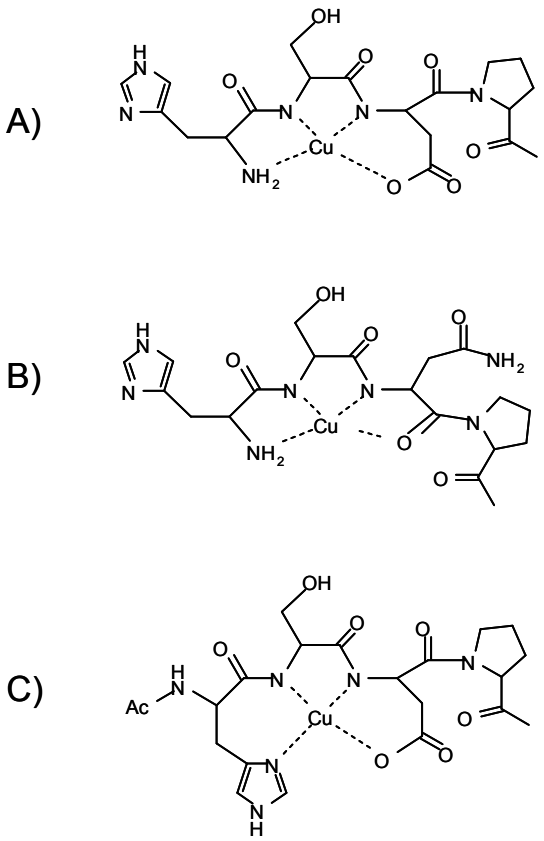

Figure 30. Schemes of [$CuLH_{-2}$] complex species: A) L= BDNF(1-12); B) L= BDNF(1-12)D3N and C) L= Ac-BDNF(1-12).

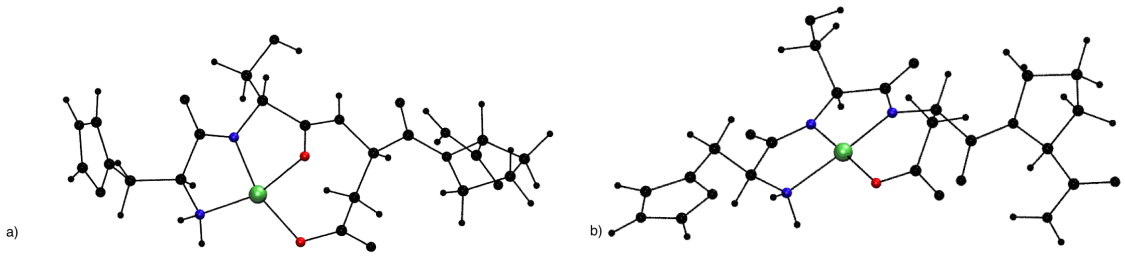

Figure 31. *Coordination polyhedron of $CuLH_{-1}$ species of HSDP sequence of BDNF. b) Coordination polyhedron of $CuLH_{-2}$ species of HSDP of BDNF. Copper is shown in green, nitrogens in blue, oxygens in red and BDNF backbone is shown in black spheres*.

[$CuLH_{-2}$] adopts a Type-II tetragonal coordination geometry in which Cu^{2+} is bound to NH_2, $2N^-$, COO^- and the metal ion lays in the ligand square plane, in agreement with experimental data. Whereas in the [$CuLH_{-1}$] the copper(II) coordination environment with lower energy involves the N-terminal amine group and the backbone nitrogen of His-1, the carbonyl oxygen of Ser-2 and carboxylate side-chain of Asp-3, and adopts a Type-II distorted tetragonal coordination geometry. The highest deviation from the planarity in the [$CuLH_{-1}$] is observed in the carbonyl oxygen of Ser-2 and in the carboxylate of Asp-3 (Fig. 31a). The former ligands are involved in a macrochelate ring upon the coordination to Cu^{2+}. In particular, at variance with the planar [$CuLH_{-2}$] polyhedron, the [$CuLH_{-1}$] complex is identified by a larger NH_2-Cu-O_{Asp} bending angle (111.3° versus 95.5° in [$CuLH_{-2}$]). Moreover, the improper torsion of the [$CuLH_{-1}$] coordination plane deviates 28.4° degree from the planarity, whereas only 5.1° is observed in the [$CuLH_{-2}$] species.

The [$CuLH_{-1}$] is only a minor species for BDNF(1-12)D3N and its spectroscopic parameters cannot be determined. Also the next deprotonation step is higher in comparison with the analogous species of BDNF(1-12). The spectroscopic parameters suggest the involvement in the binding of N_{NH2}, 2N- and carbonyl group, ruling out the presence of imidazole nitrogen atom coordinated in axial position (Table 6).[294]

The characterization of the copper(II) complex species formed by Ac-BDNF(1-12) highlights the main role played by the amino group in the metal binding to BDNF(1-12). The stability constant values of Cu-Ac-BDNF(1-12) reveal that the macrochelate formation in this case delays the first amide nitrogen deprotonation step and the metal ion coordination of amide group in the $[CuLH_{-1}]^-$. This is due to the different size of chelate rings [7,5] that occurs when the imidazole is the anchoring site and the deprotonation takes place towards the C-terminus.[280-282,290] The pK of the second amide deprotonation, owing to the metal complex formation, is very similar to that of the first, while generally is at least one logarithmic unit higher. [280-282,290] The metal ion coordination mode is characterized by the involvement of the N_{Im}, $2N^-$, COO^- donor atoms (Fig. 30). The UV-vis parameters are very different in comparison with those reported for analogous species formed by BDNF(1-12) (Table 6). This is clearly due to the formation of a sequence [7,5,6] membered chelate rings in which the more basic amino group is substituted by imidazole nitrogen. These parameters are similar to those reported for analogous species

formed with other acetylated peptides and consistent with a CuN_3O_1 coordination mode involving one imidazole and two amide deprotonated nitrogen atoms.[286,289]The relatively high λ and ε value, indirectly suggests an involvement of the carboxylate group in binding to Cu^{2+}. The EPR parameters (Table 6) indicate an apical interaction in the copper(II) complexes. In fact, differently to that observed for the Cu-BDNF system, the different chelate ring size induces a lower rigidity of the equatorial plane formed by donor atoms. The relatively high value of hyperfine coupling constant and theoretical studies carried out on similar system, suggest that the β-carboxylate group is coordinated in equatorial position in a tetrahedrically distorted square planar arrangement. [294-296]

Increasing the pH, other deprotonated species are formed. These are not relevant for biological activity, taking into account that their maximum percentage formation is over pH =9. The deprotonation step in the $[CuLH_{-3}]$ formation should involve the amide nitrogen atom of the fifth residue, alanine, water hydrolysis or guanidine group of arginine, due to the presence of a proline residue in forth position. In the Cu-BDNF(1-12) system such a species displays the same spectroscopic parameters of the previous $[CuLH_{-2}]^{2-}$, indicating the same coordination environment for the metal ion, so the deprotonation may involve a group not involved in metal binding. On the contrary, the $[CuLH_{-3}]^{2-}$ species formed by mutated BDNF(1-12)D3N shows a blu-shift in the λ_{max} and a decrease of $g_{||}$ value, indicating the formation of a 4N chromophore with the deprotonation of the alanine amide or arginine guanidine group. [294]

The presence of aspartyl carboxylate side chain in third position gives reason of the difference observed between BDNF(1-12) and BDN(1-12)D3N, the carboxylate coordination to copper(II) ion facilitates the cooperative deprotonation of the preceding two amide functions, but precludes the deprotonation of the subsequent ones. The $[CuLH_{-3}]^{3-}$ formed by Ac-BDNF(1-12) shows a blue-shift and a decrease of ε. The spectroscopic parameters indicate the presence of a 4N chromophore so involving the deprotonation of the acetyl nitrogen atom. The hyperfine coupling constant is lower than that reported for the analogous complex species with a similar coordination mode due to the binding of imidazole nitrogen in axial position, as confirmed by the presence also for this species of the $N_{Im} \rightarrow Cu^{2+}$ charge transfer band at 355 nm in the CD spectrum.

4.2.3 Speciation, stability constants and coordination modes of zinc(II) complexes with BDNF(1-12), BDNF(1-12)D3N and Ac-BDNF(1-12)

The stability constant values of the complexes of Zn^{2+} with BDNF1-12, AcBDNF1-12 and BDNF1-12D3N are listed in Table 7.

Table 7. *Stability constants (log β_{pqr}) for the Zn^{2+} and Cu^{2+} complexes with NGF(1-14) and AcNGF(1-14) (T= 298 K, I=0.10 mol dm^{-3} KNO_3).*

Species	BDNF(1-12)	BDNF(1-12) D3N	Ac-BDNF(1-12)
ZnLH	9.49 (6)	9.99 (8)	-
ZnL	5.18 (1)	5.36 (1)	2.5 (1)

The acetylation of the terminal amino group simplifies the species distribution. In fact Zn^{2+} does not form any complex with AcBDNF1-12 up to pH 5 (Fig. 32**);** above this pH only the [ZnL] species forms. The protonated species formed by BDNF1-12 with Zn^{2+}, [ZnLH], displays a stability constant value ($\log K_{(111)} = \log\beta_{(111)} - \log K_{p(011)} = 2.49$) similar to the logβ value obtained for the analogous complex species [ZnL] formed with AcBDNF1-12. This indicates that the Zn^{2+} experiences the same coordination environment with the involvement of one imidazole nitrogen atom (N_{Im},$3O_{water}$) ruling out the coordination of amino group as well as carboxylic group.

The protonated species formed by BDNF1-12 with Zn^{2+}, [ZnLH], displays a stability constant value ($\log K_{(111)} = \log\beta_{(111)} - \log K_{p(011)} = 2.05$) lower to that obtained for BDNF1-12D3N, probably due to the different network of hydrogen bonds formed (see parallel tempering simulations of ligand). Taking into account the pH range of formation, the anchoring site for this complex species could be the imidazole nitrogen atom with the amino group still protonated.

The protonated species is a minor one for both BDNF1-12 and BDNF1-12D3N. The [ZnL] is the prevailing complex species in all pH range investigated (Fig. 32). The stability constant value are similar and indicate the formation of a more stable complex species with

respect to the protonated one, with the involvement of the amino group, which substitutes a water molecule in the Zn^{2+} coordination sphere. The Zn^{2+} is bound to N_{NH2}, $2N_{Im}$ and a further evidence of this coordination mode results by the absence of analogous complex species in the acetylated peptide, in which the amino group is blocked. Further increase of pH value induces the formation of a precipitate due to the hydrolytic species formation.

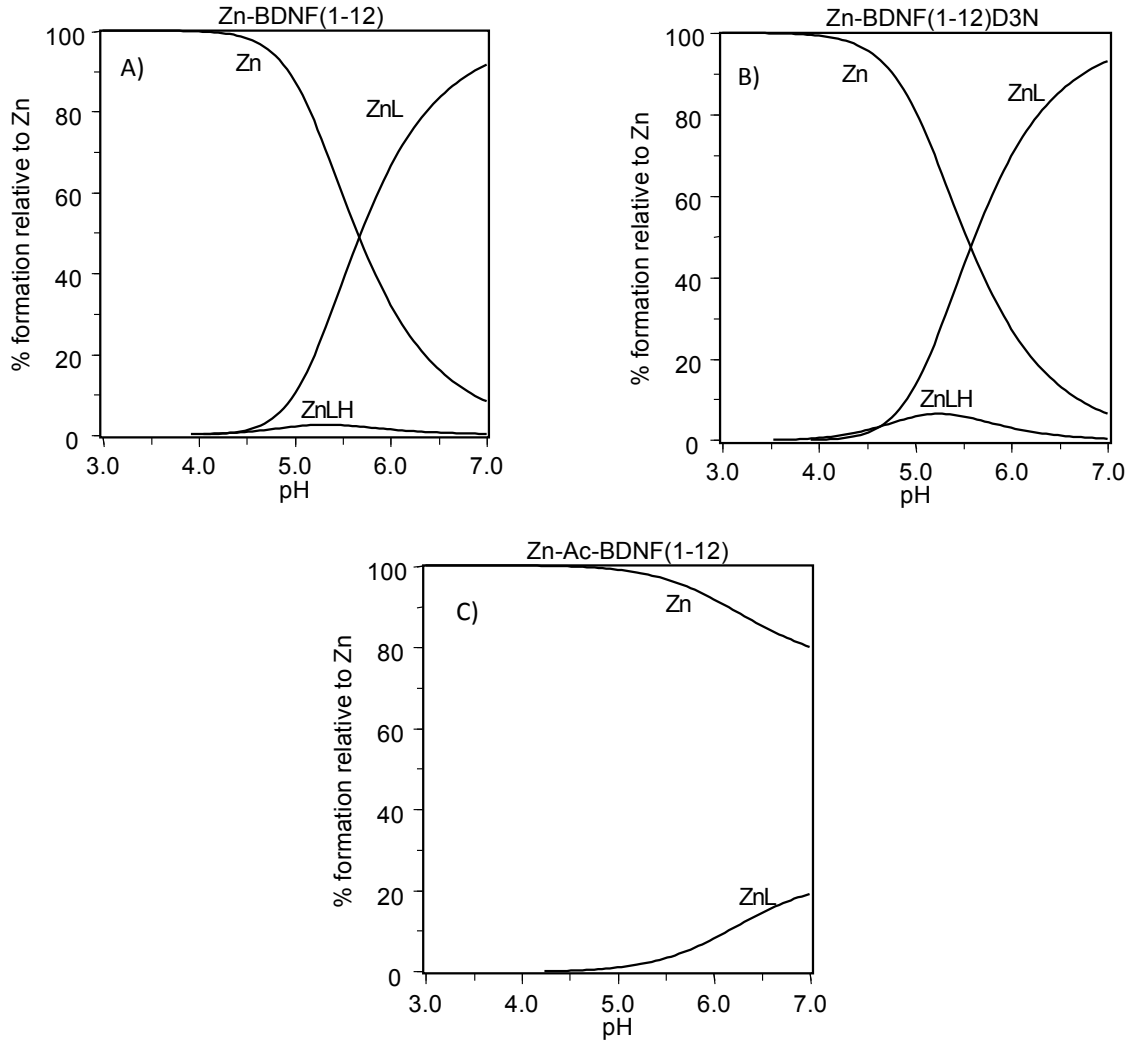

Figure32. *Species distribution diagram for the Zn(II) complexes in aqueous solution a) AcNGF1-14 and b) NGF1-14. [Zn^{2+}] = 2×10^{-3} M. Ligand to metal molar ratio is 1:1. Charges are omitted for clarity.*

This coordination mode is confirmed by DFT simulations. The minimum energy structures of the zinc complexes predicted through DFT are reported in Figure 33. All the zinc-BDNF peptides complexes adopt a distorted tetrahedral arrangement with marked differences

among the three complexes. The coordination of the zinc ion in the HSDP sequence of wild-type BDNF(1-12) involves the N-terminal amine, the N_δ nitrogen of histidine and two water molecules. Intriguingly, a hydrogen bond connects one of the two water molecules with the aspartate (Fig.33a). The coordination of zinc ion in the HSNP sequence of the BDNF(1-12)D3N is similar to the one of the BDNF(1-12), involving the N-terminal amine, the N_δ nitrogen of histidine and two water molecules. The mutation of Glu in Gln avoids the formation of hydrogen bond. The absence of the amine group completely change the coordination environment of the Ac-HSDP domain of the acetylated peptide, in which zinc is coordinated by one oxygen from aspartate, one oxygen from the histidine carbonyl, the N_δ nitrogen of histidine and one water molecule (Fig.33c).

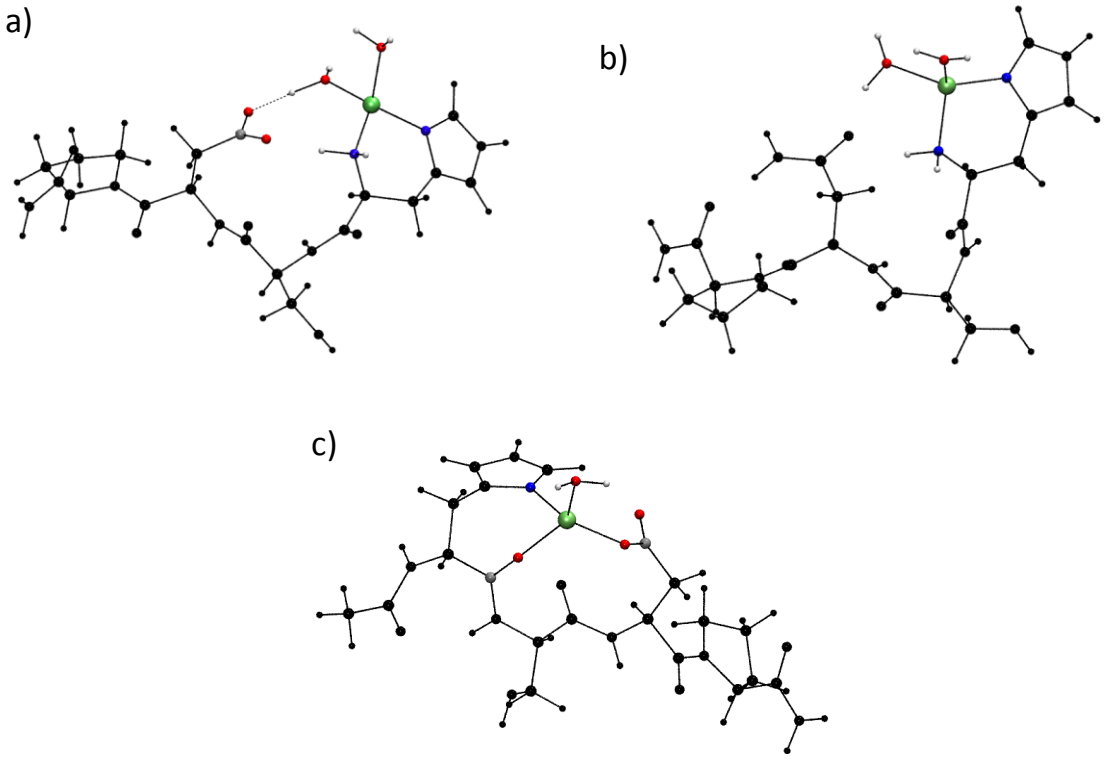

Figure 33. *Coordination polyhedron of zinc ion in a) HSDP, b) HSNP, c) Ac-HSDP of BDNF. Zinc ion is shown in green, nitrogens in blue, oxygens in red and BDNF backbone is shown in black spheres.*

The former results single out that the simultaneous coordination of the N-terminal amine and the N_{δ} nitrogen of histidine hamper the access of the aspartate in the zinc coordination site, resulting in the absence of the aspartate inside the coordination shell. However, the aspartate still interacts with the coordination site through hydrogen-bonding with the first-shell water. Such interaction is evident from the closer Zn-O_{w1} distance of the BDNF wild-type (1.89 Å) than that found in the BDNF(1-12)D3N mutant (2.01 Å). Intriguingly, when the aspartate is mutated with the asparagine, the NH_2 group turns out backward the zinc coordination site.

4.2.4 Proliferative effects of BDNF protein and its N-terminus peptide fragments BDNF(1-12) on SHSY5Y cells.

The proliferative effect of BDNF(1-12), BDNF(1-12)D3N, Ac-BDNF(1-12) has been tested on neuronal undifferentiated cell cultures (neuroblastoma SHSY5Y) at 60-70% confluence, and compared to that obtained by the whole protein BDNF both in the presence and in the absence of copper(II) ions.

Experiments carried out after 72 hours, showed an increase of the cell number following the addition of both BDNF protein and related peptides (Fig. 34).

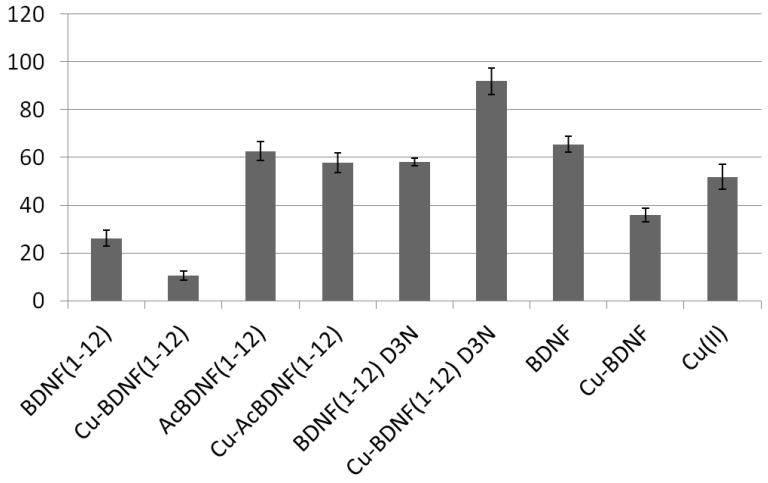

Figure 34. *Proliferative effect (after 72 hours) of BDNF(1-12), Ac-BDNF(1-12), BDNF(1-12)D3N peptides (10 μM) and the whole BDNF protein (10 nM) on neuroblastoma SHSY5Y cells in the absence and presence of Cu(II) ions (10 μM).*

It is interesting to note that Ac-BDNF(1-12) and BDNF(1-12)D3N show the same proliferative effect (+ 60%) of the whole BDNF protein. BDNF(1-12) is also able to increase the cell number but its proliferative effect is lower (+18%) in comparison with that obtained for Ac-BDNF(1-12) and BDNF(1-12)D3N. Such results indicates that these peptides can mimic the activity of the BDNF protein under these conditions, although the same proliferative effect is achieved when the peptide concentration is 100-fold higher than the whole protein as reported for the peptide fragment encompassing the N-terminal domain of the NGF protein. The difference observed between BDNF(1-12) and its

acetylated and mutated analogous can be rationalized in the different interaction with TrkB receptor due to different intramolecular interactions.

Notably, BDNF(1-12), BDNF(1-12)D3N and Ac-BDNF(1-12) peptides when docked to domain 5 of TrkB receptor (TrkB-D5) show similar binding poses to those of the N-terminal sections of neurotrophin 4/5 (pdb code 1HCF). All the peptides tend to maintain their intra-molecular interactions, as those involving Asp-3 and the N-terminal amine (Fig. 35).

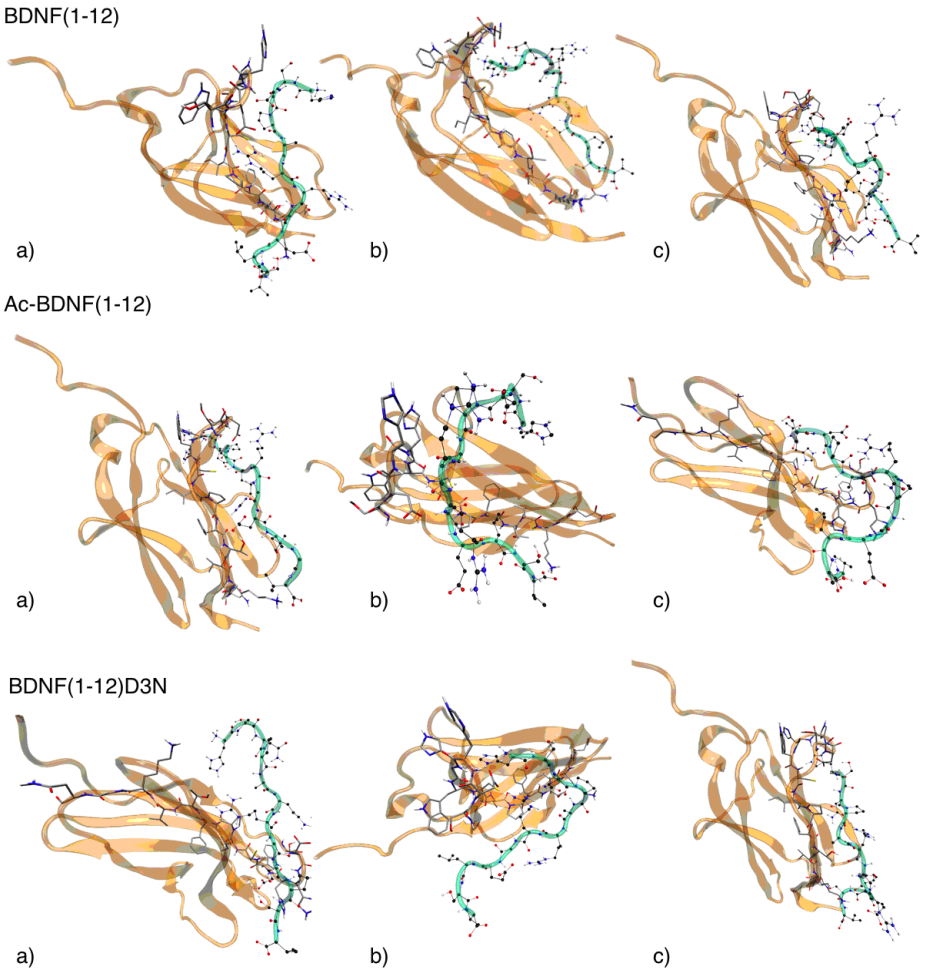

Figure 35. *Lowest energy binding modes for the TrkB-D5/BDNF(1-12), TrkB-D5/Ac-BDNF(1-12) and TrkB-D5/BDNF(1-12)D3N obtained from protein-protein docking calculations using Haddock interface.*[297] *TrkB-D5 is shown by gold ribbons, TrkB-D5 backbone is shown by sticks. BDNF sections are shown by green ribbons. BDNF backbones are shown by spheres.*

Binding poses involving Arg-6 or Arg-7 interacting with Asp-298 of TrkB-D5 are also observed (Fig. 35). In particular, when Asp-3 is mutated with Asn, this last residue tends to avoid a direct facing with TrkB-D5 (Fig. 35), and, at the same time, the Arg residue can easily interact with Asp-298, explaining its higher activity in comparison with wild type BDNF(1-12). While the higher activity of acetylated peptide may be related to the absence of protonated amino group and its conseguent higher hydrophobicity.

On the other hand the endocytosis of Trk receptor-contained vescicles is a mechanism by which neurotrophins determine long-lasting signals. Among the studied peptides, BDNF(1-12) is the less hydrophobic, thus it is assumable that internalization and/or nuclear translocation occurs with minor frequency in respect of the other peptide and the whole protein. It is interesting to note that nuclear translocation is not a forbidden mechanism to these peptides, because of they have the nuclear translocation consensus sequence Arg-Arg.

To evaluate the contribution of the copper(II) ions to cell proliferation, cell cultures have been co-treated with a mixture of metal/BDNF1-12 (10 nM, 1:1 ratio) and metal/BDNF (according concentration reported elsewhere). The proliferative effect (+ 35%) turned out to increase also in presence Cu^{2+}. Interestingly, the proliferative activity of BDNF protein is significantly decreased in the presence of Cu^{2+} (+26%,), as well as the cell culture treated with BDNF(1-12) peptide and copper(II) ions shows a decrease in cell number (+4%).

The copper addition effect on the activity of BDNF protein and of its related peptide fragment is opposite to that reported for NGF protein and the peptide NGF(1-14) encompassing the N-terminal domain, where a synergic proliferative effect is observed.

A different behavior is observed for the acetylated and single point mutated peptides: copper addition to Ac-BDNF(1-12) does not affect significantly its proliferative activity whereas significantly enhances the activity of mutated BDNF(1-12)D3N. The distribution diagram for Cu-Ac-BDNF(1-12) carried out at 10 μM (1:1 molar ratio), show that at physiological pH, free ligand (4.3×10^{-6} M) and Cu^{2+} (4.7×10^{-6} M) are present. Therefore, the proliferation activity of Cu-Ac-BDNF(1-12) system is practically determined by the

sum of free Ac-BDNF(1-12) and Cu^{2+} activity, resulting similar equal to that of single component. The distribution diagram of Cu-BDNF(1-12)D3N, as well as Cu-BDNF(1-12), at 10 μM show that at physiological pH the metal ions is bound to the ligand and the [CH-1L] and [$CuLH_{-2}$] complex species are predominant. Then the great difference in the proliferative activity of Cu-BDNF(1-12)D3N with that of Cu-BDNF(1-12) system is due to the different metal ion coordination environment. An hypothesis is that the carbonyl group bound to Cu^{2+} in the mutated peptide complex species may be substituted by another donor atoms of receptor whereas very stable [5,5,6] chelate ring determined in the [$CuLH_{-2}$] for BDNF(1-12), does not permit an analogous substitution.

Preliminary data suggest an extremely interesting effect due to zinc ions. SHSY5Y cell cultures have been co-treated with a mixture of metal/BDNF1-12 (10 μM, 1:1 ratio) and metal/BDNF. The presence of zinc turned out to increase the proliferative effect due to both BDNF(1-12). Noteworthy, also the proliferative activity of BDNF protein is significantly increased by zinc. These effects are not the mere sum of the independent effect of zinc ions and BDNF(1-12), suggesting their functional interaction.

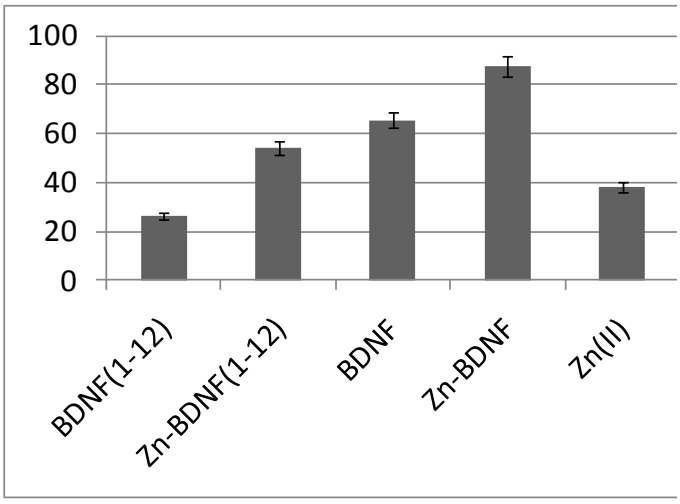

Figure 36. *Proliferative effect (after 72 hours) of BDNF(1-12) (10 μM) and the whole BDNF protein (10 nM) on neuroblastoma SHSY5Y cells in the absence and presence of Zn(II) ions (10 μM.*

Strikingly, the effect of zinc addition on the activity of BDNF and BDNF(1-12) is opposite to that reported for the same proteic system in the presence of copper.

Other studies are needed to clarify the mechanism of action of BDNF(1-12), to explain the difference with the mutated as well as acetylated peptide and how zinc affects the biological responses. Also, other hypothesis can be formulated and other experimental data as well as theoretical calculations are necessary for a full understanding of the proliferative activity of copper(II) and zinc(II) complex species of investigated peptides. However, it is evident that a prominent role is played by the amino terminus and aspartic carboxylate groups.

4.3 In vitro biochemical characterization of NGF(1-14) signaling

In vitro studies on the molecular mechanisms of action of NGF(1-14) have been performed at European Brain Research Institute in collaboration with Prof. Calissano.

We have previously reported the ability of NGF(1-14) to affect the proliferation rate of neuroblastoma cells SH-SYS5. To shed light on the molecular mechanism of NGF(1-14) and to evaluate its potential function as peptidomimetic, we decided to use PC12 cells. PC12 is a cell line, derived from a pheochromocytoma of the rat adrenal medulla and a worldwide model system used to study neuronal differentiation and validate the efficiency of NGF-like substances. Indeed, after to arrest cellular proliferation, NGF induce the differentiation of PC12, e.g. they start to extend branching processes similar to those produced by sympathetic neurons in primary cell culture.

4.3.1 NGF(1-14) does not induce and does not maintain the differentiation of PC12 cells

With the aim to ascertain the NGF(1-14) ability to mimic NGF and to activate differentiation processes, PC12 cells have been cultured in complete medium and treated with NGF(1-14) (concentration range 1-100 μM) or NGF (100 ng/ml). After 24 hours' exposure to NGF, as expected, PC12 begin to differentiate and to create a neuronal network, which is completed within 6 days. Otherwise, in the concentration range 1-100 μM, NGF(1-14) has not been able to induce any detectable sign of differentiation on PC12 within 6 days from the treatment (data not shown).

We asked if, though unable to induce axons outgrowth, NGF(1-14) is at least able to maintain the morphology of differentiated PC12. Thus, PC12 cells have been cultured for 6-7 days in RPMI medium plus 10% HS and 5% FBS, in the presence of NGF (100 ng/ml) to induce their diffentiation. Differentiated PC12 cells have been cultured for other 6-7 days in RPMI, without serum, but in the presence of NGF (100 ng/ml). Finally, the

cultures have been deprived also from the NGF, a condition that causes the spontaneous degeneration of dendrites/axons.

As expected, within 48 hours, deprived PC12 showed less and shorter axons/dendrites. The differentiated phenotype is sustained by the treatment with NGF but not by NGF(1-14), which has not been able to avoid the shrink of the neuronal processes (data not shown).

4.3.2 NGF(1-14) affects the proliferation rate of PC12 cells

Although we have ruled out the possibility that NGF(1-14) can induce/sustain differentiation states, from the above experiments we qualitatively observed a reduced confluence due to the treatment with the NGF(1-14) peptide.

We have decide to quantify the ability of NGF(1.14) to affect the proliferation of PC12 cells, as the cease of cell cycle is known to advance differentiation. Dose-response experiments showed a significant decrease of the cell number, due to the treatment with 1 to 10 μM NGF(1-14) (Fig. 37).

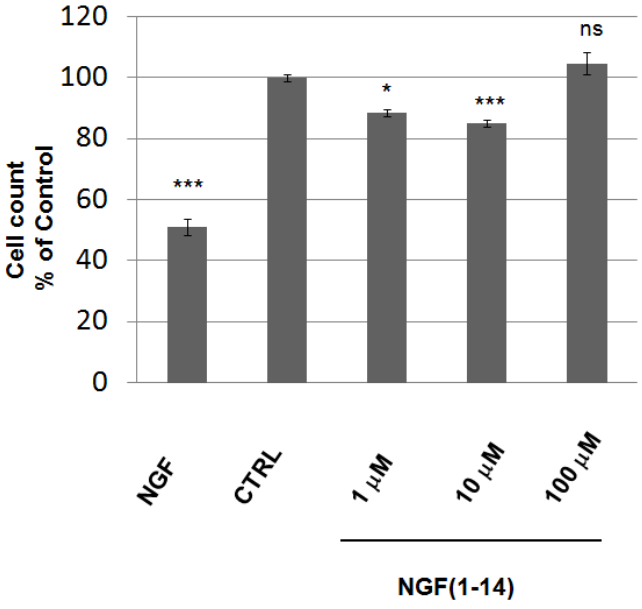

Figure 37. *Proliferative effect (72 hours after treatment) of NGF and NGF(1-14) on PC12 cells.*

The strongest effect has been observed after the treatment with NGF(1.14) 10 μM, which reduces the proliferation of PC12 cells by 15% ($P<0.001$) (Fig. 38). However, an inverted effect is observed increasing the concentration. Namely, NGF(1-14) 100 μM does not result in a reduced cell number in comparison with untreated cell (Fig. 38). Since it is a really high dose, many receptors/pathways are presumably activated. Intriguingly, the same effect has not been observed with the acetylated peptide AcNGF(1-14) in the investigated concentration range (1-100 μM).

4.3.3 NGF(1-14) triggers the phosphorylation of TrkA and induces the phosphorylation of CREB at Ser-133

The activation of TrkA is the first event of PC12 response to NGF. Namely, the binding of NGF to TrkA induces receptor dimerization and consequent autophosphorylation, followed by a kinase signaling cascade (see paragraph 1.2.1). Thus, we analyzed the ability of NGF(1-14) to induce TrkA phosphorylation in PC12 cells.

PC12 have been cultured in complete medium (10% HS, 5%FBS in RPMI) and treated with NGF(1-14) (1, 10 and 100 μM) or NGF (100 ng/ml), and the phosphorylation of TrkA receptor evaluated 5, 15 and 30 minute after the treatment. Western Blot analysis show that NGF(1-14) is able to activate TrkA receptor and its downstream signaling in a time- and concentration- dependent fashion.

The activation profile shows that NGF quickly induces the phosphorylation of TrkA receptors, with the maximum at 5 minutes and a subsequent decline. On the contrary, the phosphorylation level due to the treatment with NGF(1-14) reaches its maximum 30 minutes after treatment. It is well-known that the biological activities of proteins are due to their three-dimensional structures, which guarantee the right folding and the appropriate interaction with other proteins/receptors. We can speculate that the whole NGF represents the scaffold that allows to the N-terminal domain to be close to TrkA receptor. Conversely, the N-terminal domain alone has to explore many conformational states before to be able to bind the receptor, explaining the different temporal activation profile.

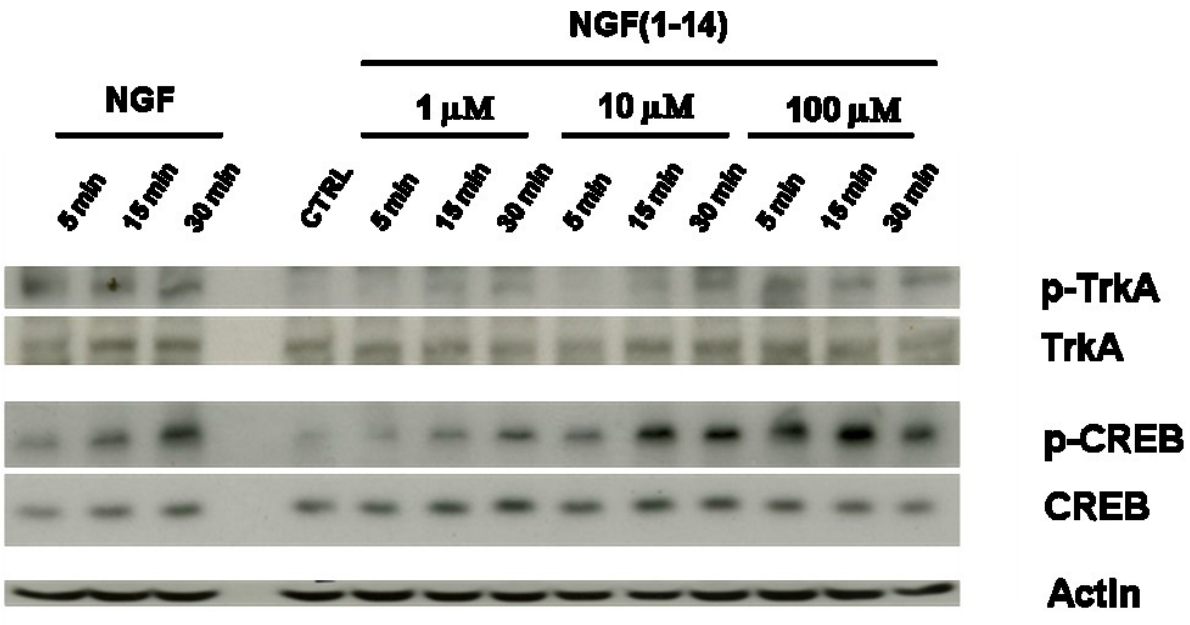

Figure 38. *Western blot of PC12 cells extract treated both with NGF and with NGF(1-14) at three different concentrations (1 μM, 10 μM and 100 μM). Control is represented by untreated PC12 cells.*

It is remarkable that, although NGF(1-14) is a just a linear and monomer peptide encompassing the 1-14 sequence of the human NGF, it is able to activate the TrkA pathway and to induce the phosphorylation of CREB Ser-133. We are currently investigating the downstream events which follow the TrkA receptor phosphorylation. Preliminary results suggest that not all the NGF signaling is activated by NGF(1-14), but only the PI3K/AKT is electively triggered, determining in turn the phosphorylation of CREB (data not shown).

4.4 In vivo biochemical characterization of BDNF signaling

In vivo studies on the molecular mechanisms of neurotrophins in memory formation have been performed at New York University in collaboration with Prof. Alberini.

Studies in the Alberini lab have recently reported that hippocampal BDNF-TrkB signaling is critical for long-term, but not short-term, inhibitory avoidance memory formation. [298] Indeed, both injecting a function-blocking antibody to BDNF or a BDNF-sequestering TrkB-Fc chimera into the dorsal hippocampus (15 min before training elicited by 0.6- or 0.9-mA foot shock) markedly and persistently disrupted memory retention at both 2 and 7 d after training compared with IgG injection, and had no effect on short-term memory.

It has been also shown that, to mediate memory consolidation, BDNF trigger the phosphorylation of CREB. [298] Thus, the inhibitory avoidance learning task has been used to identify in vivo new transcription factors activated by BDNF.

MeCP2 has recently gained attention because of its involvement in the neurodevelopmental disease Rett Syndrome. [77,83-85] Although some in vitro studies suggest that this protein might be involved in the regulation of BDNF transcription, it has not verified in vivo. Also, a physiologic role of MeCP2 in memory formation has not been taken into account. Thus, we have evaluated i) if the level of MeCP2 changes in the brain after learning ii) in which kind of cells is MeCP2 expressed iii) if MeCP2 is linked with the BDNF signaling.

4.4.1 MeCP2 is induced in many brain regions after learning

We have firstly tested the hypothesis that MeCP2 is regulated in different brain region after training of Inhibitory Avoidance (IA) Task. Briefly, IA chamber consisted of a rectangular box divided into a safe compartment and a shock compartment. The safe compartment is white and illuminated and the shock compartment is black and dark. During training

sessions, each rat is placed in the safe compartment with its head facing away from the door (Fig. 39a). After 10 seconds, the door separating the compartments is automatically opened, allowing the rat access to the shock compartment (Fig. 39b). The rats usually enter the shock (dark) compartment within 10-20 seconds of the door opening. Then, the door closed 1 second after the rat entered the shock compartment, and a 2-second foot shock (0.9mA was delivered to the grid floor of chamber (Fig. 39c). The rat was then returned to its home cage. To test the memory retention, rats have been placed back in the safe compartment and its latency to enter the shock compartment is measured (Fig. 39d). However, for biochemical studies, rats have been not tested for memory retention but directly sacrificed at the designed time-points (30 minutes, 12 hours, 20 hours, 2 days, 6 days, 3 weeks) after the learned experience to evaluate the experience-induced effect on specific neuronal markers (Fig. 39e)

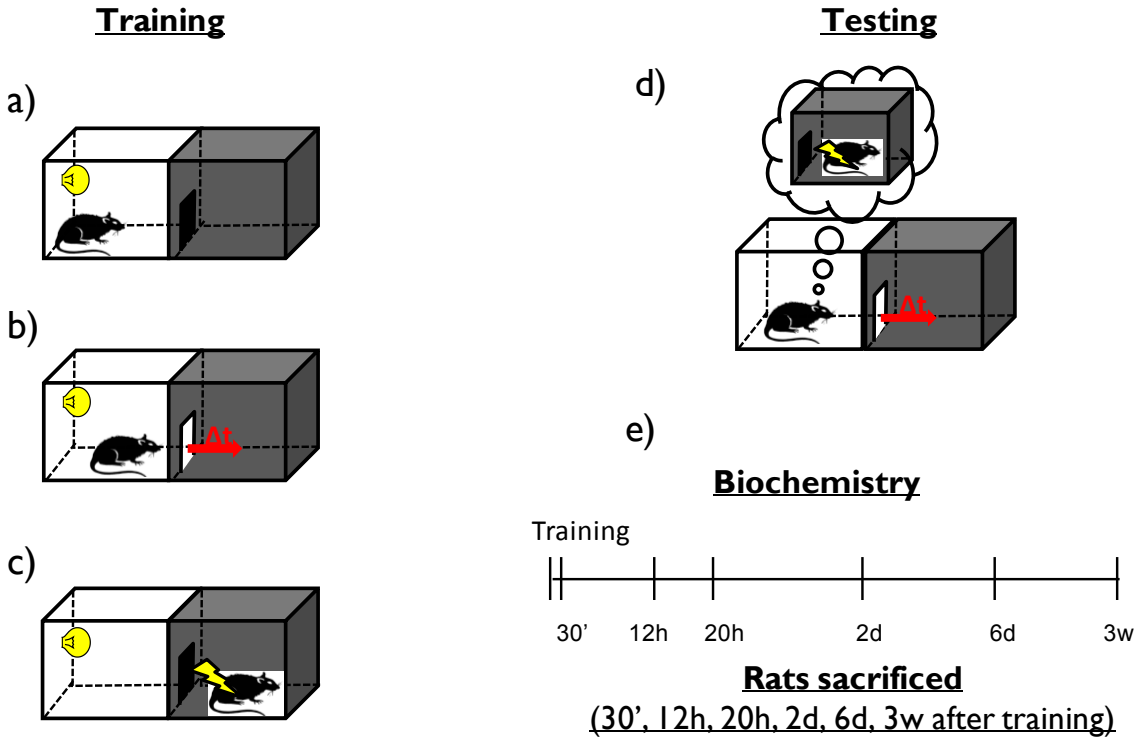

Figure 39. *Schematic representation of Inhibitory Avoidance Training.*

Western blot results suggest that MeCP2 levels are increased after training in many different brain regions compared with naïve animal (e.g. that have not been trained). Among the brain regions analyzed (cerebellum, insular cortex, retrosplenial cortex, anterior cyngulate cortex, prefrontal cortex, amygdala, hippocampus), cerebellum is the only in which has not been observed the induction in MeCP2 and the insular cortex the one with the highest induction. In the insular cortex, indeed, the up-regulation already starts 30 minutes after training, reaches the maximum value at 12-20 hours (270%) and is still higher than naïve six days after training.

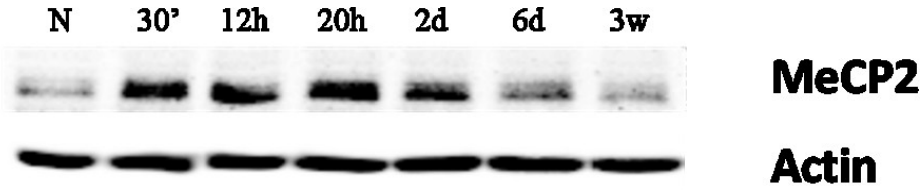

Figure 40. *Western blot of MeCP2 level in insular cortex extracts from naïve (N) and trained rats, sacrificed 30 minutes, 12 hours, 20 hours, 2 days, 6 days and 3 weeks after training. The results are expressed as % of the Naïve.*

It is interestingly to note that the each region exhibit a specific temporal activation profile. As mentioned, the insular cortex is the only region is which a significant induction is observed 30 minutes after training. Otherwise, in the amygdala, there is not a significant induction before 20 hours, though a trend is observed 12 hours after training. (Fig. 41) However, the level of expression is the same of control in 2 days. The expression of MeCP2 in the retrospleninal cortex is temporary-shifted in comparison to that observed in the amygdala (Fig. 41). Indeed, the induction massively starts only 20 hours after training but lasts for 6 days.

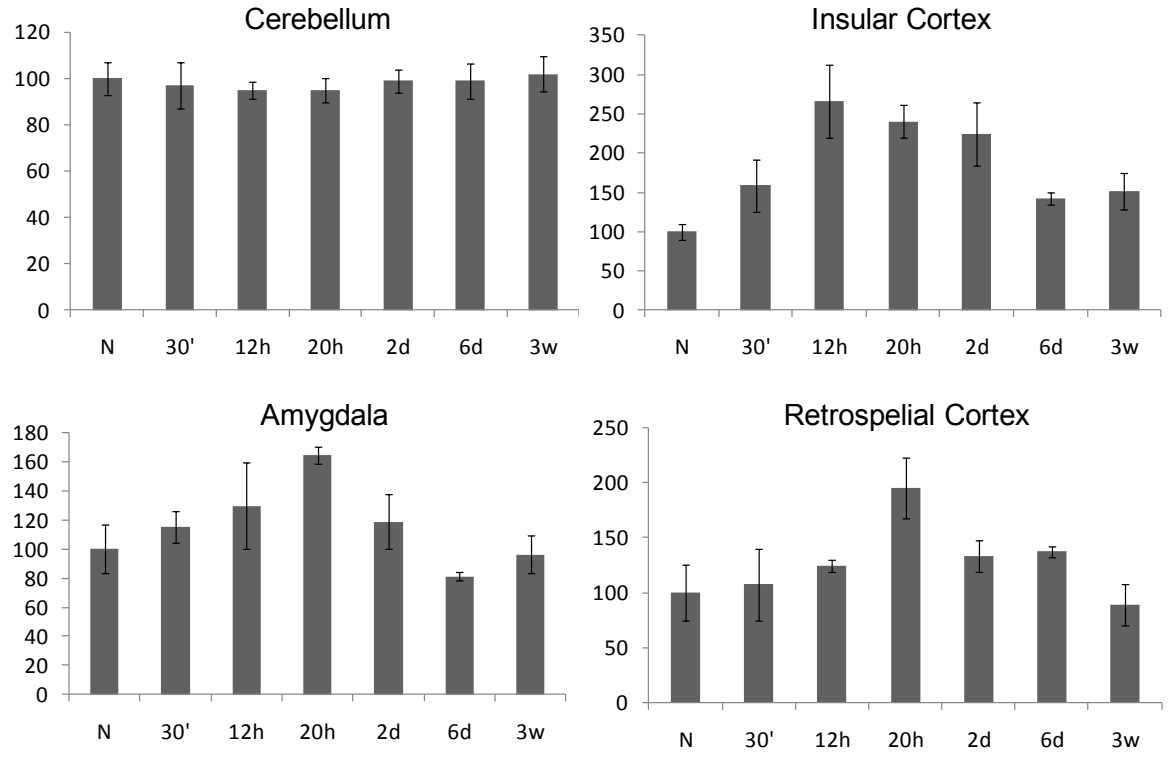

Figure 41. *Densitometric analysis of western blot of MeCP2 level in cerebellum, insular cortex, amygdale, retrosplenial cortex, from naïve (N) and trained rats, sacrificed 30 minutes, 12 hours, 20 hours, 2 days, 6 days and 3 weeks after IA training. The results are expressed as % of the Naïve.*

4.4.2 Distribution and regulation of MeCP2 in the hippocampus

Qualitative immunihistochemistry and quantitative western blot have been shed light on the distribution and regulation of MeCP2 in the hippocampus.

Immunohistochemistry studies reveal an uneven distribution of MeCP2 among different hippocampal area. CA3 neurons seem to have the lower expression of MeCP2, which is indeed highly expressed in CA1 and dentate gyrus (data not shown). Also, despite the fact that recent contributions point out the presence of MeCP2 in astrocytes, the double staining

of hippocampal dentate gyrus with MeCP2 and GFAP (a marker of astrocytes) strongly suggest that MeCP2 is exclusively expressed in neurons.

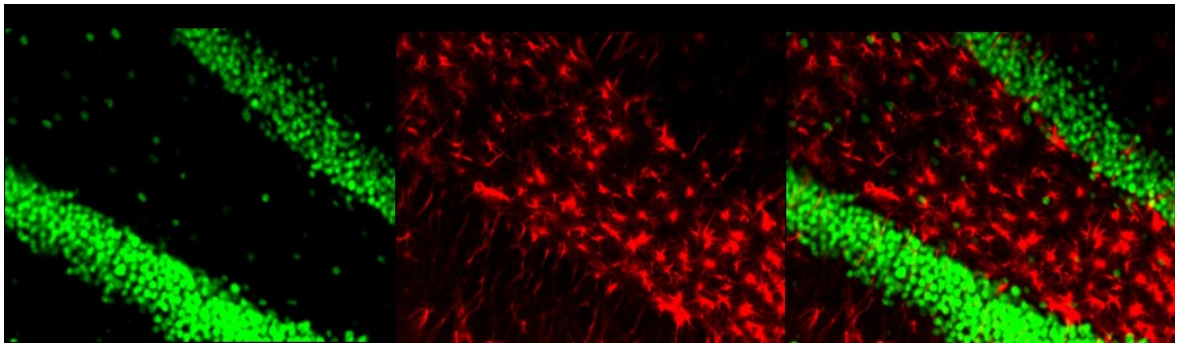

Figure 42. *Immunohistochemistry staining of hippocampus dentate gyrus.*

The temporal profile of expression of hippocampal MeCP2 resembles that observed in the amygdala. Indeed, in the hippocampus the induction of MeCP2 starts 12 hours after training but reaches the highest value at 20 hours (Fig. 42). Further studies are currently investigating in which cells/hippocampal area are responsible of the induction.

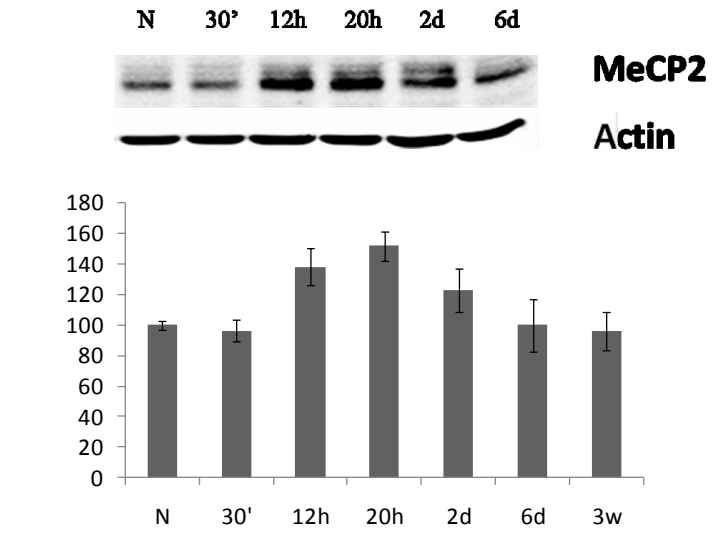

Figure 43. *Western blot and densitometric analysis of MeCP2 level in hippocampus extracts from naïve (N) and trained rats, sacrificed 30 minutes, 12 hours, 20 hours, 2 days, 6 days and 3 weeks after training. The results are expressed as % of the Naïve.*

4.4.3 BDNF signaling plays an essential role in MeCP2 upregulation.

A pivotal experiment suggest that, besides the ability of MeCP2 to regulate the expression of BDNF, MeCP2 itself is regulated by the BDNF pathway. Indeed, preliminary experiment shows that blocking the BDNF pathway, with hippocampal bilateral injection of anti-BDNF antibody 15 minutes before IA training ,blocks the training-dependent MeCP2 induction (Fig. 44) and completely disrupts memory consolidation (data not shown).

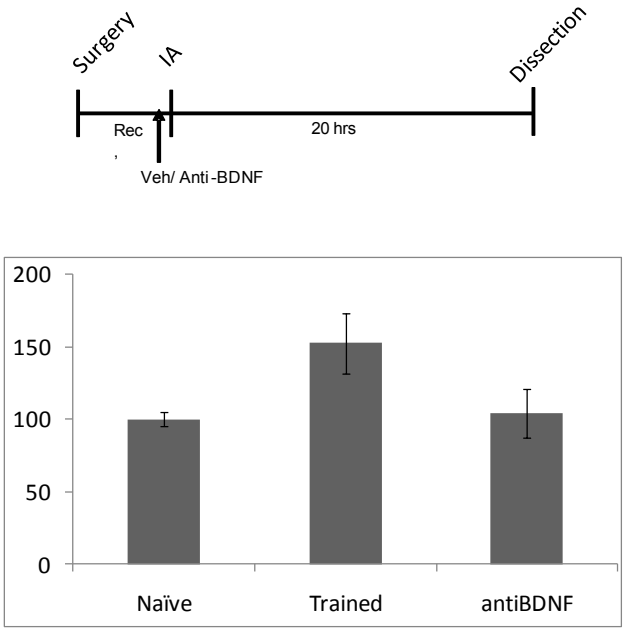

Figure 44. *Densitometric analysis of MeCP2 level in hippocampus extracts from Naïve, Trained and injected with anti-BNDF before training. The results are expressed as % of the Naïve*

Promising behavioral and biochemical studies are currently in progress to demonstrate the functional role of MeCP2 in memory formation and its link with BDNF pathway.

4.5 Characterization of lipid/neurotrophins nanoplatforms

As previously mentioned a major issue in the use of neurotrophins as therapeutic agent is their poor pharmacological properties, including the low blood-brain barrier permeability.To overcome this problem, we have studied the association of NGF(1-14) to lipid vesicles and investigated the resultant peptide-associated SLBs (both planar and nanoparticle silica surfaces), as a proof-of-concept for its application in drug delivery and imaging.

4.5.1 Association of NGF(1-14) to lipid vesicles

An electrostatic driven approach to associate the NGF(1-14) peptide to lipid vesicles by physisorption. In particular, at the physiological pH the NGF(1-14) molecules are expected to bear an overall positive charge. Accordingly, SUVs made of zwiterrionic POPC (thereafter named PC) and negatively charged POPS/POPC (1:3 molar ratio, thereafter named PS25) in the fluid phase have been used. The hydrophilic and charged residues in the peptide sequence are expected to result in the preferential placing of the NGF(1-14) molecules inside the core and/or onto the outer polar shell of the vesicles (Fig. 45)

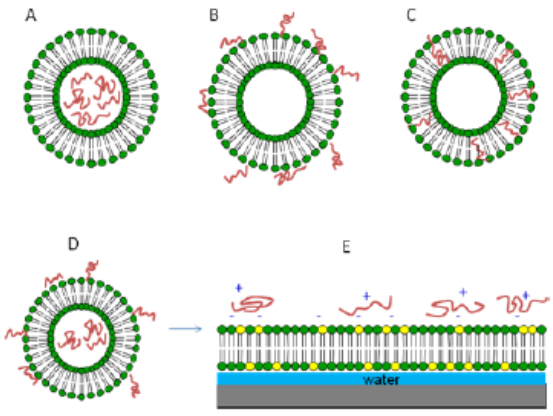

Figure 45. *Schematic representation of three limit cases of peptide-lipid interaction (A, B, C). An integrated sketch of both A and B configurations is given in (D), while the resulting peptide-associated SLB is shown in (E).*

The following interaction of NGF(1-14)-SUV systems with hydrophilic silica surfaces would eventually result into silica-supported lipid adlayers (i.e., physisorbed lipid molecules) or SLB nanoplatforms loaded with NGF(1-14) molecules (Fig. 45e).

After preparation of the various lipid vesicle dispersions, both SUV and SUV-NGF, the peptide loading efficiency has been assessed by centrifugation and spettrophotometric determinations (Fig. 46).

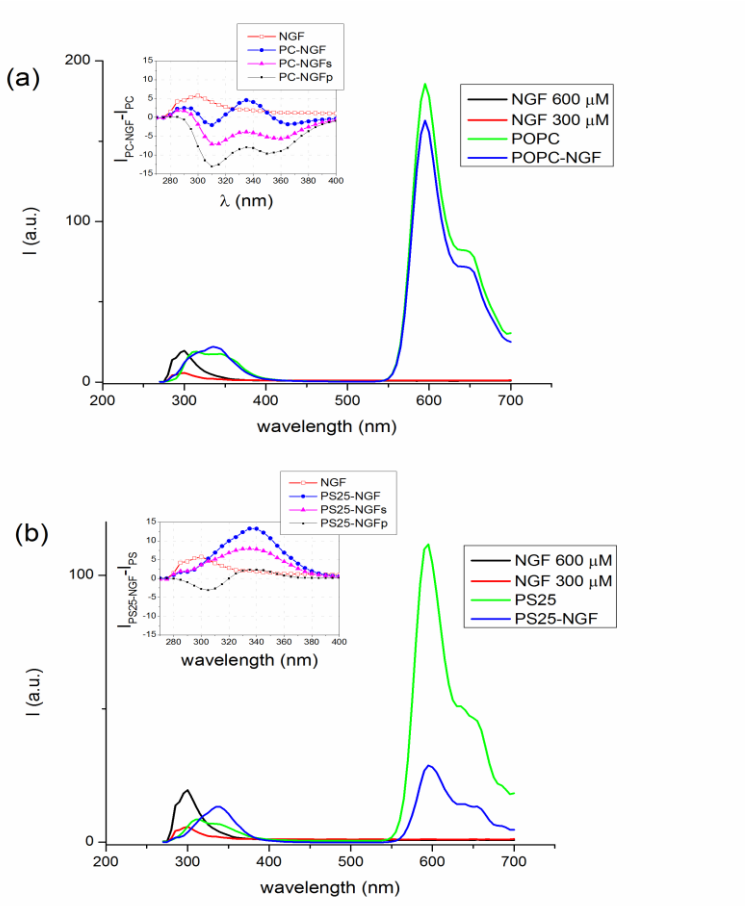

Figure 46. *Emission spectra (excitation at 260 nm) of bare and NGF-associated lipid vesicles of PC (a) and PS25 (b), in comparison with spectra of 300 and 600 μM NGF(1-14). Inset: the difference spectra between the NGF-associated vesicles and the corresponding bare vesicles are shown for as prepared and after centrifugation of the vesicle dispersions, both pellet ('p' subscript) and surnatant ('s' subscript); the spectrum of free NGF peptide at two concentrations (600 and 300 μM) is reported for comparison.*

Peptide emission spectra (black and red curves) show a broad emission band at about 300 nm, due to the presence of two phenylalanine units per each molecule fragment. On the other hand, the bare lipid vesicles (green curve) exhibit a major emission band at about 590 nm and a smaller double picked band at about 340 nm, related to the rhodamine-labeled lipids. The spectra obtained for the NGF(1-14)-SUV system (blue curve), evidence significant changes for negative PS25 (Fig.46b) but not for zwitterionic PC (Fig.46a) in comparison with bare vesicles. The difference spectra in the insets evidence for negative lipids the depletion of free NGF molecules in the pellet, confirming the efficiency of association of NGF peptide to PS25.

The actual peptide-lipid association and the preferential NGF(1-14) interaction with the negative lipids are confirmed by FT-IR spectra (Fig. 47)

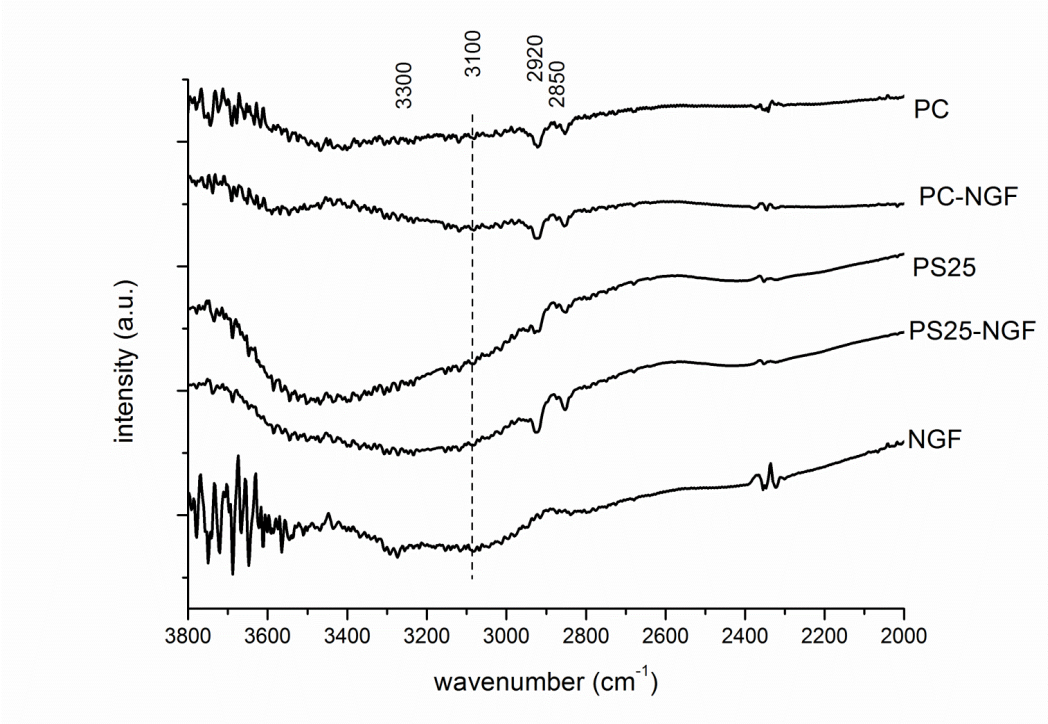

Figure 47. *FT-IR spectra of zwitterionic (PC) and negatively charged (PS25) lipid adlayers, the corresponding peptide-associated PC-NGF(1-14) and PS25-NGF(1-14) and control NGF(1-14) adlayer.*

Firstly, lipid vesicle dispersions (100 μg/mL in PBS) have been allowed to adsorb on silicon dioxide freshly cleaned by acid piranha solution. After 20 minutes of incubation the samples have been washed by multiple rinsing with PBS and dried under gentle Ar blowing. A reference 'thick' NGF(1-14) sample has been prepared by drop casting of 600 μM peptide solution until a visible film has been deposited on silicon dioxide.

The spectra in Figure 47 show the lipid characteristic peaks at 2920 cm^{-1} (CH_2 anti-symmetric stretching) and 2850 cm^{-1} (CH_2 symmetric stretching) as well as a broad band in the region of 3000-3700 cm^{-1}, due to phosphate groups and hydroxyl stretching. On the other hand, the NGF(1-14) spectrum exhibits a peak at 3300 cm^{-1}, attributed to the absorption of water molecules as well as to the contribution from the amide bonds and a band at 3000-3100 cm^{-1}, assigned to C=C-H asymmetric stretch of the aromatic rings of the phenylalanine residues. The spectra of PC-NGF(1-14) and PS25-NGF(1-14) clearly exhibit spectral features from both the lipid and the peptide, as especially evident in the 3000-3100 cm^{-1} region, thus confirming the successful association of the peptide to the lipids.

4.5.2 Adsorption processes onto planar silica surfaces: QCM-D and FRAP experiments

The adsorption processes of such systems onto planar silica surfaces have been investigated by Quartz Crystal Microbalance with Dissipation Monitoring (QCM-D) and Fluorescence Recovery after Photobleaching (FRAP) techniques. Used substrates have been either silicon dioxide (for QCM-D) or glass (for FRAP), whose surfaces are known to prompt, upon vesicle adsorption, the spontaneous lipid self-assembling into SLBs for both zwitterionic and negatively charged vesicles, this latter only in the presence of divalent ions such as Ca^{2+} or Mg^{2+}. [299-301]

QCM-D shift curves of frequency (Δf) and dissipation (ΔD) (Figure 48) indicate that *(i)* both bare and NGF-loaded vesicles form supported lipid bilayers upon adsorption to SiO_2 at the used experimental conditions, and (*ii*) the negatively charged vesicles exhibit visible

curve differences in the presence of NGF(1-14) in comparison with the corresponding bare ones.

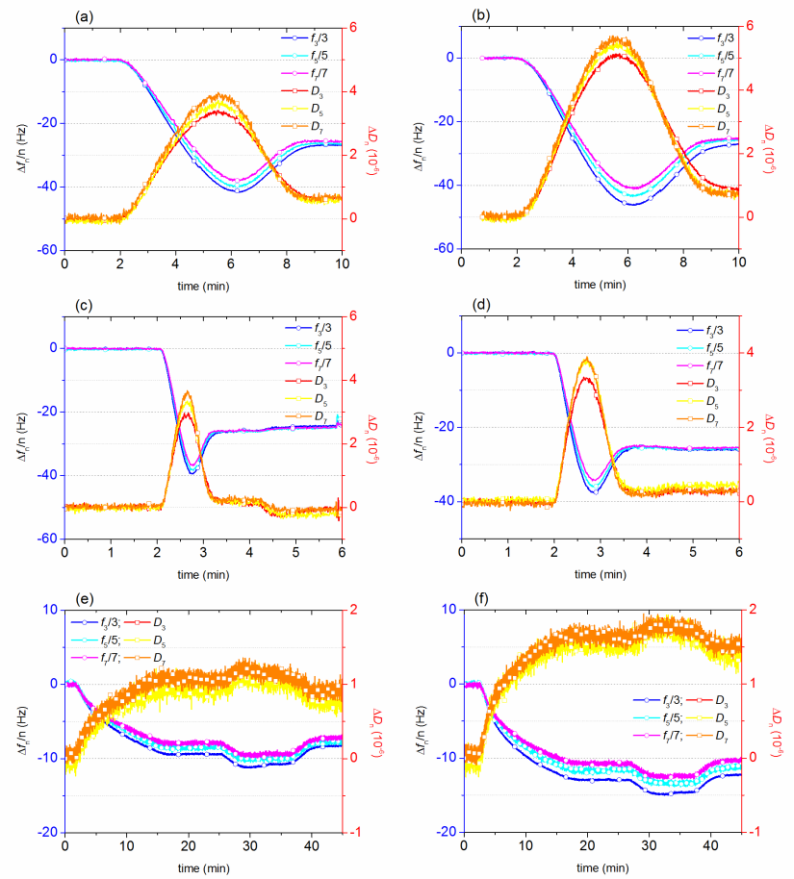

Figure 48. *QCM-D curves of f and D for three overtones (n=3,5 and 7) corresponding to vesicle adsorption on planar SiO_2 and formation of supported lipid bilayers (a-d) or lipid adlayers (e-f): (a) PC; (b) PC-NGF(1-14); (c) PS25 in 10 mM $MgCl_2$ added buffer; (d) PS25-NGF(1-14) in 10 mM $MgCl_2$ added buffer; PS25 (e) and PS25-NGF(1-14) (f) in the absence of bivalent cations. For (e) and (f) experiments the addition of 600 μM NGF(1-14) to the lipid adlayers during 10 minutes is shown.*

All the lipid vesicle solutions show the typical curve trends for the formation of a homogeneous SLB (Fig. 48a-d), i.e., an initial adsorption of intact vesicles until a minimum in *f* (or maximum in *D*) is reached, followed by vesicle rupture and fusion into the lipid bilayer, which corresponds to Δf~ -26 Hz and ΔD~0.5 (10^{-6}) values, respectively

[12]. It is to note that for PC (Fig.48a) and PC-NGF(1-14) (Fig. 48b) the kinetic curves do not display any visible difference, while for PS25 (Fig 48c) the process is slightly faster than that displayed by PS25-NGF(1-14) (Fig. 48d).

The significant interaction between the positively charged NGF(1-14) peptide and the negatively charged PS25 vesicles is highlighted by the QCM-D experiment repeated without bivalent ions addition. In such a case, as expected, SLBs are not formed but instead adlayers with different viscoelastic properties at the interface with the silica substrate are evident by the comparison of curves for PS25 (Fig. 48e) and PS25-NGF(1-14) (Fig. 48f). This observation is quantified by the $\Delta D/\Delta f$ ratio values of $1.1 \cdot 10^{-7}$ Hz^{-1} for PS25 and $1.2 \cdot 10^{-7}$ Hz^{-1} for PS25-NGF(1-14), respectively.

Moreover, the shift values of $\Delta f \sim -13$ Hz and $\Delta D \sim 1.6 \cdot 10^{-6}$ for PS25-NGF(1-14), suggest that the peptide prompts the formation of a lipid monolayer, with presence of few unruptured micelles and/or patches of bilayers. The further addition of NGF(1-14) to the adlayers induces a visible and reversible interaction, in terms of frequency decrease and dissipation increase (x-axis scale of 30-40 min in Fig. 48e-f), whereas does not result in any evident interaction with PC-based supported bilayers (data not shown).

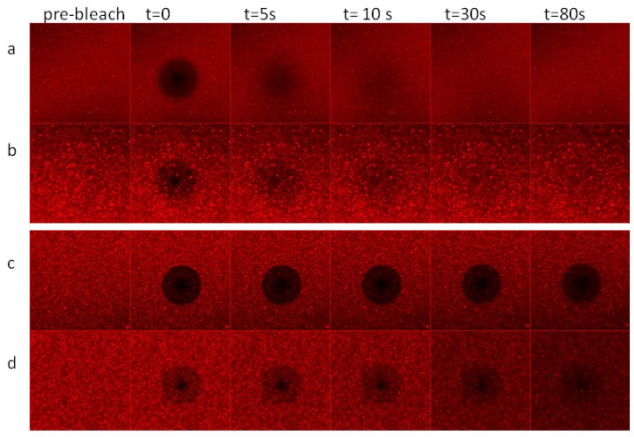

Figure 49. *Confocal microscopy images for the FRAP experiment on freshly-formed lipid adlayers from: (a) PC; (b) PC-NGF; (c) PS25 and (d) PS25-NGF. Time lapse images are shown, respectively for pre-bleach, immediately after bleach and 5s, 10s, 30s and 80s after bleach.*

FRAP experiments have been carried out by laser scanning confocal microscopy to measure the lipid lateral diffusion behaviour at the interface with the silica substrate (Fig. 49). Results confirm a higher level of interaction between positively charged peptide molecules and negative lipids in comparison with the zwitterionic ones. In fact, the lipid diffusion coefficients, calculated according to the Axelrod's algorithm, $D=0.88\cdot(w^2/4\cdot\tau_{1/2})$, where w is the radius of the bleached area and $\tau_{1/2}$ describes time for 50% recovery [14], indicate no significant changes for PC and PC-NGF(1-14), whereas a slight modification of lipid lateral diffusion is found for PS25-NGF(1-14) with respect to PS25, both in the presence of divalent cations (i.e., SLB) or not (i.e., lipid adlayers). The kinetic curves for fluorescence recovery are shown in Figure 50.

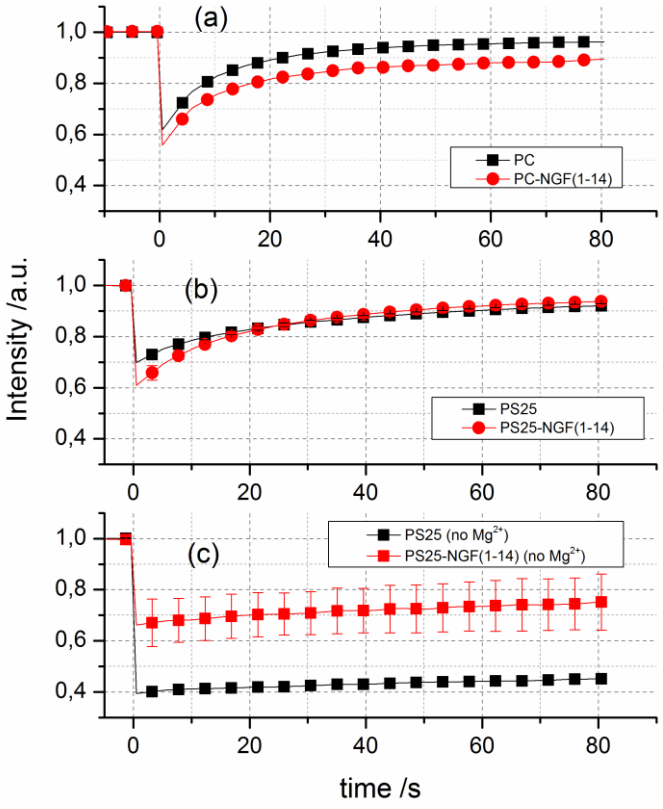

Figure 50. *Fluorescence intensity normalized to the pre-bleach values for FRAP experiments on SLBs or lipid adlayers obtained by adsorption on planar silica of SUVs made of: (a) PC and PC-NGF(1-14) in PBS; (b) PS25 and PS25-NGF(1-14) with addition of 10 mM $MgCl_2$; c) PS25 and PS25-NGF(1-14) without addition of 10 mM $MgCl_2$. Mean values of ten experiments ± S.E.M.*

As to the zwitterionic lipids similar curve trends are displayed for both bare and NGF-associated lipids, with a quick and almost complete recovery of fluorescence (Fig. 50a). Similarly, the fluorescence intensity curves for negatively charged PS25 and PS25-NGF(1-14) adsorbed on silica in the presence of divalent cations (Fig. 50b) evidence an emission recovery that is a little slower than the previous case, but still representative of the formation of mobile SLBs.

As to the negatively charged lipids without the addition of divalent cations (Fig. 50c), none or very poor lateral diffusion for PS25, but a certain level of fluorescence recovery for PS25-NGF(1-14) is found. In fact, PS25-NGF(1-14) adlayers exhibit a minimum of fluorescence emission (i.e., immediately after bleaching) very similar to that found for the SLBs (~30% bleach of the initial intensity), however the further fluorescence recovery is modest compared to the SLB. Diffusion back into the spot during irradiation can explain this behavior. This is not the case for the bare PS25 adlayers, where about 60% bleach of the initial intensity is attained. Therefore PS25-NGF(1-14) adsorption on silica, without addition of divalent cations, results in a mixed adlayer where the fraction of mobile lipids, likely as SLBs patches, is significantly higher than in the corresponding bare PS25. Further measurements by using different spot sizes and irradiation times are in progress to account for this interpretation.

4.5.3 Biocompatibility assay of NGF/lipid adlayers with neuroblastoma SHSY5Y cells.

Measurements of neuroblastoma SHSY5Y cells have been carried out in order to assess: *(i)* the suitability of the different lipid-based nanoplatforms as adhesive, non toxic supports for cells, *(ii)* if any, cellular morphological differences on the NGF-functionalized lipid adlayers with respect to the control bare ones.

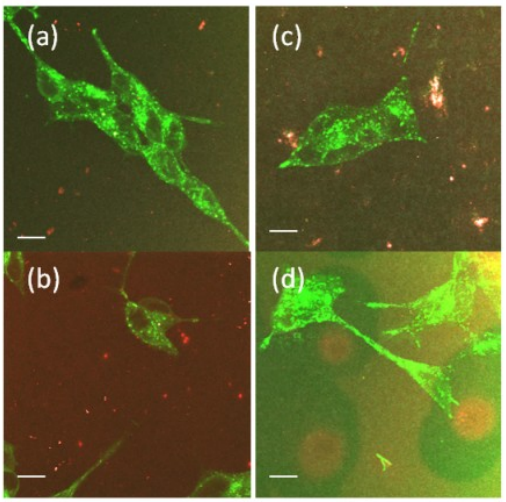

Figure 51. *Merged green ($\lambda_{ex}/\lambda_{em}$=488/519 nm, cellular staining of lysosome) and red ($\lambda_{ex}/\lambda_{em}$=543/591 nm, lipid staining with rhodamine) fluorescence channels from confocal microscopy imaging of SHSY5Y cells on: (a) PC, (b) PC-NGF, (c) PS25, (d) PS25-NGF. Scale bar=10 μm.*

Figure 51 allows visualizing different levels of interaction between cells (in green) and supported lipid adlayers (in red). According to QCM-D and FRAP results, a lipid membrane, more or less defective, is visible underneath the adhered cells for both zwitterionic and negatively charged lipids (clearly visible patches of lipid membranes for PS25-NGF). Cellular morphology clearly evidence a good adhesion and the cellular survival, even thought the prolonged time of incubation (48h) and the repeated rinsing

steps with PBS buffer, is not compromised for any of the investigated charge conditions. Moreover, the overall aspect of the cells plated on the NGF-associated in comparison to the corresponding bare lipid adlayers, indicates a lack of ameliorate for the zwitterionic lipid, but an evident improvement for the negatively charged ones.

4.5.4 Adsorption processes of NGF/lipid adlayers in silica nanoparticles

The implementation of the above-described systems from model planar surfaces to silica nanoparticles has been investigated by the use of porous core-shell silica nanoparticles (NP) dye-doped with coumarin in the interior [302-303], kindly provided by Prof. Prodi.

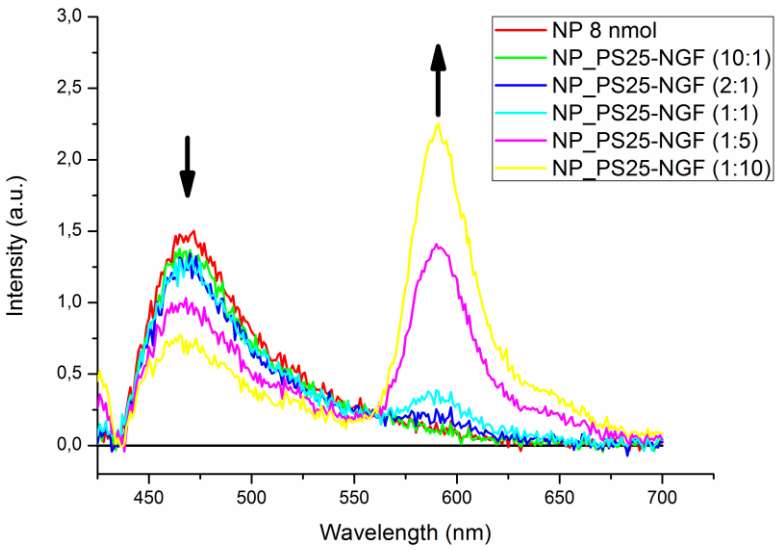

Figure 52. *Emission spectra (excitation at 380 nm) of a solution 2.7 μM of NP in 10 mM $MgCl_2$ phosphate buffer upon subsequent additions of NGF-PS25 vesicles in molar ratios from 10:1 to 1:10.*

Figure 52 shows that, by progressive additions of PS25-NGF vesicles to the silica nanoparticles, a decrease of the coumarin emission (at 475 nm) and a corresponding

increase of rhodamine emission (at 590 nm) is obtained.

The intensity values corrected for taking into account both inner filter effects and concentration changes [304] show that the decrease of the coumarin emission is not due to these artefacts, while the increase of the rhodamine emission cannot be completely explained in term of its concentration increase. Such a finding points to an energy transfer process, indicative of a close distance between the two fluorophores. This is likely due to the SLB wrapping the silica nanoparticles, a process that could modify the possible interaction among nanoparticles and cell, including cell internalization.[302-304] Moreover, we would like to underline that the coumarin moieties are covalently linked to the silica core, so that the effect cannot be due to dye leakage.

5. Concluding remarks

Many questions are attracting the attention of neuroscientists in the understanding of specific molecular processes that regulate neuronal metabolism, growth, differentiation, as well as, obviously, more qualified activities like memory formation. Researchers have been prompted to go in deep on the details of long term memory, indentifying what are the actors of memory consolidation and how they interact each other.[1-2,4,24,44]

An increasing number of evidences suggest that transition metal ions play a role in neuromodulation/neurotransmission. [177-178,185,196,198,239] The brain is an organ with extraordinary complexity and unique chemical composition. Strikingly, although they are often called "trace metals", their concentration can rise up to values 10000-fold higher than common neurotransmitters and neuropeptides and these abundance in the synaptic cleft provide a clue of their functional role in the brain and, perhaps, in memory consolidation. [177-179,185,194,196,198,204,239] Indeed, not only do these metals serve as components of various proteins and enzymes essential for normal brain function, but their labile forms, particularly those of Zn^{2+} and $Cu^{+/2+}$, are also connected to specialized brain activities. Intriguingly, the levels of zinc(II) and copper(II) ions have been found to rise up to micromolar concentration in the glutamatergic synapses if the hippocampus, the brain area involved in learning and memory, regions where neurotrophins performs their activity.[44,194,204,305]

The neurotrophin (NT) family comprises nerve growth factor (NGF), brain-derived neurotrophic factor (BDNF), neurotrophin-3 (NT-3) and neurotrophin-4 (NT-4). These are small, structurally related, proteins essential for neuronal survival and maintenance, as well as for dendritic arborization, circuit formation and wiring regulation of the central and peripheral nervous system. [37-44] The latter properties explain why, among many proteins and biochemical pathways, neurotrophins and their receptors have gained attentions as key players in the physio/pathology of the brain. [37-44]

In the last years, the direct interaction of d-block metal ions with the neurotrophines has been investigated, suggesting that metal ions can directly modulate the activities of the

neurotrophins, likely through conformational changes, and/or indirectly by activating their downstream signaling in a neurotrophin-independent mode.

Despite the importance of these modulations, the coordination features of metal ions complexes with neurotrophins have been determined only by theoretical methods. [254-256,258,260,271] The limit of these theoretical papers is the absence of experimental data inherent the coordination features. Moreover, it has not tested the hypotheses according to which Zn^{2+} and Cu^{2+} could have different binding environments, nor that Ser1 α-amino group could be involved in coordination. However, computational studies have predicted that the N-terminal domain of the protein represents the main metal ion binding region. This is really interesting because biochemical, crystallographic and computational studies converge to suggest that the N-terminal residues of neurotrophins are crucial for specific activities toward their cognate Trk receptor.[47,163,172,174,179,306]

We have synthesized the peptide fragments encompassing the N-terminal domain of NGF and BDNF and their Cu^{2+} and Zn^{2+} complexes have been characterized by means of a multi-technique approach. [307-308]

The Zn^{2+} and Cu^{2+} complexes with the peptide fragments encompassing the N-terminal sequence 1-14 of human NGF have been characterized by means of potentiometric and NMR, EPR, CD, UV-vis techniques. We have demonstrated that copper and zinc bind the the N-terminal domain with different coordination modes. Ser1 amino group is not only involved in Cu^{2+} binding also at acidic pH but it represents the main metal anchoring site as shown by the data obtained for the free and the acetylated peptide. Similar studied have been carried out to characterize the Zn^{2+} and Cu^{2+} complexes with the peptide fragment BDNF(1-12) encompassing the N-terminal sequence 1-12 of BDNF, stressing again the importance of the amino group.

The proliferative effect of NGF and BDNF peptides, as well as the whole protein, has been tested on neuronal SHSY5Y cell cultures.

The addition of both copper(II) and zinc(II) ions induces a remarkable difference in the activity of NGF(1-14) and its acetylated analogous AcNGF(1-14). NGF(1-14) proliferative

effect is significantly increased in the presence of Zn^{2+} or Cu^{2+} ions, while the AcNGF(1-14) activity is practically unaffected in the same experimental conditions, reinforcing the thermodynamic and spectroscopic results and highlight the role played by the N-terminus amine group. Cu^{2+} and Zn^{2+} influence the NGF proliferative activity in a different manner: the addition of Cu^{2+} induces a synergic effect similar to NGF(1-14) peptide, whilst Zn^{2+} causes a decrease of the protein proliferative activity.

As regarding BDNF peptides, interestingly, Ac-BDNF(1-12) and BDNF(1-12)D3N peptides display higher proliferative activity than wild type BDNF(1-12). Computational studies show that Ac-BDNF and BDNF(1-12)D3N may better interact with receptor recognition site due to the absence of determined intra-molecular interaction involving the N-terminal amino group and/or the aspartate carboxylate side chain. The addition of Cu^{2+} induces a decrease in both the proliferative activity of BDNF(1-12) and the whole BDNF protein. Intriguingly, zinc exerts the opposite effect, increasing both the activity of the whole protein and wild type BDNF(1-12). This result is opposite to that observed for the peptide NGF(1-14) and the NGF protein.

It is remarkable that zinc and copper differently modulate the activity of the neurotrophins. Copper is s positive modulator of NGF and a negative modulator of BDNF. On the other side, zinc has exactly the opposite role: it reduces the activity of NGF and increases the activity of BDNF. Though the biological tests presented here are to be regarded as preliminary results, undoubtedly they indicate that Cu^{2+} and Zn^{2+} may drive differently the activity of the two neurotrophins NGF and BDNF.

From an inorganic perspective, we can speculate that metal ions are able to modulate the activity of the neurotrophins also in function of the pH values. We can speculate that metal ions directly modulate the activities of the NGF and BDNF, likely through conformational changes that involve the N-terminal domain. The distribution diagrams reported in Figure 53 can be used to compare the metal binding affinity of the peptides NGF(1-14) and BDNF(1-12). Indeed, Figure 53 clearly shows that BDNF(1-12) is able to bind a single copper(II) ion more tightly than NGF(1-12) at acidic pH. In the pH range 6-6.5, the copper(II) is distributed among the two peptides. Increasing the pH, there is an inversion with the copper(II) ion bound prevalently to NGF(1-14). In particular, at physiological pH,

NGF(1-14) binds the 90% of metal ion. It is interesting to note that pH variation can occur in pathological condition, but also in local environment such us intracellular compartments or in the synaptic cleft. Thus, N-terminal domain of the neurotrophins, recognition binding domain, may be differently regulated by Cu^{2+} ions, also as function of pH value. Generalizing, we can speculate that such mechanism is responsible of neurotrophins modulation in physiological condition and might have a role in cognitive function as memory formation.

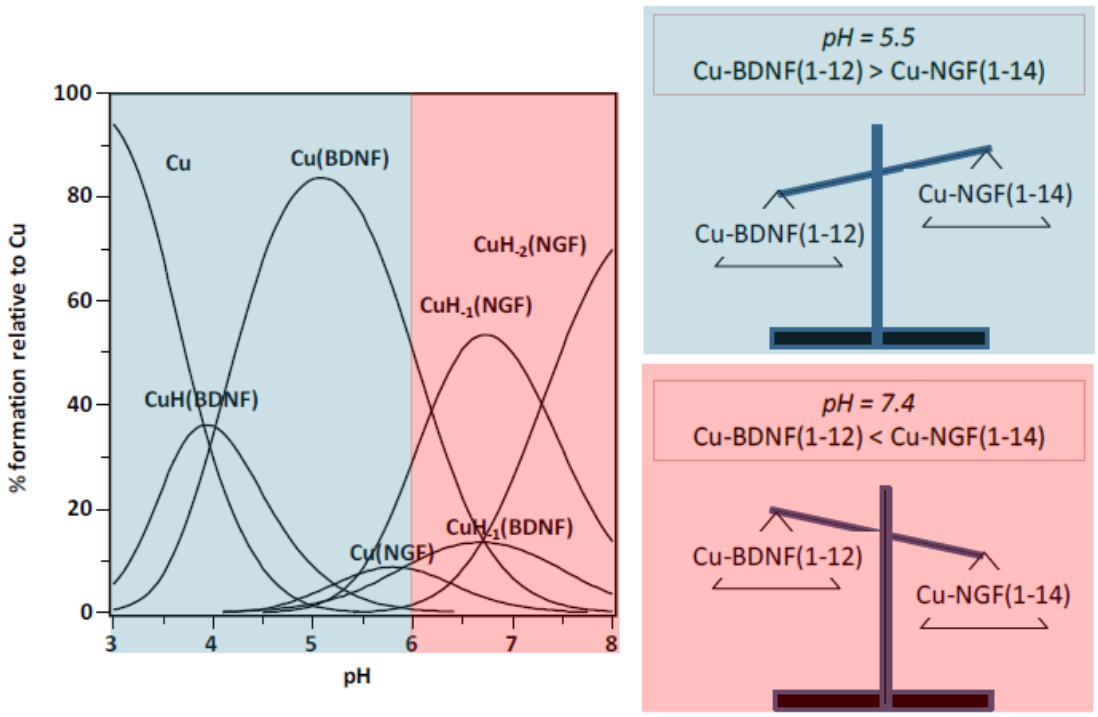

Figure 53. *Species distribution diagram for the Cu(II) complexes in aqueous solution with NGF(1-14) and BDNF(1-12).*

Further studies are in progress to clarify the role of metals on the neurotrophins activities and their role in synaptic plasticity.

Moreover, beside their physiological role, neurotrophins and their receptor have recently gained attention as potential target for neurological disease. Indeed, the alteration of neurotrophins homeostasis has been observed in pathological condition, as well neurotrophins exert a key role in the glutamatergic synapses if the hippocampus, thus overlapping with the area involved in learning and memory and of early occurrence of Aβ amyloid plaques in Alzheimer Disease (Fig. 54).[179]

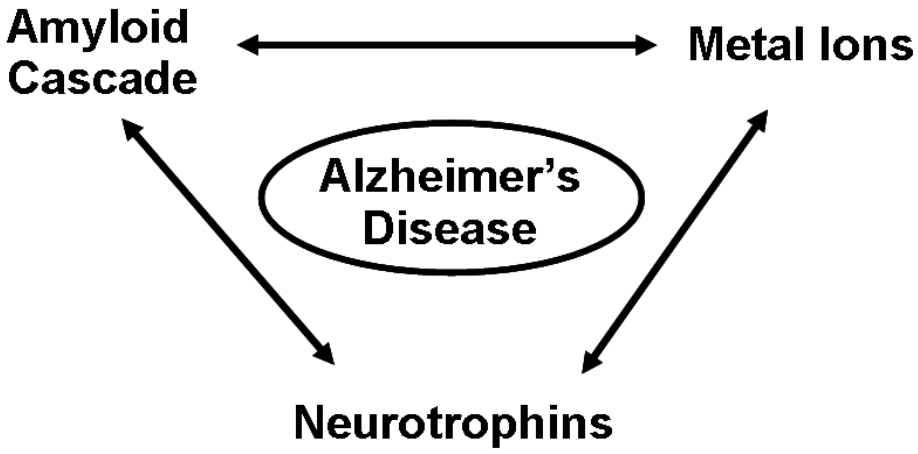

Figure 54. *Metal ions: the missing link between neurotrophins and β-amyloid.*

Neurodeurodegenerative diseases are pathologies without cures. Considerable efforts have been made to obtain agents able to interact with selective receptors mimicking or antagonizing the neurotrophins activities.[309] Linear peptides, containing loops 1 and 4 and the N-terminal region of the trophic protein, have been reported to show inhibitory but to lack agonist activity.[147,310] Conversely, cyclic peptides have been reported to have agonist activity *in vitro*. [311]

Even though the treatment with our peptide fragments has not induced any morphological difference on PC12, NGF(1-14) is able to activate the TrkA pathway and to induce the phosphorylation of CREB Ser-133.

It is the first time that a linear peptide is able to activate the Trk signaling, instead of conformational restricted peptides. Second, NGF(1-14) is not only a peptidomimetic, but a small portion of NGF. It is unusual that a piece of a protein display, at least in part, the same action of the whole protein. We could speculate that the regulated degradation/digestion of the whole neurotrophins, and subsequent formation of small N-terminal domain peptides, has a physiological role. Third, since the peptide induce the phosphorylation of TrkA, reduce the proliferation rate of PC12 without affecting the morphological state of PC12 cells (e.g. without inducing differentiation), it drives to the conclusion that our peptide active some, but not all, the NGF signaling. Among the biochemical signals activated, it is really interesting the ability of NGF(1-14) to induce the phosphorylation of CREB. Due to the role of CREB phosphorylation on memory consolidation and its underlying synaptic plasticity, such a molecule has potential application as memory enhancer. Also, our preliminary studies on the ability of NGF(1-14) to activate the PI3K/AKT signaling provide an explanation for the strong synergic effect observed after the co-treatment of NGF(1-14) and copper.

Further studies will unravel the molecular pathway activated by NGF(1-14) as well the effect of this peptide and its metal complexes in memory formation.

Neurotrophins are attractive therapeutic option for several diseases, including neurodegenerative disorders, inflammation, distinct types of cancers and (maybe) Rett Syndrome. The discovery that BDNF signaling recruits MeCP2 is extremely attractive. Our findings suggest that MeCP2 has a physiological role in memory formation. Many different brain regions show a peculiar induction of MeCP2 after the learning experience, though the functional meaning of these results is not clear and need further investigations. Also, despite the fact that recent contributions point out the presence of MeCP2 in astrocytes, the double staining of hippocampal dentate gyrus with MeCP2 and GFAP strongly suggest that MeCP2 is exclusively expressed in neurons. All together, these results might provide new therapeutic strategies for patients affected by Rett Syndrome.

However, both the use of NGF and BDNF is prevented by their poor pharmacological properties, such as the scarce blood-brain barrier permeability and adverse relevant side effects.

Adlayers and/or supported lipid bilayers, formed by the NGF(1-14)-SUV adsorption on silica (both planar model and nanoparticles), have been characterized in view of application as functional nanoplatforms for cell adhesion and drug delivery (Fig. 55). This study is very promising to overcome the major obstacles limit in the clinical application of neurotrophins, as lipid/polymeric biocompatible materials have the huge advantage to potentially be administrated intravenously. Further investigations are in progress to set the optimal lipid composition/charge conditions, the subsequent transfer to SLB-wrapped silica nanoparticles, as well as in-depth cellular assays.

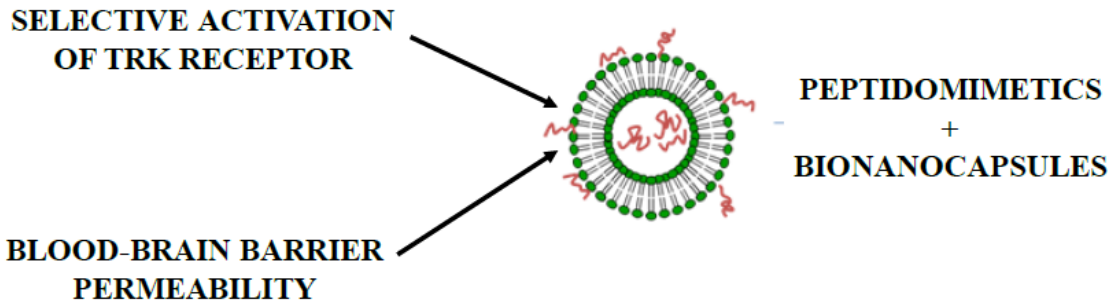

Figure 55. *Peptidomimetics and bionanocapsule, a challenge to overcome the major issues in neurotrophins based therapies.*

The emerging importance of the role of biometals and the mounting evidences on the different, not yet fully understood, mechanisms of signal transduction in which they are involved producing significant derangements, or guaranteeing the perfect function of neural networks, underlines the need to get deeper inside the knowledge of metallostasis in the CNS.

The interaction of metals and neurotrophins might represent a crossroad for neuronal

physiology. Better understanding of metal ion-driven neurotrophins signal transduction and intercellular signaling, as well as vice versa, the role of neurotrophins in the control of metallostasis, could disclose helpful information , and it is therefore strongly rising as one of the most critical step in the study of neurodegenerative diseases as well physiological mechanisms of memory.

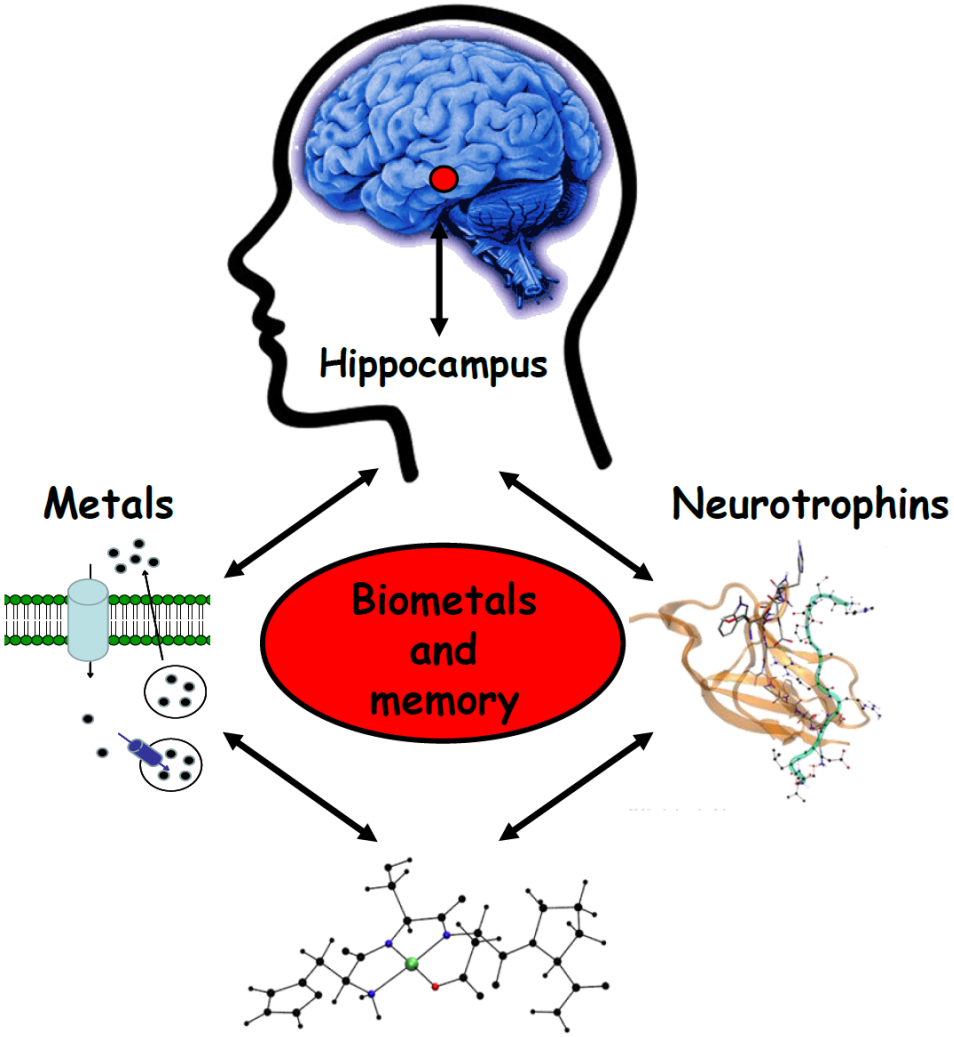

Figure 56. *Memory, metals and neurotrophins. The overlapping functions of neurotrophins and biometals in the hippocampus, as well as the ability of metal ionsto modulate the activities of the neurotrophins provide a clue of their functional role in the brain and in memory consolidation.*

Acknowledgements

Many thanks, for their invaluable contributions, to all the people that participated to this project.

UNIVERSITÀ di CATANIA

Prof Rizzarelli
Prof Arena
Prof Nicoletti
Dr Satriano

ALMA MATER STUDIORUM UNIVERSITÀ DI BOLOGNA

Prof Prodi

FONDAZIONE EBRI "RITA LEVI-MONTALCINI"

Prof Calissano

UNIVERSITÀ DI PISA

Prof La Mendola

[redacted]

Prof Fattorusso
Prof Isernia

NEW YORK UNIVERSITY

Prof Alberini
Dr Bambah-Mukku

IBB

Dr. Magrì
Dr Giuffrida

UMG Università Magna Graecia di Catanzaro

Dr Pietropaolo

References

(1) McGaugh, J. L. *Science* **2000**, *287*, 248.

(2) Dudai, Y. *Annu Rev Psychol* **2004**, *55*, 51.

(3) Tronson, N. C.; Taylor, J. R. *Nat Rev Neurosci* **2007**, *8*, 262.

(4) Kandel, E. R. *Science* **2001**, *294*, 1030.

(5) Squire, L. R. *Memory and Brain*; New York: Oxford Univ. Press, 1987.

(6) Alberini, C. M.; Milekic, M. H.; Tronel, S. *Cell Mol Life Sci* **2006**, *63*, 999.

(7) Diekelmann, S.; Buchel, C.; Born, J.; Rasch, B. *Nat Neurosci* **2011**, *14*, 381.

(8) Miller, R. R.; Matzel, L. D. *Nat Rev Neurosci* **2000**, *1*, 214.

(9) Bailey, C. H.; Bartsch, D.; Kandel, E. R. *Proc Natl Acad Sci U S A* **1996**, *93*, 13445.

(10) Lee, J. L.; Everitt, B. J.; Thomas, K. L. *Science* **2004**, *304*, 839.

(11) Kandel, E. R.; Klein, M.; Castellucci, V. F.; Schacher, S.; Goelet, P. *Neurosci Res* **1986**, *3*, 498.

(12) Bliss, T. V.; Collingridge, G. L. *Nature* **1993**, *361*, 31.

(13) Squire, L. R.; Davis, H. P. *Annu Rev Pharmacol Toxicol* **1981**, *21*, 323.

(14) Squire, L. R.; Davis, H. P.; Spanis, C. W. *Science* **1980**, *209*, 836.

(15) Goelet, P.; Castellucci, V. F.; Schacher, S.; Kandel, E. R. *Nature* **1986**, *322*, 419.

(16) Alberini, C. M. *Trends Neurosci* **2005**, *28*, 51.

(17) Sara, S. J. *Learn Mem* **2000**, *7*, 73.

(18) Malenka, R. C. *Nat Rev Neurosci* **2003**, *4*, 923.

(19) Malenka, R. C.; Nicoll, R. A. *Science* **1999**, *285*, 1870.

(20) Malenka, R. C. *Mol Neurobiol* **1991**, *5*, 289.

(21) Malenka, R. C.; Kauer, J. A.; Perkel, D. J.; Mauk, M. D.; Kelly, P. T.; Nicoll, R. A.; Waxham, M. N. *Nature* **1989**, *340*, 554.

(22) Kauer, J. A.; Malenka, R. C.; Nicoll, R. A. *Neuron* **1988**, *1*, 911.

(23) Alberini, C. M. *Neurobiol Learn Mem* **2008**, *89*, 234.

(24) Alberini, C. M. *Physiol Rev* **2009**, *89*, 121.

(25) Gold, P. E. *Neurobiol Learn Mem* **2008**, *89*, 201.

(26) van Praag, H.; Schinder, A. F.; Christie, B. R.; Toni, N.; Palmer, T. D.; Gage, F. H. *Nature* **2002**, *415*, 1030.

(27) Shors, T. J.; Miesegaes, G.; Beylin, A.; Zhao, M.; Rydel, T.; Gould, E. *Nature* **2001**, *410*, 372.

(28) Tronel, S.; Milekic, M. H.; Alberini, C. M. *PLoS Biol* **2005**, *3*, e293.

(29) Taubenfeld, S. M.; Muravieva, E. V.; Garcia-Osta, A.; Alberini, C. M. *Proc Natl Acad Sci U S A* **2010**, *107*, 12345.

(30) Taubenfeld, S. M.; Riceberg, J. S.; New, A. S.; Alberini, C. M. *Biol Psychiatry* **2009**, *65*, 249.

(31) Nader, K.; Schafe, G. E.; LeDoux, J. E. *Nat Rev Neurosci* **2000**, *1*, 216.

(32) Morris, R. G.; Inglis, J.; Ainge, J. A.; Olverman, H. J.; Tulloch, J.; Dudai, Y.; Kelly, P. A. *Neuron* **2006**, *50*, 479.

(33) Milekic, M. H.; Alberini, C. M. *Neuron* **2002**, *36*, 521.

(34) Levi-Montalcini, R.; Calissano, P. *Sci Am* **1979**, *240*, 68.

(35) Levi-Montalcini, R. *Science* **1987**, *237*, 1154.

(36) Cohen, S.; Levi-Montalcini, R.; Hamburger, V. *Proc Natl Acad Sci U S A* **1954**, *40*, 1014.

(37) Fox, K.; Zahs, K. *Curr Opin Neurobiol* **1994**, *4*, 112.

(38) Thoenen, H. *Science* **1995**, *270*, 593.

(39) Kang, H.; Schuman, E. M. *Science* **1995**, *267*, 1658.

(40) Kang, H.; Schuman, E. M. *Science* **1996**, *273*, 1402.

(41) Lohof, A. M.; Ip, N. Y.; Poo, M. M. *Nature* **1993**, *363*, 350.

(42) Minichiello, L. *Nat Rev Neurosci* **2009**, *10*, 850.

(43) Huang, E. J.; Reichardt, L. F. *Annu Rev Neurosci* **2001**, *24*, 677.

(44) McAllister, A. K.; Katz, L. C.; Lo, D. C. *Annu Rev Neurosci* **1999**, *22*, 295.

(45) Wiesmann, C.; de Vos, A. M. *Cell Mol Life Sci* **2001**, *58*, 748.

(46) Lewin, G. R.; Barde, Y. A. *Annu Rev Neurosci* **1996**, *19*, 289.

(47) Ibanez, C. F. *J Neurobiol* **1994**, *25*, 1349.

(48) Ilag, L. L.; Lonnerberg, P.; Persson, H.; Ibanez, C. F. *J Biol Chem* **1994**, *269*, 19941.

(49) Lee, R.; Kermani, P.; Teng, K. K.; Hempstead, B. L. *Science* **2001**, *294*, 1945.

(50) Chao, M. V.; Bothwell, M. *Neuron* **2002**, *33*, 9.

(51) Chao, M. V. *Nat Rev Neurosci* **2003**, *4*, 299.

(52) Schecterson, L. C.; Bothwell, M. *Dev Neurobiol* **2010**, *70*, 332.

(53) Barbacid, M. *J Neurobiol* **1994**, *25*, 1386.

(54) Huang, E. J.; Reichardt, L. F. *Annu Rev Biochem* **2003**, *72*, 609.

(55) Al-Shawi, R.; Hafner, A.; Chun, S.; Raza, S.; Crutcher, K.; Thrasivoulou, C.; Simons, P.; Cowen, T. *Ann N Y Acad Sci* **2007**, *1119*, 208.

(56) Wang, Y. J.; Valadares, D.; Sun, Y.; Wang, X.; Zhong, J. H.; Liu, X. H.; Majd, S.; Chen, L.; Gao, C. Y.; Chen, S.; Lim, Y.; Pollard, A.; Salegio, E. A.; Gai, W. P.; Yang, M.; Zhou, X. F. *Neurotox Res* **2010**, *17*, 257.

(57) Nykjaer, A.; Lee, R.; Teng, K. K.; Jansen, P.; Madsen, P.; Nielsen, M. S.; Jacobsen, C.; Kliemannel, M.; Schwarz, E.; Willnow, T. E.; Hempstead, B. L.; Petersen, C. M. *Nature* **2004**, *427*, 843.

(58) Frade, J. M.; Rodriguez-Tebar, A.; Barde, Y. A. *Nature* **1996**, *383*, 166.

(59) Frade, J. M.; Barde, Y. A. *Bioessays* **1998**, *20*, 137.

(60) Montarolo, P. G.; Goelet, P.; Castellucci, V. F.; Morgan, J.; Kandel, E. R.; Schacher, S. *Science* **1986**, *234*, 1249.

(61) Neale, J. H.; Klinger, P. D.; Agranoff, B. W. *Science* **1973**, *179*, 1243.

(62) Agranoff, B. W.; Davis, R. E.; Casola, L.; Lim, R. *Science* **1967**, *158*, 1600.

(63) Agranoff, B. W.; Davis, R. E. *Science* **1967**, *158*, 523.

(64) Alberini, C. M. *J Exp Biol* **1999**, *202*, 2887.

(65) Han, J. H.; Kushner, S. A.; Yiu, A. P.; Cole, C. J.; Matynia, A.; Brown, R. A.; Neve, R. L.; Guzowski, J. F.; Silva, A. J.; Josselyn, S. A. *Science* **2007**, *316*, 457.

(66) Bonni, A.; Brunet, A.; West, A. E.; Datta, S. R.; Takasu, M. A.; Greenberg, M. E. *Science* **1999**, *286*, 1358.

(67) Ghosh, A.; Greenberg, M. E. *Science* **1995**, *268*, 239.

(68) DeCoster, M. A. *Adv Neuroimmunol* **1995**, *5*, 233.

(69) Shaywitz, A. J.; Greenberg, M. E. *Annu Rev Biochem* **1999**, *68*, 821.

(70) Sheng, M.; Thompson, M. A.; Greenberg, M. E. *Science* **1991**, *252*, 1427.

(71) Saura, C. A.; Valero, J. *Rev Neurosci* **2011**, *22*, 153.

(72) Nan, X.; Ng, H. H.; Johnson, C. A.; Laherty, C. D.; Turner, B. M.; Eisenman, R. N.; Bird, A. *Nature* **1998**, *393*, 386.

(73) McGraw, C. M.; Samaco, R. C.; Zoghbi, H. Y. *Science* **2011**, *333*, 186.

(74) Lewis, J. D.; Meehan, R. R.; Henzel, W. J.; Maurer-Fogy, I.; Jeppesen, P.; Klein, F.; Bird, A. *Cell* **1992**, *69*, 905.

(75) Guy, J.; Cheval, H.; Selfridge, J.; Bird, A. *Annu Rev Cell Dev Biol* **2011**, *27*, 631.

(76) Amir, R. E.; Van den Veyver, I. B.; Wan, M.; Tran, C. Q.; Francke, U.; Zoghbi, H. Y. *Nat Genet* **1999**, *23*, 185.

(77) Guy, J.; Hendrich, B.; Holmes, M.; Martin, J. E.; Bird, A. *Nat Genet* **2001**, *27*, 322.

(78) Chahrour, M.; Jung, S. Y.; Shaw, C.; Zhou, X.; Wong, S. T.; Qin, J.; Zoghbi, H. Y. *Science* **2008**, *320*, 1224.

(79) Chahrour, M.; Zoghbi, H. Y. *Neuron* **2007**, *56*, 422.

(80) Skene, P. J.; Illingworth, R. S.; Webb, S.; Kerr, A. R.; James, K. D.; Turner, D. J.; Andrews, R.; Bird, A. P. *Mol Cell* **2010**, *37*, 457.

(81) Cohen, S.; Gabel, H. W.; Hemberg, M.; Hutchinson, A. N.; Sadacca, L. A.; Ebert, D. H.; Harmin, D. A.; Greenberg, R. S.; Verdine, V. K.; Zhou, Z.; Wetsel, W. C.; West, A. E.; Greenberg, M. E. *Neuron* **2011**, *72*, 72.

(82) Li, H.; Zhong, X.; Chau, K. F.; Williams, E. C.; Chang, Q. *Nat Neurosci* **2011**, *14*, 1001.

(83) Zhou, Z.; Hong, E. J.; Cohen, S.; Zhao, W. N.; Ho, H. Y.; Schmidt, L.; Chen, W. G.; Lin, Y.; Savner, E.; Griffith, E. C.; Hu, L.; Steen, J. A.; Weitz, C. J.; Greenberg, M. E. *Neuron* **2006**, *52*, 255.

(84) Chen, W. G.; Chang, Q.; Lin, Y.; Meissner, A.; West, A. E.; Griffith, E. C.; Jaenisch, R.; Greenberg, M. E. *Science* **2003**, *302*, 885.

(85) Martinowich, K.; Hattori, D.; Wu, H.; Fouse, S.; He, F.; Hu, Y.; Fan, G.; Sun, Y. E. *Science* **2003**, *302*, 890.

(86) Thompson, L. M. *Nature* **2008**, *452*, 707.

(87) Bredesen, D. E.; Rao, R. V.; Mehlen, P. *Nature* **2006**, *443*, 796.

(88) Ferri, C. P.; Prince, M.; Brayne, C.; Brodaty, H.; Fratiglioni, L.; Ganguli, M.; Hall, K.; Hasegawa, K.; Hendrie, H.; Huang, Y.; Jorm, A.; Mathers, C.; Menezes, P. R.; Rimmer, E.; Scazufca, M. *Lancet* **2005**, *366*, 2112.

(89) Hardy, J. A.; Higgins, G. A. *Science* **1992**, *256*, 184.

(90) Haass, C.; Selkoe, D. J. *Nat Rev Mol Cell Biol* **2007**, *8*, 101.

(91) Shoji, M.; Golde, T. E.; Ghiso, J.; Cheung, T. T.; Estus, S.; Shaffer, L. M.; Cai, X. D.; McKay, D. M.; Tintner, R.; Frangione, B.; et al. *Science* **1992**, *258*, 126.

(92) Mattson, M. P. *Nature* **2004**, *430*, 631.

(93) Bossy-Wetzel, E.; Schwarzenbacher, R.; Lipton, S. A. *Nat Med* **2004**, *10 Suppl*, S2.

(94) Giuffrida, M. L.; Caraci, F.; De Bona, P.; Pappalardo, G.; Nicoletti, F.; Rizzarelli, E.; Copani, A. *Rev Neurosci* **2010**, *21*, 83.

(95) Giuffrida, M. L.; Caraci, F.; Pignataro, B.; Cataldo, S.; De Bona, P.; Bruno, V.; Molinaro, G.; Pappalardo, G.; Messina, A.; Palmigiano, A.; Garozzo, D.; Nicoletti, F.; Rizzarelli, E.; Copani, A. *J Neurosci* **2009**, *29*, 10582.

(96) Shigenaga, M. K.; Hagen, T. M.; Ames, B. N. *Proc Natl Acad Sci U S A* **1994**, *91*, 10771.

(97) Levine, B.; Kroemer, G. *Cell* **2008**, *132*, 27.

(98) Conner, J. M.; Lauterborn, J. C.; Yan, Q.; Gall, C. M.; Varon, S. *J Neurosci* **1997**, *17*, 2295.

(99) Connor, B.; Young, D.; Yan, Q.; Faull, R. L.; Synek, B.; Dragunow, M. *Brain Res Mol Brain Res* **1997**, *49*, 71.

(100) Korsching, S.; Auburger, G.; Heumann, R.; Scott, J.; Thoenen, H. *EMBO J* **1985**, *4*, 1389.

(101) Calissano, P.; Amadoro, G.; Matrone, C.; Ciafre, S.; Marolda, R.; Corsetti, V.; Ciotti, M. T.; Mercanti, D.; Di Luzio, A.; Severini, C.; Provenzano, C.; Canu, N. *Cell Death Differ* **2010**, *17*, 1126.

(102) Calissano, P.; Matrone, C.; Amadoro, G. *Dev Neurobiol* **2010**, *70*, 372.

(103) Yuen, E. C.; Howe, C. L.; Li, Y.; Holtzman, D. M.; Mobley, W. C. *Brain Dev* **1996**, *18*, 362.

(104) Auburger, G.; Heumann, R.; Hellweg, R.; Korsching, S.; Thoenen, H. *Dev Biol* **1987**, *120*, 322.

(105) Coulson, E. J.; May, L. M.; Sykes, A. M.; Hamlin, A. S. *Neuroscientist* **2009**, *15*, 317.

(106) Mufson, E. J.; Counts, S. E.; Perez, S. E.; Ginsberg, S. D. *Expert Rev Neurother* **2008**, *8*, 1703.

(107) Capsoni, S.; Cattaneo, A. *Cell Mol Neurobiol* **2006**, *26*, 619.

(108) Zhou, Y.; Lu, T. J.; Xiong, Z. Q. *Cell Res* **2009**, *19*, 525.

(109) Boissiere, F.; Faucheux, B.; Ruberg, M.; Agid, Y.; Hirsch, E. C. *Exp Neurol* **1997**, *145*, 245.

(110) Boissiere, F.; Lehericy, S.; Strada, O.; Agid, Y.; Hirsch, E. C. *Mol Chem Neuropathol* **1996**, *28*, 219.

(111) Hock, C.; Heese, K.; Hulette, C.; Rosenberg, C.; Otten, U. *Arch Neurol* **2000**, *57*, 846.

(112) Hock, C.; Heese, K.; Muller-Spahn, F.; Hulette, C.; Rosenberg, C.; Otten, U. *Neurosci Lett* **1998**, *241*, 151.

(113) Hock, C. H.; Heese, K.; Olivieri, G.; Hulette, C. H.; Rosenberg, C.; Nitsch, R. M.; Otten, U. *J Neural Transm Suppl* **2000**, *59*, 171.

(114) Salehi, A.; Verhaagen, J.; Dijkhuizen, P. A.; Swaab, D. F. *Neuroscience* **1996**, *75*, 373.

(115) Costantini, C.; Della-Bianca, V.; Formaggio, E.; Chiamulera, C.; Montresor, A.; Rossi, F. *Exp Cell Res* **2005**, *311*, 126.

(116) Capsoni, S.; Tiveron, C.; Vignone, D.; Amato, G.; Cattaneo, A. *Proc Natl Acad Sci U S A* **2010**, *107*, 12299.

(117) Aboulkassim, T.; Tong, X. K.; Tse, Y. C.; Wong, T. P.; Woo, S. B.; Neet, K. E.; Brahimi, F.; Hamel, E.; Saragovi, H. U. *Mol Pharmacol* **2011**, *80*, 498.

(118) Kelly, A.; Maguire, C.; Lynch, M. A. *Neuroscience* **2000**, *95*, 359.

(119) Terry, A. V., Jr.; Kutiyanawalla, A.; Pillai, A. *Physiol Behav* **2011**, *102*, 149.

(120) Cattaneo, A.; Capsoni, S.; Paoletti, F. *J Alzheimers Dis* **2008**, *15*, 255.

(121) Larkfors, L.; Ebendal, T.; Whittemore, S. R.; Persson, H.; Hoffer, B.; Olson, L. *Brain Res* **1987**, *427*, 55.

(122) Narisawa-Saito, M.; Wakabayashi, K.; Tsuji, S.; Takahashi, H.; Nawa, H. *Neuroreport* **1996**, *7*, 2925.

(123) Phillips, H. S.; Hains, J. M.; Armanini, M.; Laramee, G. R.; Johnson, S. A.; Winslow, J. W. *Neuron* **1991**, *7*, 695.

(124) Peng, S.; Wuu, J.; Mufson, E. J.; Fahnestock, M. *J Neuropathol Exp Neurol* **2004**, *63*, 641.

(125) Cuello, A. C.; Bruno, M. A.; Allard, S.; Leon, W.; Iulita, M. F. *J Mol Neurosci* **2010**, *40*, 230.

(126) Pedraza, C. E.; Podlesniy, P.; Vidal, N.; Arevalo, J. C.; Lee, R.; Hempstead, B.; Ferrer, I.; Iglesias, M.; Espinet, C. *Am J Pathol* **2005**, *166*, 533.

(127) Kichev, A.; Ilieva, E. V.; Pinol-Ripoll, G.; Podlesniy, P.; Ferrer, I.; Portero-Otin, M.; Pamplona, R.; Espinet, C. *Am J Pathol* **2009**, *175*, 2574.

(128) Bruno, M. A.; Leon, W. C.; Fragoso, G.; Mushynski, W. E.; Almazan, G.; Cuello, A. C. *J Neuropathol Exp Neurol* **2009**, *68*, 857.

(129) Hofer, M.; Pagliusi, S. R.; Hohn, A.; Leibrock, J.; Barde, Y. A. *EMBO J* **1990**, *9*, 2459.

(130) Durany, N.; Michel, T.; Kurt, J.; Cruz-Sanchez, F. F.; Cervos-Navarro, J.; Riederer, P. *Int J Dev Neurosci* **2000**, *18*, 807.

(131) Holsinger, R. M.; Schnarr, J.; Henry, P.; Castelo, V. T.; Fahnestock, M. *Brain Res Mol Brain Res* **2000**, *76*, 347.

(132) Michalski, B.; Fahnestock, M. *Brain Res Mol Brain Res* **2003**, *111*, 148.

(133) Fahnestock, M.; Garzon, D.; Holsinger, R. M.; Michalski, B. *J Neural Transm Suppl* **2002**, 241.

(134) Peng, S.; Wuu, J.; Mufson, E. J.; Fahnestock, M. *J Neurochem* **2005**, *93*, 1412.

(135) Matrone, C.; Di Luzio, A.; Meli, G.; D'Aguanno, S.; Severini, C.; Ciotti, M. T.; Cattaneo, A.; Calissano, P. *J Alzheimers Dis* **2008**, *13*, 81.

(136) Matrone, C.; Ciotti, M. T.; Mercanti, D.; Marolda, R.; Calissano, P. *Proc Natl Acad Sci U S A* **2008**, *105*, 13139.

(137) Capsoni, S.; Giannotta, S.; Cattaneo, A. *Mol Cell Neurosci* **2002**, *21*, 15.

(138) Costantini, C.; Weindruch, R.; Della Valle, G.; Puglielli, L. *Biochem J* **2005**, *391*, 59.

(139) Matrone, C.; Marolda, R.; Ciafre, S.; Ciotti, M. T.; Mercanti, D.; Calissano, P. *Proc Natl Acad Sci U S A* **2009**, *106*, 11358.

(140) Yaar, M.; Zhai, S.; Pilch, P. F.; Doyle, S. M.; Eisenhauer, P. B.; Fine, R. E.; Gilchrest, B. A. *J Clin Invest* **1997**, *100*, 2333.

(141) Chakravarthy, B.; Gaudet, C.; Menard, M.; Atkinson, T.; Brown, L.; Laferla, F. M.; Armato, U.; Whitfield, J. *J Alzheimers Dis* **2010**, *19*, 915.

(142) Sotthibundhu, A.; Sykes, A. M.; Fox, B.; Underwood, C. K.; Thangnipon, W.; Coulson, E. J. *J Neurosci* **2008**, *28*, 3941.

(143) Susen, K.; Blochl, A. *J Mol Med (Berl)* **2005**, *83*, 720.

(144) Arevalo, M. A.; Roldan, P. M.; Chacon, P. J.; Rodriguez-Tebar, A. *J Neurochem* **2009**, *111*, 1425.

(145) Aliaga, E.; Silhol, M.; Bonneau, N.; Maurice, T.; Arancibia, S.; Tapia-Arancibia, L. *Neurobiol Dis* **2010**, *37*, 208.

(146) LeSauteur, L.; Cheung, N. K.; Lisbona, R.; Saragovi, H. U. *Nat Biotechnol* **1996**, *14*, 1120.

(147) Longo, F. M.; Massa, S. M. *J Alzheimers Dis* **2004**, *6*, S13.

(148) Wahlberg, L. U.; Lind, G.; Almqvist, P. M.; Kusk, P.; Tornoe, J.; Juliusson, B.; Soderman, M.; Sellden, E.; Seiger, A.; Eriksdotter-Jonhagen, M.; Linderoth, B. *J Neurosurg* **2012**, *117*, 340.

(149) Eriksdotter-Jonhagen, M.; Linderoth, B.; Lind, G.; Aladellie, L.; Almkvist, O.; Andreasen, N.; Blennow, K.; Bogdanovic, N.; Jelic, V.; Kadir, A.; Nordberg, A.; Sundstrom, E.; Wahlund, L. O.; Wall, A.; Wiberg, M.; Winblad, B.; Seiger, A.; Almqvist, P.; Wahlberg, L. *Dement Geriatr Cogn Disord* **2012**, *33*, 18.

(150) Fjord-Larsen, L.; Kusk, P.; Emerich, D. F.; Thanos, C.; Torp, M.; Bintz, B.; Tornoe, J.; Johnsen, A. H.; Wahlberg, L. U. *Gene Ther* **2012**, *19*, 1010.

(151) Fjord-Larsen, L.; Kusk, P.; Tornoe, J.; Juliusson, B.; Torp, M.; Bjarkam, C. R.; Nielsen, M. S.; Handberg, A.; Sorensen, J. C.; Wahlberg, L. U. *Mol Ther* **2010**, *18*, 2164.

(152) de Boer, R.; Knight, A. M.; Spinner, R. J.; Malessy, M. J.; Yaszemski, M. J.; Windebank, A. J. *J Biomed Mater Res A* **2010**, *95*, 1067.

(153) Camarata, P. J.; Suryanarayanan, R.; Turner, D. A.; Parker, R. G.; Ebner, T. J. *Neurosurgery* **1992**, *30*, 313.

(154) Cho, Y.; Shi, R.; Ivanisevic, A.; Ben Borgens, R. *Nanotechnology* **2009**, *20*, 275102.

(155) Cho, Y.; Shi, R.; Borgens, R.; Ivanisevic, A. *Small* **2008**, *4*, 1676.

(156) Cho, Y.; Shi, R.; Borgens, R. B.; Ivanisevic, A. *Nanomedicine (Lond)* **2008**, *3*, 507.

(157) Xie, Y.; Ye, L.; Zhang, X.; Cui, W.; Lou, J.; Nagai, T.; Hou, X. *J Control Release* **2005**, *105*, 106.

(158) Irvine, D. J. *Nat Mater* **2011**, *10*, 342.

(159) Ashley, C. E.; Carnes, E. C.; Phillips, G. K.; Padilla, D.; Durfee, P. N.; Brown, P. A.; Hanna, T. N.; Liu, J.; Phillips, B.; Carter, M. B.; Carroll, N. J.; Jiang, X.; Dunphy, D. R.; Willman, C. L.; Petsev, D. N.; Evans, D. G.; Parikh, A. N.; Chackerian, B.; Wharton, W.; Peabody, D. S.; Brinker, C. J. *Nat Mater* **2011**, *10*, 389.

(160) Alam, M. I.; Beg, S.; Samad, A.; Baboota, S.; Kohli, K.; Ali, J.; Ahuja, A.; Akbar, M. *Eur J Pharm Sci* **2010**, *40*, 385.

(161) Holland, D. R.; Cousens, L. S.; Meng, W.; Matthews, B. W. *J Mol Biol* **1994**, *239*, 385.

(162) Ultsch, M. H.; Wiesmann, C.; Simmons, L. C.; Henrich, J.; Yang, M.; Reilly, D.; Bass, S. H.; de Vos, A. M. *J Mol Biol* **1999**, *290*, 149.

(163) Wiesmann, C.; Ultsch, M. H.; Bass, S. H.; de Vos, A. M. *Nature* **1999**, *401*, 184.

(164) Zampieri, N.; Chao, M. V. *Science* **2004**, *304*, 833.

(165) Butte, M. J.; Hwang, P. K.; Mobley, W. C.; Fletterick, R. J. *Biochemistry* **1998**, *37*, 16846.

(166) Robinson, R. C.; Radziejewski, C.; Stuart, D. I.; Jones, E. Y. *Biochemistry* **1995**, *34*, 4139.

(167) Jungbluth, S.; Bailey, K.; Barde, Y. A. *Eur J Biochem* **1994**, *221*, 677.

(168) Wehrman, T.; He, X.; Raab, B.; Dukipatti, A.; Blau, H.; Garcia, K. C. *Neuron* **2007**, *53*, 25.

(169) He, X. L.; Garcia, K. C. *Science* **2004**, *304*, 870.

(170) Kahle, P.; Burton, L. E.; Schmelzer, C. H.; Hertel, C. *J Biol Chem* **1992**, *267*, 22707.

(171) Woo, S. B.; Neet, K. E. *J Biol Chem* **1996**, *271*, 24433.

(172) Woo, S. B.; Timm, D. E.; Neet, K. E. *J Biol Chem* **1995**, *270*, 6278.

(173) Shih, A.; Laramee, G. R.; Schmelzer, C. H.; Burton, L. E.; Winslow, J. W. *J Biol Chem* **1994**, *269*, 27679.

(174) Berrera, M.; Cattaneo, A.; Carloni, P. *Biophys J* **2006**, *91*, 2063.

(175) Settanni, G.; Cattaneo, A.; Carloni, P. *Biophys J* **2003**, *84*, 2282.

(176) Berg, J. M.; Shi, Y. *Science* **1996**, *271*, 1081.

(177) Mounicou, S.; Szpunar, J.; Lobinski, R. *Chem Soc Rev* **2009**, *38*, 1119.

(178) Milardi, D.; Rizzarelli, E. *Neurodegeneration, Metallostasis and Proteostasis*; Eds. RSC, Cambridge, 2011.

(179) Travaglia, A.; Pietropaolo, A.; La Mendola, D.; Nicoletti, V. G.; Rizzarelli, E. *J Inorg Biochem* **2012**, *111*, 130.

(180) Liuzzi, J. P.; Cousins, R. J. *Annu Rev Nutr* **2004**, *24*, 151.

(181) Palmiter, R. D.; Huang, L. *Pflugers Arch* **2004**, *447*, 744.

(182) Eide, D. J. *Pflugers Arch* **2004**, *447*, 796.

(183) Devirgiliis, C.; Zalewski, P. D.; Perozzi, G.; Murgia, C. *Mutat Res* **2007**, *622*, 84.

(184) Sekler, I.; Moran, A.; Hershfinkel, M.; Dori, A.; Margulis, A.; Birenzweig, N.; Nitzan, Y.; Silverman, W. F. *J Comp Neurol* **2002**, *447*, 201.

(185) Frederickson, C. J.; Suh, S. W.; Silva, D.; Thompson, R. B. *J Nutr* **2000**, *130*, 1471S.

(186) Huang, X.; Cuajungco, M. P.; Atwood, C. S.; Moir, R. D.; Tanzi, R. E.; Bush, A. I. *J Nutr* **2000**, *130*, 1488S.

(187) Vasak, M. *J Trace Elem Med Biol* **2005**, *19*, 13.

(188) Balesaria, S.; Ramesh, B.; McArdle, H.; Bayele, H. K.; Srai, S. K. *FEBS Lett* **2010**, *584*, 719.

(189) Smirnova, I. V.; Bittel, D. C.; Ravindra, R.; Jiang, H.; Andrews, G. K. *J Biol Chem* **2000**, *275*, 9377.

(190) Heuchel, R.; Radtke, F.; Georgiev, O.; Stark, G.; Aguet, M.; Schaffner, W. *EMBO J* **1994**, *13*, 2870.

(191) Pena, M. M.; Lee, J.; Thiele, D. J. *J Nutr* **1999**, *129*, 1251.

(192) Valentine, J. S.; Gralla, E. B. *Science* **1997**, *278*, 817.

(193) Prohaska, J. R.; Gybina, A. A. *J Nutr* **2004**, *134*, 1003.

(194) Que, E. L.; Domaille, D. W.; Chang, C. J. *Chem Rev* **2008**, *108*, 1517.

(195) Frederickson, C. J. *Int Rev Neurobiol* **1989**, *31*, 145.

(196) Frederickson, C. J.; Koh, J. Y.; Bush, A. I. *Nat Rev Neurosci* **2005**, *6*, 449.

(197) Suh, S. W.; Won, S. J.; Hamby, A. M.; Yoo, B. H.; Fan, Y.; Sheline, C. T.; Tamano, H.; Takeda, A.; Liu, J. *J Cereb Blood Flow Metab* **2009**, *29*, 1579.

(198) Frederickson, C. J.; Giblin, L. J.; Krezel, A.; McAdoo, D. J.; Mueller, R. N.; Zeng, Y.; Balaji, R. V.; Masalha, R.; Thompson, R. B.; Fierke, C. A.; Sarvey, J. M.; de Valdenebro, M.; Prough, D. S.; Zornow, M. H. *Exp Neurol* **2006**, *198*, 285.

(199) Tamano, H.; Takeda, A. *Metallomics* **2011**, *3*, 656.

(200) Smart, T. G.; Xie, X.; Krishek, B. J. *Prog Neurobiol* **1994**, *42*, 393.

(201) Lee, J. Y.; Cole, T. B.; Palmiter, R. D.; Koh, J. Y. *J Neurosci* **2000**, *20*, RC79.

(202) Howell, G. A.; Welch, M. G.; Frederickson, C. J. *Nature* **1984**, *308*, 736.

(203) Bush, A. I. *Curr Opin Chem Biol* **2000**, *4*, 184.

(204) Vogt, K.; Mellor, J.; Tong, G.; Nicoll, R. *Neuron* **2000**, *26*, 187.

(205) Ando, M.; Oku, N.; Takeda, A. *Neurochem Int* **2010**, *57*, 608.

(206) Pan, E.; Zhang, X. A.; Huang, Z.; Krezel, A.; Zhao, M.; Tinberg, C. E.; Lippard, S. J.; McNamara, J. O. *Neuron* **2011**, *71*, 1116.

(207) Lopantsev, V.; Wenzel, H. J.; Cole, T. B.; Palmiter, R. D.; Schwartzkroin, P. A. *Neuroscience* **2003**, *116*, 237.

(208) Takeda, A.; Fuke, S.; Minami, A.; Oku, N. *J Neurosci Res* **2007**, *85*, 1310.

(209) Takeda, A.; Nakajima, S.; Fuke, S.; Sakurada, N.; Minami, A.; Oku, N. *Brain Res Bull* **2006**, *68*, 442.

(210) Minami, A.; Sakurada, N.; Fuke, S.; Kikuchi, K.; Nagano, T.; Oku, N.; Takeda, A. *J Neurosci Res* **2006**, *83*, 167.

(211) Weiss, J. H.; Sensi, S. L.; Koh, J. Y. *Trends Pharmacol Sci* **2000**, *21*, 395.

(212) Takeda, A.; Takada, S.; Nakamura, M.; Suzuki, M.; Tamano, H.; Ando, M.; Oku, N. *PLoS One* **2011**, *6*, e28615.

(213) Colvin, R. A.; Holmes, W. R.; Fontaine, C. P.; Maret, W. *Metallomics* **2010**, *2*, 306.

(214) Adlard, P. A.; Parncutt, J. M.; Finkelstein, D. I.; Bush, A. I. *J Neurosci* **2010**, *30*, 1631.

(215) Martel, G.; Hevi, C.; Kane-Goldsmith, N.; Shumyatsky, G. P. *Behav Brain Res* **2011**, *223*, 233.

(216) Sindreu, C.; Palmiter, R. D.; Storm, D. R. *Proc Natl Acad Sci U S A* **2011**, *108*, 3366.

(217) Lutsenko, S.; Bhattacharjee, A.; Hubbard, A. L. *Metallomics* **2010**, *2*, 596.

(218) Rongzhu, L.; Suhua, W.; Guangwei, X.; Chunlan, R.; Fangan, H.; Junjie, J.; Aschner, M. *Biol Trace Elem Res* **2009**, *130*, 39.

(219) Gybina, A. A.; Tkac, I.; Prohaska, J. R. *Nutr Neurosci* **2009**, *12*, 114.

(220) Jackson, B.; Harper, S.; Smith, L.; Flinn, J. *Anal Bioanal Chem* **2006**, *384*, 951.

(221) Dobrowolska, J.; Dehnhardt, M.; Matusch, A.; Zoriy, M.; Palomero-Gallagher, N.; Koscielniak, P.; Zilles, K.; Becker, J. S. *Talanta* **2008**, *74*, 717.

(222) Becker, J. S.; Zoriy, M. V.; Pickhardt, C.; Palomero-Gallagher, N.; Zilles, K. *Anal Chem* **2005**, *77*, 3208.

(223) Zatta, P.; Drago, D.; Zambenedetti, P.; Bolognin, S.; Nogara, E.; Peruffo, A.; Cozzi, B. *J Chem Neuroanat* **2008**, *36*, 1.

(224) Tarohda, T.; Ishida, Y.; Kawai, K.; Yamamoto, M.; Amano, R. *Anal Bioanal Chem* **2005**, *383*, 224.

(225) Hershey, C. O.; Hershey, L. A.; Varnes, A.; Vibhakar, S. D.; Lavin, P.; Strain, W. H. *Neurology* **1983**, *33*, 1350.

(226) Basun, H.; Forssell, L. G.; Wetterberg, L.; Winblad, B. *J Neural Transm Park Dis Dement Sect* **1991**, *3*, 231.

(227) Schlief, M. L.; Gitlin, J. D. *Mol Neurobiol* **2006**, *33*, 81.

(228) Schlief, M. L.; Craig, A. M.; Gitlin, J. D. *J Neurosci* **2005**, *25*, 239.

(229) Walter, P. L.; Kampkotter, A.; Eckers, A.; Barthel, A.; Schmoll, D.; Sies, H.; Klotz, L. O. *Arch Biochem Biophys* **2006**, *454*, 107.

(230) Ostrakhovitch, E. A.; Lordnejad, M. R.; Schliess, F.; Sies, H.; Klotz, L. O. *Arch Biochem Biophys* **2002**, *397*, 232.

(231) Kim, S.; Jung, Y.; Kim, D.; Koh, H.; Chung, J. *J Biol Chem* **2000**, *275*, 25979.

(232) Bao, S.; Knoell, D. L. *Am J Physiol Lung Cell Mol Physiol* **2006**, *290*, L433.

(233) Liang, J.; Slingerland, J. M. *Cell Cycle* **2003**, *2*, 339.

(234) Barthel, A.; Ostrakhovitch, E. A.; Walter, P. L.; Kampkotter, A.; Klotz, L. O. *Arch Biochem Biophys* **2007**, *463*, 175.

(235) White, A. R.; Du, T.; Laughton, K. M.; Volitakis, I.; Sharples, R. A.; Xilinas, M. E.; Hoke, D. E.; Holsinger, R. M.; Evin, G.; Cherny, R. A.; Hill, A. F.; Barnham, K. J.; Li, Q. X.; Bush, A. I.; Masters, C. L. *J Biol Chem* **2006**, *281*, 17670.

(236) Finney, L. A.; O'Halloran, T. V. *Science* **2003**, *300*, 931.

(237) Zatta, P.; Drago, D.; Bolognin, S.; Sensi, S. L. *Trends Pharmacol Sci* **2009**, *30*, 346.

(238) Bonda, D. J.; Lee, H. G.; Blair, J. A.; Zhu, X.; Perry, G.; Smith, M. A. *Metallomics* **2011**, *3*, 267.

(239) White, A. R.; Barnham, K. J.; Bush, A. I. *Expert Rev Neurother* **2006**, *6*, 711.

(240) Lovell, M. A.; Robertson, J. D.; Teesdale, W. J.; Campbell, J. L.; Markesbery, W. R. *J Neurol Sci* **1998**, *158*, 47.

(241) Faller, P. *Chembiochem* **2009**, *10*, 2837.

(242) Bush, A. I.; Pettingell, W. H.; Multhaup, G.; d Paradis, M.; Vonsattel, J. P.; Gusella, J. F.; Beyreuther, K.; Masters, C. L.; Tanzi, R. E. *Science* **1994**, *265*, 1464.

(243) Lin, C. J.; Huang, H. C.; Jiang, Z. F. *Brain Res Bull* **2010**, *82*, 235.

(244) Cherny, R. A.; Atwood, C. S.; Xilinas, M. E.; Gray, D. N.; Jones, W. D.; McLean, C. A.; Barnham, K. J.; Volitakis, I.; Fraser, F. W.; Kim, Y.; Huang, X.; Goldstein, L. E.; Moir, R. D.; Lim, J. T.; Beyreuther, K.; Zheng, H.; Tanzi, R. E.; Masters, C. L.; Bush, A. I. *Neuron* **2001**, *30*, 665.

(245) Squitti, R.; Lupoi, D.; Pasqualetti, P.; Dal Forno, G.; Vernieri, F.; Chiovenda, P.; Rossi, L.; Cortesi, M.; Cassetta, E.; Rossini, P. M. *Neurology* **2002**, *59*, 1153.

(246) Squitti, R.; Bressi, F.; Pasqualetti, P.; Bonomini, C.; Ghidoni, R.; Binetti, G.; Cassetta, E.; Moffa, F.; Ventriglia, M.; Vernieri, F.; Rossini, P. M. *Neurology* **2009**, *72*, 50.

(247) Squitti, R.; Zito, G. *Recent Pat CNS Drug Discov* **2009**, *4*, 209.

(248) Lovell, M. A.; Smith, J. L.; Xiong, S.; Markesbery, W. R. *Neurotox Res* **2005**, *7*, 265.

(249) Smith, J. L.; Xiong, S.; Markesbery, W. R.; Lovell, M. A. *Neuroscience* **2006**, *140*, 879.

(250) Wenzel, H. J.; Cole, T. B.; Born, D. E.; Schwartzkroin, P. A.; Palmiter, R. D. *Proc Natl Acad Sci U S A* **1997**, *94*, 12676.

(251) Lee, J. Y.; Cole, T. B.; Palmiter, R. D.; Suh, S. W.; Koh, J. Y. *Proc Natl Acad Sci U S A* **2002**, *99*, 7705.

(252) Phinney, A. L.; Drisaldi, B.; Schmidt, S. D.; Lugowski, S.; Coronado, V.; Liang, Y.; Horne, P.; Yang, J.; Sekoulidis, J.; Coomaraswamy, J.; Chishti, M. A.; Cox, D. W.; Mathews, P. M.; Nixon, R. A.; Carlson, G. A.; St George-Hyslop, P.; Westaway, D. *Proc Natl Acad Sci U S A* **2003**, *100*, 14193.

(253) Leung, K. W.; Liu, M.; Xu, X.; Seiler, M. J.; Barnstable, C. J.; Tombran-Tink, J. *Invest Ophthalmol Vis Sci* **2008**, *49*, 1221.

(254) Maitra, R.; Shamovsky, I. L.; Wang, W.; Solc, M.; Lawrance, G.; Dostaler, S. M.; Ross, G. M.; Riopelle, R. J. *Neurotox Res* **2000**, 321.

(255) Wang, W.; Post, J. I.; Dow, K. E.; Shin, S. H.; Riopelle, R. J.; Ross, G. M. *Neurosci Lett* **1999**, *259*, 115.

(256) Ross, G. M.; Shamovsky, I. L.; Lawrance, G.; Solc, M.; Dostaler, S. M.; Jimmo, S. L.; Weaver, D. F.; Riopelle, R. J. *Nat Med* **1997**, *3*, 872.

(257) Zhao, G. H.; Yu, P.; Hu, X. S.; Zhao, L. *Acta Biochim Biophys Sin (Shanghai)* **2004**, *36*, 99.

(258) Allington, C.; Shamovsky, I. L.; Ross, G. M.; Riopelle, R. J. *Cell Death Differ* **2001**, *8*, 451.

(259) Frade, J. M.; Barde, Y. A. *Neuron* **1998**, *20*, 35.

(260) Ross, G. M.; Shamovsky, I. L.; Woo, S. B.; Post, J. I.; Vrkljan, P. N.; Lawrance, G.; Solc, M.; Dostaler, S. M.; Neet, K. E.; Riopelle, R. J. *J Neurochem* **2001**, *78*, 515.

(261) Huang, Y. Z.; Pan, E.; Xiong, Z. Q.; McNamara, J. O. *Neuron* **2008**, *57*, 546.

(262) Huang, Y. Z.; McNamara, J. O. *J Biol Chem* **2010**, *285*, 8207.

(263) Hwang, J. J.; Park, M. H.; Choi, S. Y.; Koh, J. Y. *J Biol Chem* **2005**, *280*, 11995.

(264) Hwang, J. J.; Park, M. H.; Koh, J. Y. *J Neurosci Res* **2007**, *85*, 2160.

(265) Kheirvari, S.; Uezu, K.; Sakai, T.; Nakamori, M.; Alizadeh, M.; Sarukura, N.; Yamamoto, S. *J Nutr Sci Vitaminol (Tokyo)* **2006**, *52*, 421.

(266) Kheirvari, S.; Uezu, K.; Yamamoto, S.; Nakaya, Y. *Nutr Neurosci* **2008**, *11*, 228.

(267) Corona, C.; Masciopinto, F.; Silvestri, E.; Viscovo, A. D.; Lattanzio, R.; Sorda, R. L.; Ciavardelli, D.; Goglia, F.; Piantelli, M.; Canzoniero, L. M.; Sensi, S. L. *Cell Death Dis* **2010**, *1*, e91.

(268) Sowa-Kucma, M.; Legutko, B.; Szewczyk, B.; Novak, K.; Znojek, P.; Poleszak, E.; Papp, M.; Pilc, A.; Nowak, G. *J Neural Transm* **2008**, *115*, 1621.

(269) Birkaya, B.; Aletta, J. M. *J Neurobiol* **2005**, *63*, 49.

(270) Pattison, S. E.; Dunn, M. F. *Biochemistry* **1975**, *14*, 2733.

(271) Shamovsky, I. L.; Ross, G. M.; Riopelle, R. J.; Weaver, D. F. *Protein Sci* **1999**, *8*, 2223.

(272) Gans, P.; Sabatini, A.; Vacca, A. *Talanta* **1996**, *43*, 1739.

(273) Wishart, D. S.; Sykes, B. D.; Richards, F. M. *Biochemistry* **1992**, *31*, 1647.

(274) Wishart, D. S.; Sykes, B. D.; Richards, F. M. *J Mol Biol* **1991**, *222*, 311.

(275) Wishart, D. S.; Sykes, B. D.; Richards, F. M. *FEBS Lett* **1991**, *293*, 72.

(276) La Mendola, D.; Bonomo, R. P.; Impellizzeri, G.; Maccarrone, G.; Pappalardo, G.; Pietropaolo, A.; Rizzarelli, E.; Zito, V. *J Biol Inorg Chem* **2005**, *10*, 463.

(277) Di Natale, G.; Osz, K.; Nagy, Z.; Sanna, D.; Micera, G.; Pappalardo, G.; Sovago, I.; Rizzarell, E. *Inorg Chem* **2009**, *48*, 4239.

(278) Damante, C. A.; Osz, K.; Nagy, Z.; Grasso, G.; Pappalardo, G.; Rizzarelli, E.; Sovago, I. *Inorg Chem* **2011**, *50*, 5342.

(279) Galanis, A. S.; Spyroulias, G. A.; Pierattelli, R.; Tzakos, A.; Troganis, A.; Gerothanassis, I. P.; Pairas, G.; Manessi-Zoupa, E.; Cordopatis, P. *Biopolymers* **2003**, *69*, 244.

(280) Gaggelli, E.; Janicka-Klos, A.; Jankowska, E.; Kozlowski, H.; Migliorini, C.; Molteni, E.; Valensin, D.; Valensin, G.; Wieczerzak, E. *J Phys Chem B* **2008**, *112*, 100.

(281) Valensin, D.; Szyrwiel, L.; Camponeschi, F.; Rowinska-Zyrek, M.; Molteni, E.; Jankowska, E.; Szymanska, A.; Gaggelli, E.; Valensin, G.; Kozlowski, H. *Inorg Chem* **2009**, *48*, 7330.

(282) Camponeschi, F.; Gaggelli, E.; Kozlowski, H.; Valensin, D.; Valensin, G. *Dalton Trans* **2009**, 4643.

(283) La Mendola, D.; Magri, A.; Hansson, O.; Bonomo, R. P.; Rizzarelli, E. *J Inorg Biochem* **2009**, *103*, 758.

(284) Damante, C. A.; Osz, K.; Nagy, Z.; Pappalardo, G.; Grasso, G.; Impellizzeri, G.; Rizzarelli, E.; Sovago, I. *Inorg Chem* **2009**, *48*, 10405.

(285) Boka, B.; Myari, A.; Sovago, I.; Hadjiliadis, N. *J Inorg Biochem* **2004**, *98*, 113.

(286) Myari, A.; Malandrinos, G.; Deligiannakis, Y.; Plakatouras, J. C.; Hadjiliadis, N.; Nagy, Z.; Sovago, I. *J Inorg Biochem* **2001**, *85*, 253.

(287) La Mendola, D.; Magri, A.; Campagna, T.; Campitiello, M. A.; Raiola, L.; Isernia, C.; Hansson, O.; Bonomo, R. P.; Rizzarelli, E. *Chemistry* **2010**, *16*, 6212.

(288) Orfei, M.; Alcaro, M. C.; Marcon, G.; Chelli, M.; Ginanneschi, M.; Kozlowski, H.; Brasun, J.; Messori, L. *J Inorg Biochem* **2003**, *97*, 299.

(289) Myari, A.; Malandrinos, G.; Plakatouras, J.; Hadjiliadis, N.; Sovago, I. *Bioinorg Chem Appl* **2003**, 99.

(290) Sovago, I.; Osz, K. *Dalton Trans* **2006**, 3841.

(291) La Mendola, D.; Magri, A.; Santoro, A. M.; Nicoletti, V. G.; Rizzarelli, E. *J Inorg Biochem* **2012**, *111*, 59.

(292) La Mendola, D.; Magri, A.; Vagliasindi, L. I.; Hansson, O.; Bonomo, R. P.; Rizzarelli, E. *Dalton Trans* **2010**, *39*, 10678.

(293) Galey, J. F.; Kozlowski, H.; Pettit, L. D. *J Inorg Biochem* **1991**, *44*, 149.

(294) Kowalik-Jankowska, T.; Jankowska, E.; Kasprzykowski, F. *Inorg Chem* **2010**, *49*, 2182.

(295) Yajima, T.; Maccarrone, G.; Takani, M.; Contino, A.; Arena, G.; Takamido, R.; Hanaki, M.; Funahashi, Y.; Odani, A.; Yamauchi, O. *Chemistry* **2003**, *9*, 3341.

(296) Vagliasindi, L. I.; Arena, G.; Bonomo, R. P.; Pappalardo, G.; Tabbi, G. *Dalton Trans* **2011**, *40*, 2441.

(297) de Vries, S. J.; van Dijk, M.; Bonvin, A. M. *Nat Protoc* **2010**, *5*, 883.

(298) Chen, D.; Bambah-Mukku, D.; Pollonini, G.; Alberini, C. M. *Nat Neurosci* **2012**, 1707.

(299) Satriano, C.; Edvardsson, M.; Ohlsson, G.; Wang, G.; Svedhem, S.; Kasemo, B. *Langmuir* **2010**, *26*, 5715.

(300) Keller, C. A.; Glasmastar, K.; Zhdanov, V. P.; Kasemo, B. *Phys Rev Lett* **2000**, *84*, 5443.

(301) Keller, C. A.; Kasemo, B. *Biophys J* **1998**, *75*, 1397.

(302) Bonacchi, S.; Genovese, D.; Juris, R.; Montalti, M.; Prodi, L.; Rampazzo, E.; Sgarzi, M.; Zaccheroni, N. *Top Curr Chem* **2011**, *300*, 93.

(303) Bonacchi, S.; Genovese, D.; Juris, R.; Montalti, M.; Prodi, L.; Rampazzo, E.; Zaccheroni, N. *Angew Chem Int Ed Engl* **2011**, *50*, 4056.

(304) Rampazzo, E.; Bonacchi, S.; Genovese, D.; Juris, R.; Sgarzi, M.; Montalti, M.; Prodi, L.; Zaccheroni, N.; Tomaselli, G.; Gentile, S.; Satriano, C.; Rizzarelli, E. *Chemistry* **2011**, *17*, 13429.

(305) McAllister, A. K.; Katz, L. C.; Lo, D. C. *Neuron* **1996**, *17*, 1057.

(306) Banfield, M. J.; Naylor, R. L.; Robertson, A. G.; Allen, S. J.; Dawbarn, D.; Brady, R. L. *Structure* **2001**, *9*, 1191.

(307) Travaglia, A.; Arena, G.; Fattorusso, R.; Isernia, C.; La Mendola, D.; Malgieri, G.; Nicoletti, V. G.; Rizzarelli, E. *Chemistry* **2011**, *17*, 3726.

(308) Travaglia, A.; La Mendola, D.; Magri, A.; Nicoletti, V. G.; Pietropaolo, A.; Rizzarelli, E. *Chemistry* **2012**, *18*, 15618.

(309) Peleshok, J.; Saragovi, H. U. *Biochem Soc Trans* **2006**, *34*, 612.

(310) Longo, F. M.; Vu, T. K.; Mobley, W. C. *Cell Regul* **1990**, *1*, 189.

(311) Colangelo, A. M.; Bianco, M. R.; Vitagliano, L.; Cavaliere, C.; Cirillo, G.; De Gioia, L.; Diana, D.; Colombo, D.; Redaelli, C.; Zaccaro, L.; Morelli, G.; Papa, M.; Sarmientos, P.; Alberghina, L.; Martegani, E. *J Neurosci* **2008**, *28*, 2698.

Annex 1: List of publication and communications

Publications

1) A. Travaglia, G. Arena, R. Fattorusso, C. Isernia, D. La Mendola, G. Malgieri, V.G. Nicoletti, E. Rizzarelli, *Chem. Eur. J.*, 2011, 17, 3726-3738)

2) A. Travaglia, A. Pietropaolo, D. La Mendola, V.G. Nicoletti, E. Rizzarelli, *J. Inorg. Biochem.*, 2012, 111, 130-137

3) D. La Mendola, D. Farkas, F. Bellia, A. Magrì, A. Travaglia, O. Hansson, E. Rizzarelli; *Inorg Chem*. 2012,51,128-41

4) A. Travaglia, D. La Mendola, A. Magrì, VG Nicoletti, A. Pietropaolo, E. Rizzarelli, Chem. Eur. J, 2012, *18*, 15618.-15631

5) A. Travaglia, C. Satriano, M.L. Giuffrida, D. La Mendola, E. Rampazzo, L. Prodi and E. Rizzarelli, *Submitted*

6) A. Travaglia, D. La Mendola, A. Magrì, VG Nicoletti, A. Pietropaolo, E. Rizzarelli, *Submitted*

7) A. Travaglia, G. Arena, C. Sgarlata, GI Grasso, D. La Mendola, E. Rizzarelli, *In preparation*

8) A. Travaglia, P. Calissano , E. Rizzarelli, *In Preparation*

9) A.Travaglia, G. Di Natale, E. Rizzarelli, *In Preparation*

Oral communications

1) A. Travaglia, R.P. Bonomo, G. Grasso, D. La Mendola, D. Milardi, G. Pappalardo, E. Rizzarelli, 9th workshop on PharmacoBioMetallics-BIOMET, Certosa di Pontignano (SI), Italy; 6-8 November 2009

2) A. Travaglia, G. Arena, R.P. Bonomo, D. La Mendola, V. Nicoletti, E. Rizzarelli, Joint conference of the sections Calabria - Sicily, Aci Castello (CT), Italy, 1-2 December 2009

3) G. Arena, D. La Mendola, V.G. Nicoletti, A. Travaglia, Nation meeting of PhD student in neuroscience, Busto Arsizio (VA), Italy; 27-28 May 2010,

4) A. Travaglia, D. La Mendola, R. Fattorusso, G. Arena, C. Isernia, G. Malgieri, V.G. Nicoletti, E. Rizzarelli, National Meeting of Italian Chemical Society, Lecce (LE), Italy; 11-16 September 2011

5) D. La Mendola, A. Travaglia, A. Magrì, A. Pietropaolo, VG Nicoletti, E. Rizzarelli, XL National Conference of Inorganic Chemistry, Sestri Levante (GE) Italy; 9-13 September 2012

6) A. Travaglia, D. La Mendola, A. Magrì, A. Pietropaolo, VG Nicoletti, E. Rizzarelli, 12th workshop on PharmacoBioMetallics-BIOMET, Padova, Italy, 26-28 October 2012

7) E. Rizzarelli, A. Travaglia, Samic 2012- Synthesis and Methodologies in Inorganic Chemistry, Bressanone, Italy, 2-6 December 2012

Poster communications

1) A. Travaglia, G. Arena, R.P. Bonomo, D. La Mendola, V. Nicoletti, E. Rizzarelli; XIV School of pure and applied biophysics, Biophysics school on the molecular mechanisms of neurodegeneration, Venezia(VE), Italy, 25-29 January 2010.

2) V.G. Nicoletti, D. La Mendola, A. Travaglia, G. Caruso, DA Distefano, E Rizzarelli, 55th National Meeting SIB, Milan (MI), Italy, 14-17 September 2010.

3) D. La Mendola, A. Magrì, F. Bellia, A. Travaglia, O. Hansson, F. Arnesano, G. Natile, L. De Gioia, RP Bonomo, E. Rizzarelli, 11th International Symposium on Applied Bioinorganic Chemistry, Barcelona (Spain), 2-5 Dicember 2011.

4) D. La Mendola, A. Travaglia, ML Giuffrida, C. Satriano, E. Rizzarelli, XIV Congress of the italian Society for Neurosciences, Catania (Italy) 19-22 April 2012

5) A. Magrì, A. Travaglia, D. La Mendola, VG Nicoletti, E. Rizzarelli, XIV Congress of the italian Society for Neurosciences, Catania (Italy) 19-22 April 2012

Annex 2: Research experiences

18/01/2010 → 30/10/2012 **PhD student, Advanced School of University of Catania, Italy.** Role of biometals, in physiological and pathological conditions, and their ability to modulate the activities of neurotrophins. Synthesis and structural characterization of neurotrophins peptidomimetics. Development of nanocapsules for drugs delivery. (Prof Rizzarelli).

22/02/2012 → 31/07/2012 **Visiting scholar, New York University, Center for Neural Science, New York, NY.** *In vivo* biochemical studies on molecular mechanisms of memory (Prof. Alberini).

20/03/2011 → 19/06/2011 **Visiting scholar, European Brain Research Institute, Rome, Italy.** *In vitro* biochemical studies on peptide fragments with pharmacological activity (Prof. Calissano).

29/08/2009 → 12/09/2009 **Visiting scholar, University of Gothenburg, Sweden.** Expression and characterization of human Angiogenin (prof. Hansson).